OO5-OO4
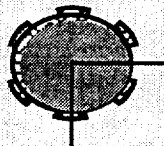
Texas A&M University
Mechanical Engineering Department

Analysis of Two-Phase Flow in Damper Seals for Cryogenic Turbopumps

NASA Grant NAG3-1434

Grigory L Arauz
Research Assistant

Principal Investigator:
Luis San Andres
Associate Professor

December 1996

Thermohydrodynamic Analysis of Cryogenic
Liquid Turbulent Flow Fluid Film Bearings.
(Phase III)

ANALYSIS OF TWO-PHASE FLOW IN DAMPER SEALS

FOR CRYOGENIC TURBOMACHINERY

A Dissertation

by

GRIGORY L. ARAUZ

Submitted to the Office of Graduate Studies of
Texas A&M University
in partial fulfillment of the requirements for the degree of

DOCTOR OF PHILOSOPHY

May 1997

Major Subject: Mechanical Engineering

ABSTRACT

Analysis of Two-Phase Flow in Damper Seals for Cryogenic Turbomachinery.

(May 1997)

Grigory L. Arauz, B.S. Escuela Politécnica Nacional, Ecuador;

M.S. Texas A&M University

Chair of Advisory Committee: Dr. Luis San Andrés

Cryogenic damper seals operating close to the liquid-vapor region (near the critical point or slightly sub-cooled) are likely to present two-phase flow conditions. Under single phase flow conditions the mechanical energy conveyed to the fluid increases its temperature and causes a phase change when the fluid temperature reaches the saturation value.

A bulk-flow analysis for the prediction of the dynamic force response of damper seals operating under two-phase flow conditions is presented as: all-liquid, liquid-vapor, and all-vapor, i.e. a "continuous vaporization" model. The two-phase region is considered as a homogeneous saturated mixture in thermodynamic equilibrium. The flow in each region is described by continuity, momentum and energy transport equations. The interdependency of fluid temperature and pressure in the two-phase region (saturated mixture) does not allow the use of an energy equation in terms of fluid temperature. Instead the energy transport is expressed in terms of fluid enthalpy. Temperature in the single-phase regions, or mixture composition in the two-phase region are determined based on the fluid enthalpy. The flow is also regarded as adiabatic since the large axial velocities

typical of the seal application determine small levels of heat conduction to the walls as compared to the heat carried by fluid advection. Static and dynamic force characteristics for the seal are obtained from a perturbation analysis of the governing equations. The solution expressed in terms of zeroth and first order fields provide the static (leakage, torque, velocity, pressure, temperature and mixture composition fields) and dynamic (rotordynamic force coefficients) seal parameters.

Theoretical predictions show good agreement with experimental leakage and pressure profiles available from a Nitrogen at cryogenic temperatures. Force coefficients predictions for two-phase flow conditions show significant fluid compressibility effects, particularly for mixtures with low mass content of vapor. Under these conditions, an increase on direct stiffness and reduction of whirl frequency ratio are shown to occur. Prediction of such important effects will motivate experimental studies as well as a more judicious selection of the operation conditions for the seals used in cryogenic turbomachinery.

TABLE OF CONTENTS

LIST OF FIGURES

LIST OF TABLES

NOMENCLATURE

c: radial clearance [m].

E_I: i_* / U_*^2, dimensionless parameter in energy equation.

$f_{r,s}$: $a_m[1+(c_m r_{r,s}/H+b_m/Re_{r,s})^{e_m}]$, turbulent friction factors at rotor and stator surfaces.

     $a_m=0.001375$; $b_m=5x10^5$; $c_m=10^4$; $e_m=1/3$

H: film thickness [m].

h: H/c, dimensionless film thickness

$h_{X,Y}$: $\cos\theta$, $\sin\theta$

i,i_*:   fluid enthalpy, characteristic enthalpy at supply [J/kg].

$\bar{i}$: i/i_*, dimensionless enthalpy.

i_l: liquid saturated enthalpy [J/kg].

i_g: vapor saturated enthalpy [J/kg].

i_{lg}: i_g-i_l, vapor-liquid saturated relative enthalpy [J/kg].

$K_{\alpha\beta},C_{\alpha\beta}$: stiffness and damping rotordynamic force coefficients [N/m, N.s/m]. $\alpha\beta=X,Y$

k_r,k_s: f_sRe_s, f_rRe_r, turbulent shear parameters at stator and rotor surfaces.

k_x,k_y: $(k_r+k_s)/2$, dimensionless shear parameters in X and Y directions.

L: seal length [m].

n: μ_g/μ_l, vapor-to-liquid viscosity ratio.

P: fluid pressure [Pa].

P_s, P_a: supply and discharge pressure [Pa].

p: $(P-P_a)/(P_s-P_a)$, dimensionless fluid pressure.

Q: $\rho V \pi Dc$, leakage [kg/s].

Qs: heat flux to bearing and journal surfaces [W/m^2]

R: rotor radius [m].

Re$_r$: $\rho H[(U-\Omega R)^2+V^2]^{0.5}/\mu$, Reynolds number relative to rotor surface.

Re$_s$: $\rho H[U^2+V^2]^{0.5}/\mu$, Reynolds number relative to stator surface.

Re$_S$: $\rho_* \omega_* c^2/\mu_*$, squeeze film Reynolds number.

Re$_p^*$: $\rho_* U_* c^2/(\mu_* R)$, modified reference pressure flow Reynolds number.

r$_r$,r$_s$: mean roughness depth at rotor and stator surfaces [m].

T,T$_*$: fluid temperature, characteristic temperature ['K].

$\overline{T}$: T/T_*, dimensionless temperature.

t: time [s].

U,V: circumferential and axial bulk-flow velocities [m/s].

u,v: $(U,V)/U_*$, dimensionless mean flow velocities.

U$_*$: $c^2(P_s-P_a)/(\mu R)$, characteristic velocity [m/s].

WFR: $K_{XY}/\Omega C_{XX}$, whirl frequency ratio.

X,Y: inertial coordinates for rotor center position within seal stator [m].

x,y: circumferential and axial coordinates [m].

$\overline{x}$: $x/R=\theta$, dimensionless circumferential coordinate.

$\overline{y}$: y/R, dimensionless axial coordinate.

α: circumferential velocity entrance swirl factor.

$\in_{X,Y}$:   dimensionless rotor eccentricities in X and Y directions.

Ψ: void fraction (vapor-to-mixture volume ratio).

Γ: first order coefficients (Appendix 1).

γ: first order shear coefficients (Appendix 1).

Λ: $\Omega R/U_*$, dimensionless rotor velocity.

λ: vapor-to-mixture mass ratio (quality).

μ, μ_* :   fluid viscosity, characteristic viscosity [Pa.s].

$\bar{\mu}$: μ/μ_*, dimensionless viscosity.

Ω: rotational speed of journal [rad/s].

ω: excitation whirl frequency [rad/s].

ρ, ρ_*:   fluid density, characteristic density [kg/m^3].

$\bar{\rho}$: ρ/ρ_*, dimensionless density.

σ: $\omega R/U_*$, dimensionless frequency parameter.

τ_{ij}:   wall shear stresses [Pa].

ξ: empirical entrance loss coefficient.

Subscripts:

o: refers to zeroth order solution.

α: refers to first order solution.

l: refers to liquid phase.

g: refers to vapor or gaseous phase.

i: refers to seal inlet conditions.

s: refers to seal external supply conditions.

sat: refers to fluid saturation conditions.

+:   refers to mixture properties when void fraction $\Psi=0.3$.

1. INTRODUCTION

The importance of process fluid damper bearing seals and hybrid journal bearings (HJBs) in high performance turbomachinery has grown steadily in the past few years. These thin fluid film bearing devices allow for more compact and lighter rotors, supercritical rotor operation and no bearing life limitations. These characteristics along with increased durability, reduced wear and friction, and more importantly, predictable rotordynamic force coefficients have fueled the advance of an "all-fluid-film-bearing" technology for advanced cryogenic turbomachinery (San Andres,1994).

Within this context, the roll of interstage seals in cryogenic turbomachinery has been expanded. In addition to their original function reducing leakage flow between interstages, seals are now required to operate as rotor load supports providing damping to improve the stability of the rotor-bearing system. Therefore the need for accurate analytical and experimental tools to determine the dynamic force response of these dampers seals has grown in recent years.

Operation close to the fluid critical point, likely to occur in damper seals using cryogenic fluids due to the steep variations of pressure and temperature within the seal, may result in fluid vaporization and the consequent formation of a single component two-phase fluid (Hendricks et al., 1987, Yang et al., 1993a). In any case, the transformation from a single-phase to concentration a two-phase fluid implies considerable variations in the overall material properties of the fluid such as its viscosity and density, and therefore

---

The journal style followed is the *ASME Journal of Tribology*.

affects the pressure and temperature gradients within the seal. Important seal performance characteristics such as leakage rate, power dissipation and rotordynamic force coefficients are closely related to the pressure field within the seal. Thus, a pronounced change in the seal static and dynamic performance characteristics is expected under two-phase flow conditions.

A brief description of the main concepts used in the rotordynamic analysis of seals is appropriate. The typical geometry of a pressure annular seal is presented in Figure 1. The seal is comprised by two concentric cylinders, the inner one (rotor) spins at speed (Ω) and the outer cylinder (stator) is stationary. A thin fluid film of thickness H, exaggerated in the figure for clarity, separates the rotor from the stator. This thin gap acts as a resistance path to the fluid flow from the high pressure supply (P_s) zone to the relatively low pressure discharge side (P_a) and creating the sealing effect of the device. The pressure difference between supply and discharge is usually very high in inter-stage seals in turbomachinery. A typical pressure distribution along a centered seal operating with an incompressible fluid is also shown in Figure 1. After a sudden drop at the seal entrance due to fluid acceleration from the supply sump to the seal inlet, the pressure decreases almost linearly along the seal until it reaches the discharge conditions. This pressure distribution is the same around the seal under concentric operation. If the rotor becomes off-centered by means of any applied load, the pressure distributions in the locations of minimum and maximum film thickness are as shown by the dotted lines in Figure 1. This difference in pressure produces a restoring force that opposes the rotor displacement, i.e. the seal provides a direct stiffness force coefficient (Childs, 1993).

Figure 1. Seal geometry and restoring fluid forces.

In addition to this hydrostatic effect, fluid rotation, drag and fluid inertia also promote restoring forces. Therefore, the fluid film forces generated in damper seals, and fluid film bearings in general, are typically described in terms of frequency independent rotordynamic force coefficients as given by:

$$\begin{bmatrix} F_X \\ F_Y \end{bmatrix} = \begin{bmatrix} K_{XX} & K_{XY} \\ K_{YX} & K_{YY} \end{bmatrix} \begin{bmatrix} X \\ Y \end{bmatrix} + \begin{bmatrix} C_{XX} & C_{XY} \\ C_{YX} & C_{YY} \end{bmatrix} \begin{bmatrix} \dot{X} \\ \dot{Y} \end{bmatrix} + \begin{bmatrix} M_{XX} & M_{XY} \\ M_{YX} & M_{YY} \end{bmatrix} \begin{bmatrix} \ddot{X} \\ \ddot{Y} \end{bmatrix}$$

The force is expressed in terms of stiffness (K_{ij}), damping (C_{ij}) and fluid inertia (M_{ij}) coefficients which represent the force components proportional to the rotor displacements, velocities and accelerations, respectively. The coefficients in the main diagonal are called direct coefficients and characterize a force that is in the same direction as the motion; whereas the off diagonal coefficients represent forces that although proportional to the generalized displacement, velocity or acceleration, act in a direction perpendicular to it. Note that the rotordynamic model presented in the above equation is valid only for incompressible fluids, rigid surface seals operating at sufficiently low frequencies.

Rotor instability in turbomachinery is usually produced by forces that are tangential to the rotor whirl orbit and acting in the same direction as the instantaneous motion of the rotor. Most destabilizing effects in turbomachinery are represented by cross-coupled stiffness coefficients (Vance, 1988). On the other hand, damping forces, which are proportional to the rotor speed and therefore are also tangential to the whirl orbit, oppose the rotor motion and are thus considered as stabilizing forces. The ratio of these two type of forces (destabilizing-to-stabilizing), known as "Whirl Frequency Ratio" (WFR), is commonly used to describe the stability of the rotor support system.

2. LITERATURE REVIEW

The study of two-phase flow phenomena in fluid film bearings such as dampers seals and journal bearings for cryogenic turbomachinery applications is of current interest. The present literature review focuses on the flow mechanics of a mixture of a liquid and a dispersed compressible fluid (gas or vapor). A two-phase flow condition is attained when the thermodynamic critical point (coexistence of liquid and vapor) of the gaseous phase is reached. A gaseous phase may be present in hydrodynamic bearings and squeeze film dampers by either fluid vaporization or release of gases dissolved in the fluid.

There have been two main streams in the study of multi-component flows as a direct result of their practical applications. The first of them considers the fluid as a two-component mixture with no mass transfer between the constituents (i.e. lubrication with emulsions and contaminated lubricants). The second branch of research regards the fluid as a one-component, two-phase fluid where the vaporization of the liquid requires mass transfer between the phases (face seals and annular pressure seals). The following is a review of the relevant research on two-phase flow under these two considerations.

The continuum theory of mixtures

One of the approaches used to model a two-phase fluid is through the continuum theory of mixtures where the fluid is regarded as a homogeneous mixture of two immiscible components. This method has been applied to lubrication problems in order to analyze the behavior of oil on water (O/W) emulsions used in metal forming processes. Nakahara et al. (1988) present an experimental study of the droplet behavior on O/W emulsion lubrication on a metal rolling process. The observations demonstrate that the oil

droplets which penetrate into the elasto-hydrodynamic-lubrication zone (EHL) form an "oil pool", i.e. an oil zone containing water droplets. In other words, a phase inversion occurs producing a water on oil (W/O) emulsion with a higher mixture viscosity in the EHL zone. The extent of this oil pool was found to be influenced by the oil concentration and the roller speed. However, at high roller speeds, coarse oil droplets cannot enter to the EHL zone due to back flow in the water phase. Only the fine droplets close to the moving surfaces enter the EHL zone producing a very fine O/W emulsion.

Al-Sharif (1992), Al-Sharif et al. (1993), and Wang et al. (1993) have applied the continuum theory of mixtures to the lubrication problem with liquid-liquid emulsions. In Al-Sharif's work, the continuum theory of mixtures developed by Atkin et al. (1976) and Muller (1968) are thoroughly discussed. The main assumption of this theory relates to the "equipresence principle", which states that every spatial position of a N component mixture is occupied by N material particles, one per each component. Conservation equations for each component are derived and coupled by the mutual interaction of the components. The lubrication approximation (i.e. a thin film) is applied to the mass and momentum equations to render an extended Reynolds equation for mixtures. When applied to a hydrodynamic journal bearing, the model shows some results that agree qualitatively with Nakahara et al. (1988) observations, e.g. a "filtration" phenomenon occurs in the converging region of the fluid film. The model also predicts that the maximum peak bearing pressure increases as the oil content increases.

In Wang et al. (1993), the continuum mixture theory is applied to elasto-hydrodynamic conjunctions. An expression for the film thickness as function of velocity,

load and material properties is obtained. Results of the proposed model applied to a oil-in-water emulsion show that the film thickness varies linearly with the inlet volume fraction of the oil. An increase in the of oil is observed close to the minimum film thickness, i.e. an oil pooling. Under this phenomenon the film thickness in the EHD conjunction is defined by the viscosity of the oil.

The next advancement in the mixture theory approach is related to gas-liquid mixtures. This type of mixture usually termed as a "bubbly" mixture may be present in oil ring seals, squeeze film dampers and hydrodynamic journal bearings vented to ambient conditions and operating under dynamic loading. Tonder (1975,1976a) presents a model for a homogeneous mixture of bubbles and lubricant where the size of the bubbles is small compared to the film thickness and with a low bubble solubility. The model neglects temperature changes and viscosity variations due to the presence of bubbles, i.e. it regards the mixture as isoviscous. It also shows there is a gain in load capacity in externally pressurized bearings when bubbles are trapped in the lubricant (mixtures with up to 10% in gas-to-lubricant volume ratio). This load gain is proportional to bubble content, bearing load factor, and inversely proportional to pressure drop. Tonder's model presents only qualitative agreement with load capacity experimental data presented by Cameron (1966) and with later findings of Tonder (1976b).

Khalil et al. (1980) extend Tonder's model to account for variation in lubricant properties due to changes in pressure and temperature along the flow. The model combines continuity, momentum and energy transport equations to obtain expressions for the bearing mass flow and temperature and pressure gradients. Application of the model to

externally pressurized bearings shows that the pressure distribution and load-carrying capacity improve with air bubble content for both rotating and non-rotating bearings.

Chamniprasart (1992) and Chamniprasart et al. (1993) extend the original research of Al-Sharif et al. (1993) on binary mixtures to bubbly-oil mixtures. The model considers the fluid as a mixture of a newtonian fluid and an ideal gas (typically air). However, the analysis does not account for mass transfer between component and makes the model unsuitable to handle lubricant vapor cavitation. The analysis when applied to a finite hydrodynamic journal bearing shows that the concentration of air (gas) affects significantly the bearing pressure distribution. Comparison of numerical predictions with some experimental pressure measurements of Braun and Hendricks (1981) shows moderate qualitative agreement.

In general the models based on the continuum theory of mixtures present qualitative agreement with experimental and practical observations provided that accurate empirical rheological and constitutive equations are used. Results depend on how close the modeled flow process (laminar flow with isothermal, isoviscous, adiabatic conditions) resembles the actual flow. Note that these models do not account yet for mass transfer between phases, and therefore, are not suitable for two-phase flows where fluid vaporization/condensation is present. Furthermore, a number of yet unknown rheological parameters are needed for accurate results. It is important to note that all the models referred consider the fluid flow as laminar. This is not an appropriate assumption in applications with cryogenic fluids where operation at higher rotational speeds and the use of rough surfaces to improve rotordynamic stability lead to turbulent flow conditions.

Vapor Cavitation

Zuber et al. (1982) present an early attempt to treat the two-phase flow problem arising from fluid vaporization as a homogeneous mixture in thermodynamic non-equilibrium. The model considers the conservation equations for each component and a "constitutive equation of condensation or of evaporation" specifying the mass rate of liquid formation or extraction per unit volume of mixture. The inclusion of this sink or source term is the only difference with the standard Reynolds equation for compressible fluids. Results from the analysis show that this added term has a significant effect on the static and dynamic bearing force characteristics. Unfortunately, according to the authors, the equation of evaporation and condensation which governs this source/sink term "is not known for some flow regimes and only in a rudimentary way manner for others."

Feng et al. (1986) present density and viscosity models for two-phase homogeneous fluids used in dynamically loaded hydrodynamic bearings and squeeze film dampers. The authors show that when the fluid vapor pressure is low it has little influence in the gas phase and can be safely regarded as zero (absolute). An empirical correlation for viscosity of certain oil products known as the Hayward model (1961) is used to represent the mixture viscosity.

Pinkus (1990) discusses the differences in the heat transfer process in the flow regions of a hydrodynamic fluid film bearing. In the all-liquid region heat generation is large and its temperature is slightly higher than the bearing wall temperature. Thus, heat is transferred from the fluid to the bearing walls. In the two-phase region the temperature is lower than that of the walls and the heat generation drops with the increments of mixture

quality. The mixture then extracts heat from the walls to maintain the vaporization. In the all-vapor section the heat generation is minimum, which when added to the low temperature at the end of the two-phase region causes a heat transfer from the walls and the temperature of the vapor to increase.

Two-Phase Flow in Annular Pressure Seals and Face Seals

The theoretical treatment of multi-phase flow in annular seal applications is only recent. Several analysis present modifications to the classical lubrication theory in order to account for the multi-phase phenomena. Unfortunately, due to the lack of experimental data and the variety of approaches used, most of these efforts show different results.

Hughes et al. (1978) study the vaporization of a lubricant in liquid face seals. The flow through the seal is divided into two separate regions, one liquid and one gaseous with separate equations of motion for pressure, temperature and mass flow rate in each fluid phase. The two flow zones are coupled by the boundary conditions at the interphase surface. Hughes et al. further assume that both phases are at the same temperature (vaporization temperature). The model predicts that the maximum flow rate is reached when the fluid is fully liquid. On the other hand, when two-phase flow occurs most of the pressure drop takes place in the vapor phase. The temperature variations across the film are found not to be significant, with the main cause for liquid boiling as due to "flashing" occurring as the pressure decreases along the seal. However, the theoretical predictions for fluid pressure and temperature show evidence of a transition region where both liquid and vapor phases coexist. Yasuna and Hughes (1990) present a "continuous boiling" model as opposed to the previous "discrete boiling" analysis. In the novel model the flow along the

seal is divided into three regions: all-liquid, liquid-gas, and all-gas. The two-phase region is considered as an homogeneous mixture of saturated liquid and vapor in thermodynamic equilibrium. Results show the extent of the two-phase region to be considerable in all cases, even when the flow is nearly isothermal (discrete model). For nearly isothermal and viscous dissipation dominated conditions, the quality of the mixture is very low (close to zero), explaining why the mixture behaves as a saturated liquid. Results also show that energy convection effects are important and often dominant with respect to the dissipation effects for the typical range of clearances used in laminar flow face seals. The "discrete boiling" model developed earlier is then inadequate is such situation.

Yasuna and Hughes (1992) present an analysis for two-phase face seals including squeeze film effects and thermal transients. The model is based on the "discrete boiling" model referred earlier. Results for simulations to step perturbations of the film thickness are presented. For step increments the response decays as the rotor approaches the initial steady state conditions. For large enough film thickness step decrements the seal collapses due to the onset of an unstable vibration. For small step decrements of film thickness the rotor approaches the steady state asymptotically in a stable oscillatory motion. The assumption of discrete boiling and laminar flow are appropriate only for small film thickness (low leakage rate) and limit greatly Yasuna et al.'s model. As the film thickness increases, thermal convection gains importance and a two-phase zone may appear. For even larger film thickness the flow becomes turbulent. At this increased velocity condition the thermal transport process may be considered as adiabatic.

Beatty and Hughes (1987) present a turbulent flow, steady and adiabatic model for concentric annular pressure seals. Here the fluid flow is also divided into three regions: all liquid, liquid-vapor, and all vapor. Numerical results for a case example emulating the inter-stage seal of the Space Shuttle Main Engine High-Pressure Oxidizer Turbo-Pump show that the leakage rate is reduced by clearance reduction, increment of rotational speed, lengthening of the seal, and vapor production. It is concluded that subcooling of the liquid before the seal inlet reduces vapor production, therefore increasing the leakage rate.

Beatty and Hughes (1990) later introduce a different approach in a model for turbulent flow annular seals based on the stratified flow of the boiling liquid and vapor phases. Stratification of the phases is attributed to the centrifugal inertia due to shaft rotation. Governing equations for film-averaged liquid and vapor properties and flow variables are presented. The model regards the fluid streams as adiabatic and moving at different bulk-flow velocities, with the vapor layer closer to the rotating shaft. This model is similar to those used by continuum theory of mixtures discussed earlier. Conservation equations for each phase and for the mixture are presented. Although this is a more sound approach to account for the interfacial action between liquid and vapor, it presents the same weakness as the models based continuum theory, i.e. it lacks of appropriate constitutive equations for the interfacial shear stresses as a function of the interfacial velocity to provide closure to the model. Calculations for seal cases show that the variations of seal leakage rate with speed, seal length, vapor generation, etc., are similar to those predicted with the earlier "homogeneous mixture" model. However, the stratified model predicts slightly larger leakage rates and it is less sensitive to rotational speed than

the homogeneous-mixture model. These small deviations show that the centrifugal effects are not important in a configuration such as annular seals where curvature effects are negligible due to the smallness of the film thickness compared to the length, diameter and the rest of the seal dimensions. It also shows that the two phases are moving closely together and therefore a one component mixture suffices to model the fluid. In addition, the large level of turbulence present in annular seals in cryogenic turbomachinery tend to enhance mixing and homogenize the liquid-vapor mixture.

Hendricks (1987) presents a unique experimental study on uniform clearance, non-rotating, cylindrical seals for high performance turbomachines like the Space Shuttle Main Engine Fuel Turbo Pump. The work focuses on the measurement of leakage rates and pressure profiles for several fluid conditions, and for concentric and fully eccentric seal positions. The experiments demonstrate that low back pressures may lead to a two-phase flow condition at the seal discharge. A model based on one-dimensional, steady state isentropic, two-phase momentum and energy equations provides expressions for the mass flux and pressure. These expressions are normalized to use the corresponding-states theory to compare results using different fluids. Experimental results show two-phase choked flow near the seal exit as denoted by a large positive slope of the pressure profiles in that region. The work of Hendricks is relevant because it presents useful experimental data for cryogenic fluids, namely nitrogen and hydrogen. Hydrogen flow rate and fluid pressure distribution experimental data are quite sensitive to the inlet temperature for concentric seal configuration. For eccentric operation the liquid hydrogen and liquid nitrogen pressure fields were determined to be very sensitive to the inlet temperature.

Hendricks et al. (1987) present a theoretical model for laminar flow of a variable properties fluid through cylindrical seals, and show that two-phase flow regions may appear even when the supply and discharge pressures are well above the critical point. For seals or bearings operating highly eccentric the minimum pressure associated with the maximum film thickness location may be low enough to fall below the critical pressure and reach saturation conditions. These "nested" two-phase regions will affect the fluid pressure and temperature fields and therefore seal static and dynamic force characteristics may differ significantly to those of a full single-phase seal.

Salhi et al. (1992) present an experimental study on the pressure gradient in a two-phase flow (nitrogen on diluted oil) at low void fractions (~5%) in a narrow annular space between concentric cylinders. The measured flow rate and pressure drop along the seal are combined in a "pressure drop coefficient" ($\lambda=4\Delta P/[L\rho V^2/c]$) which represents the friction factor for the mixture. Salhi's experimental study demonstrates that the conventional pressure drop coefficient correlation ($\lambda = a\ Re^{\ n}$) used for single-phase flows is valid for two-phase mixtures with low vapor concentration .

Iwatsubo et al. (1993) present an experimental study on the static and dynamic forced response of an annular seal using a mixture of water and air as working fluid. Rotordynamic force coefficients are identified for mixtures with void fractions (gas-to-mixture volume ratios) up to 70 %. Results show the significant effect of two-phase flow condition on the seal dynamic forceperformance However, due to the large difference in density between the two mixture components (air and water) the compositions tested represent very small concentrations of gas in terms of mixture quality (gas-to-mixture

mass ratio) compared to the expected values in a seal for cryogenic applications where the two-phase flow condition is a result of fluid vaporization, i.e. the mixture has only one material component.

One of the weaknesses of the analyses for two-phase flow models referred so far is the lack of firm theoretical grounds for the multi-phase transport phenomena (mass, momentum and energy). Gray (1975) presents a general equation for multi-phase transport of a fluid material property. This work demonstrates the importance of the correct definition of the convective and diffusive components of the transport process. Gros D'Aillon et al. (1981) present a experimental study of two-phase flow through nozzles. The measurements, representative of the flow under steep pressure gradients in nuclear reactors, show the great influence that interface mass and momentum transfer have in critical flows. It seems that an appropriate treatment of the interface mass, momentum and energy transfer could be the key to a more accurate prediction of two-phase flows.

San Andres et al (1991, 1992, 1995), Yang et al. (1993a,b) have developed a theoretical model for prediction of bearing and seal performance that accounts for most of the important flow phenomena present in cryogenic applications. Thermal effects, flow turbulence, fluid inertia at the entrance, discharge and within the seal, different geometries (grooves, recesses, etc.) have been progressively included in the model, and which has shown good agreements with experimental results. The next step in the development of this theoretical analysis is the inclusion of two-phase flow phenomena.

3. OBJECTIVES

The importance of two-phase flow on the performance of fluid film bearings is detailed in the previous section. San Andres et al. (1991, 1995), Yang et al. (1993,a,b) at Texas A&M University have developed bulk flow analyses that account for most of the flow phenomena of importance in fluid film bearings used in cryogenic turbomachinery. These are namely turbulence, fluid inertia, and thermal effects.

The objective of this dissertation is to extend the work performed at Texas A&M University and advance a bulk-flow analysis for the prediction of the dynamic forced response of damper seals for cryogenic turbomachinery operating under two-phase flow conditions. The starting point of this research is the analysis of two-phase flow in a concentric annular seal working with cryogenic fluids. As for the structure of the flow, the Beatty and Hughes approach (1987) dividing the flow inside the seal into three sections: all-liquid, vapor-liquid, and all-gas ("continuous boiling" model) is assumed.

Special attention is given to two aspects: the inter-phase interaction (mass and energy transfer) expressed by the liquid-vapor mixture composition, and the effect of two-phase flow on the dynamic force coefficients of damper seals for cryogenic turbopumps.

4. THEORETICAL MODEL

Annular pressure seals (damper seals) in cryogenic turbomachinery commonly operate close to the fluid saturation conditions. The typical thermodynamic process for the fluid across the seal is depicted in the temperature-entropy (T-S) diagram shown in Figure 2. Two examples of seals working with liquid oxygen (LOX) are presented in the Figure. One example depicts the typical process for a typical damper seal designed for the space shuttle fuel pump, and the other corresponds to an example presented by Beatty and Hughes (1987) designed to show two-phase flow conditions. Three points are marked in each case indicating the supply condition (s), the seal entrance or inlet condition (i) and the exit or discharge condition (e). The nearly isentropic pressure drop between supply and entrance(s-i) is a result of the acceleration of the fluid as it flows from the fluid sump at supply conditions to the narrow seal entrance. The remaining segment of the curves (i-e) correspond to the change in state of the fluid within the seal itself.

The case shown in dotted lines represent the design for the inter-stage seal of the oxidizer pump (HPOTP) of the space shuttle main engine (SSME) (San Andres, 1995). The supply conditions are 55.6 MPa and 115 °K, the discharge pressure is equal to 2.55 MPa and the shaft rotational speed is equal to 30,367 rpm. As it can be seen in the figure, the fluid is very close to saturation condition at the seal exit. Even this proximity to the saturation line may lead to two-phase flow conditions during eccentric motions of the rotor within the seal as described by Hendricks, et al. (1987).
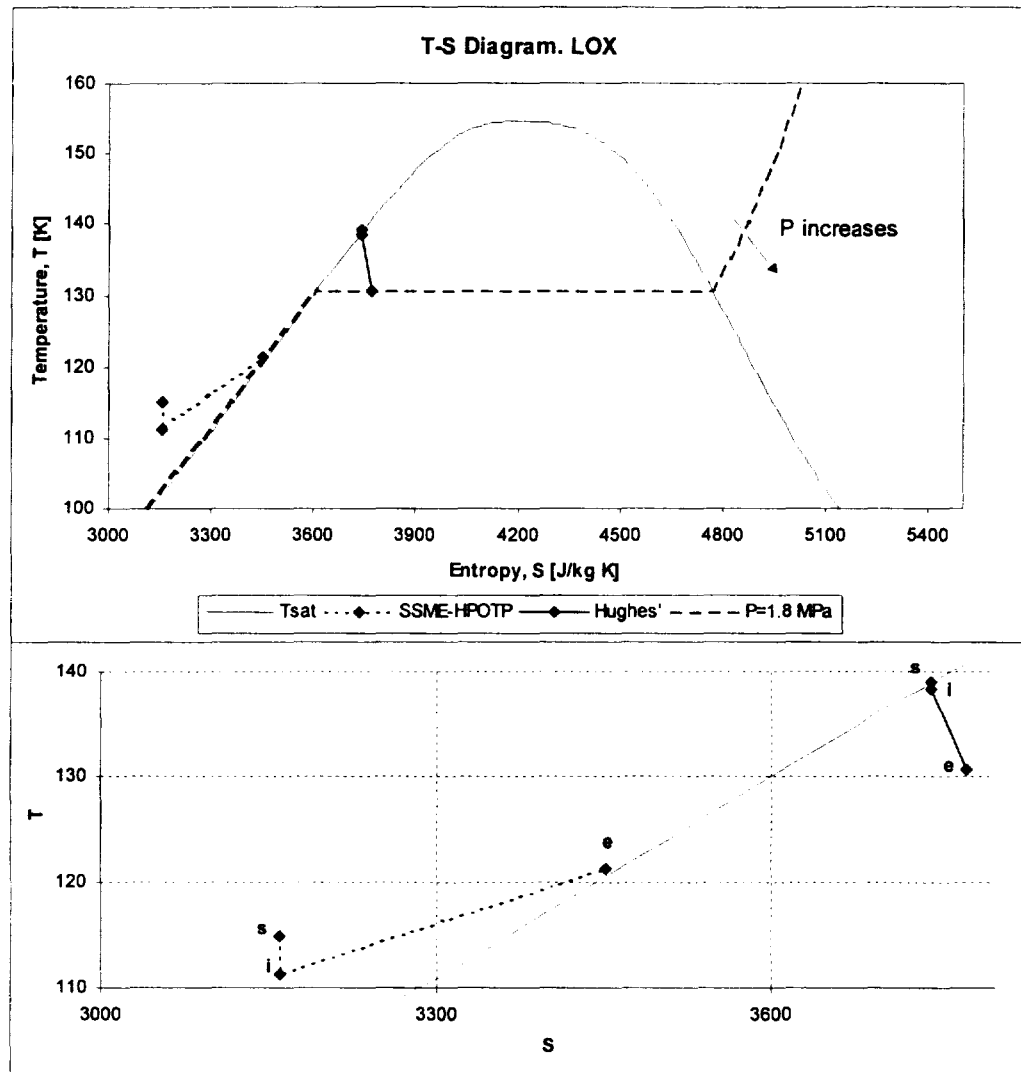
Figure 2. Typical trajectory of a fluid element through a LO_2 seal in the T-S plane.

The case shown in solid lines corresponds to the seal example presented by Beatty and Hughes (1987), where the operating conditions of the above mentioned seal have been changed to bring the seal supply state close to saturation enabling the presence of two-phase flow within the seal. Supply conditions are 2.79 MPa and 139 °K while the discharge pressure is equal to 1.8 MPa at a rotational speed equal to 37,300 rpm. The

figure shows that the fluid reaches two-phase flow conditions after the sudden contraction at the inlet and remains as a vapor-liquid mixture throughout the seal.

The purpose of these examples is not only to show the proximity to saturation conditions in a real application seal, but also to show the dramatic change in the character of the process along the seal once two-phase flow conditions occur.

Figure 3 shows a schematic view of an annular pressure seal and the coordinate system used. The radial clearance is exaggerated for clarity. A cryogenic fluid flows through the very thin annular space between the rotating shaft (rotor) and the stationary housing (stator) due to a difference in pressure between supply (P_s) and discharge (P_a) values. The pressure drop (P_s-P_a) is typically very large (usually a function of speed square) due to their application as inter-stage seals. These peculiar conditions enable the use of the following general assumptions for the flow within the seal:

- The flow is considered as two-dimensional bulk-flow (in the circumferential and axial directions) due to the smallness of the film thickness as compared to the other seal dimensions. This also allows to neglect the effect of rotor and stator curvatures leading to a cartesian coordinate system (x,y) on the plane of the seal.

- The large pressure gradient along the seal produces large axial velocities. Hence the flow is considered as fully developed turbulent. Typical Reynolds numbers based on pressure flow for the considered cryogenic applications are around 50,000 and higher.
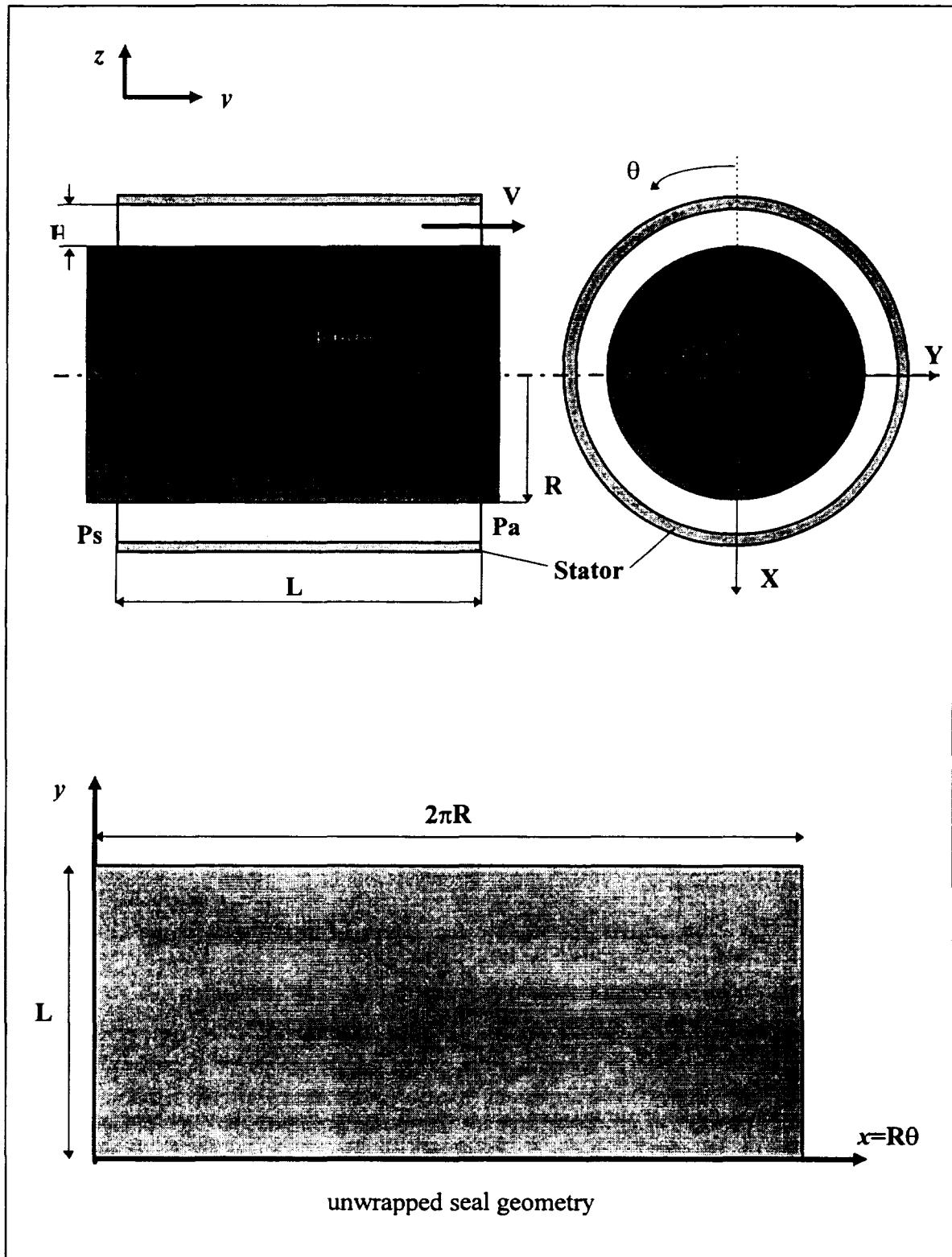
Figure 3. Schematic annular pressure seal geometry and coordinate system.

- Due to this large axial velocity the heat flow carried by convection is significantly higher than the heat transferred to the walls. Consequently, the bulk-flow can be regarded as adiabatic (Yang et al., 1993a).

In the event of two-phase flow conditions within the seal the following additional assumptions are made:

- Under two-phase conditions the flow is divided into three regions: all-liquid, liquid-vapor, and all-vapor, i.e. a "continuous" vaporization model is assumed (Beatty and Hughes, 1987).

- All three regions satisfy the general assumptions given above.

- The liquid-vapor mixture is regarded as homogeneous and saturated, and considered to be in thermodynamic equilibrium.

At the beginning of this investigation a more fundamental approach was tried for the two-phase flow region. The continuum theory for mixtures(Atkin et al., 1976, and Muller, 1968) was used. Conservation equations for mass, momentum and energy were developed for each component (liquid and vapor) and for the mixture as a whole. This approach provided a more direct way to treat the phase interaction through explicit terms in the component governing equations. However, it required a series of constitutive equations for the interface stresses and interface surface tensions which have been developed empirically for some fluids and are non-existing for others, in particular for turbulent flows. This approach was discarded due to the lack of firm knowledge needed to provide closure to the theoretical model.

4.1 Bulk-flow governing equations

Taking into account the above assumptions, the turbulent bulk-flow of a variable properties fluid inside an annular pressure seal is described by the continuity, momentum and energy transport equations given by Yang (1992). These equations are valid for any single-phase compressible fluid, and thus can be applied directly to the all-liquid or the all-vapor regions. The main modification to account for two-phase flow is the use of the energy transport equation in terms of fluid enthalpy instead of an equation using fluid temperature. In the two-phase region the fluid temperature is no longer independent of pressure, and therefore, a different fluid property such as mixture composition, enthalpy, entropy, etc, is needed to describe the thermophysical state of the fluid. Unlike a mixture composition which is not defined in the single-phase regions, enthalpy provides a continuous flow variable that allows the use of the same energy equation in the single or two-phase regions. Under two-phase flow conditions the fluid properties used in the governing equations (density and viscosity) are those of the mixture and therefore they convey the effect of the two-phase flow to the continuity and momentum equations.

With all the considerations presented above the bulk-flow transport governing equations are given as follows (Yang, 1992):

Continuity:

$$\frac{\partial(\rho H)}{\partial t} + \frac{\partial(\rho HU)}{\partial x} + \frac{\partial(\rho HV)}{\partial y} = 0 \tag{1}$$

Circumferential Momentum:

$$\frac{\partial(\rho HU)}{\partial t} + \frac{\partial(\rho HU^2)}{\partial x} + \frac{\partial(\rho HUV)}{\partial y} = -H\frac{\partial P}{\partial x} + \tau_{xz}\Big|_0^H \tag{2}$$

Axial Momentum:

$$\frac{\partial(\rho HV)}{\partial t} + \frac{\partial(\rho HUV)}{\partial x} + \frac{\partial(\rho HV^2)}{\partial y} = -H\frac{\partial P}{\partial y} + \tau_{yz}\Big|_0^H \qquad (3)$$

Energy:

$$\frac{\partial(\rho Hi)}{\partial t} + \frac{\partial(\rho HUi)}{\partial x} + \frac{\partial(\rho HVi)}{\partial y} = H\left[\frac{\partial P}{\partial t} + U\frac{\partial P}{\partial x} + V\frac{\partial P}{\partial y}\right] - Q_s$$
$$+ R\Omega\tau_{xz}\Big|^H - U\tau_{xz}\Big|_0^H - V\tau_{yz}\Big|_0^H \qquad (4)$$

4.2 Shear stress model

Yang et al. (1993a) uses Hirs' bulk-flow theory for turbulence in thin films flows. This model works well for all-liquid and all-gaseous flows. The use of friction factors based on Moody's formulae facilitates the inclusion of macroscopically rough stator surfaces into the model. These considerations and the assumption of a homogeneous mixture for the two-phase region makes Hirs' shear stress model adequate for the proposed two-phase flow model. The validity of this model for low gas concentration two-phase mixtures is also demonstrated by the experimental work of Salhi et al. (1992), as explained in the literature review (section 2). Thus, the wall shear stresses presented in the bulk flow governing equations are defined as:

$$\tau_{xz}\Big|_0^H = -\frac{\mu}{H}\left(k_x U - k_r \frac{R\Omega}{2}\right)$$

$$\tau_{yz}\Big|_0^H = -\frac{\mu}{H}k_y V \qquad (5)$$

$$\tau_{xz}\Big|^H = \frac{H}{2}\frac{\partial P}{\partial x} + \frac{\mu}{4H}\left[U k_s - (U - R\Omega)k_r\right]$$

with the turbulent shear parameters (k_x, k_y) and (k_r, k_s) are local functions of the Reynolds numbers and the friction factors based on Moody's formulae.

$$k_x = k_y = \frac{k_s + k_r}{2} \quad ; \qquad k_{s,r} = f_{s,r} \, \mathrm{Re}_{s,r}$$

$$f_{s,r} = 0.001375 \left[1 + \left(10^4 \, \frac{r_{s,r}}{H} + \frac{5 \times 10^5}{\mathrm{Re}_{s,r}} \right)^{1/3} \right] \qquad (6)$$

$$\mathrm{Re}_r = \frac{\rho H \sqrt{(U - \Omega R)^2 + V^2}}{\mu} \quad ; \quad \mathrm{Re}_s = \frac{\rho H \sqrt{U^2 + V^2}}{\mu}$$

4.3 Boundary conditions

The type of damper seal considered is used as inter-stage seal in cryogenic turbopump applications. Thus, supply pressure and temperature and the discharge pressure are determined by the performance and operation requirements of the machine. Therefore the boundary conditions for the flow field variables are summarized as follows:

a) A sudden drop in pressure occurs at the seal inlet due to the local acceleration of the fluid from stagnant conditions (P_s, T_s) to an inlet velocity at the seal entrance. The entrance pressure (P_i) is given by (Childs, 1993):

$$P_i = P_s - \frac{(1 + \xi)}{2} \rho_i V_i^2 \qquad (7)$$

where the subscripts s and i denote supply and seal inlet conditions respectively. (ξ) is an empirical entrance loss coefficient to account for the non-isentropic effects of the process. This Bernoulli like equation is obtained from a balance of mechanical energy between stagnant and entrance conditions along an isentropic path.

b) The entrance enthalpy is also affected by the acceleration of the fluid through the seal entrance and is given by:

$$i_i = i_s - \frac{(1 + \xi)}{2} V_i^2 \qquad (8)$$

This equation arises from a total energy balance in an infinitesimal control volume at the seal inlet plane. The enthalpy at the supply conditions (i_s) is determined by the known pressure and temperature if the fluid is in single-phase condition. If the fluid is

supplied as a two-phase mixture its composition in terms of quality (vapor-to-mixture mass ratio) has to be specified along with the supply pressure and temperature ($T_s = T_{sat(Ps)}$) in order to determine the supply enthalpy. Note that this equation arises from a balance of total energy at the seal entrance and is independent from the expression for pressure drop at the entrance (equation 7) which is based on a balance of mechanical energy along an isentropic path and where the irreversibilities are accounted for through the entrance loss coefficient..

c) Depending on upstream conditions like fluid preswirl and seal straightening vanes, the circumferential velocity at the seal entrance is given as a fraction of the rotor surface speed.

$$U = \alpha \Omega R \qquad (9)$$

where α is a preswirl factor .

d) At the seal exit (Y=L), under subsonic flow conditions, the fluid pressure is taken to be equal to the ambient or discharge pressure (P_a). No fluid inertia effects producing a pressure recovery are considered at the seal exit.

$$P_{(Y=L)} = P_a \qquad (10)$$

If the flow reaches sonic conditions the velocity at the exit is equal to the fluid sound velocity, and the mass flow rate is determined by the supply (stagnant) conditions and the area where the flow chokes.

4.4 Determination of two-phase flow condition

The existence of a two-phase flow condition within the seal is determined by comparison of the estimated enthalpy (i) with the liquid (i_l) and vapor (i_g) saturated enthalpies corresponding to the local pressure.

$$
\begin{array}{lll}
\text{If} & i \leq i_{l(P)} & \Rightarrow \text{LIQUID} \\[1em]
\text{If} & i \geq i_{g(P)} & \Rightarrow \text{VAPOR} \qquad (11) \\[1em]
\text{If} & i_{l(P)} < i < i_{g(P)} & \Rightarrow \text{TWO-PHASE}
\end{array}
$$

In the two-phase region the mixture quality (λ), i.e. the vapor to mixture mass ratio, is given by:

$$\lambda = \frac{i - i_l}{i_g - i_l} \tag{12}$$

Recall that vapor-liquid two-phase mixtures can only exist below the fluid critical point, above this point there is no distinction between vapor and liquid and the substance is regarded simply as a fluid. Fluid material properties at the critical point for oxygen, nitrogen and hydrogen are given in Table 1, as obtained from NBS database developed by McCarty (1986).

Table 1. Material properties for hydrogen, oxygen and nitrogen at the critical point.

	Hydrogen, H_2	Oxygen, O_2	Nitrogen, N_2
Pressure [MPa]	32.938	154.58	126.26
Temperature [°K]	1.2838	5.043	3.3991
Density [kg/m³]	32.199	707.96	254.06
Enthalpy [J/kg]	33965	-9623.8	44834
Entropy [J/kg °K]	17445	3927	4337.9

4.5 Two-phase mixture fluid properties

Under two-phase flow conditions the thermodynamic state of the mixture cannot be determined by pressure and temperature since these are not independent material properties. Fluid pressure and a different thermophysical property such as enthalpy or mixture quality (composition) are necessary to define the state. Once the fluid enthalpy and pressure are known (primitive flow variables) the mixture quality is determined, and thus all the other physical properties can be determined.

Most of the mixture properties such as its entropy, internal energy, specific heat, specific volume ($1/\rho$) are defined in terms of the quality (mixture composition) as (Look, 1986):

$$\Phi = \lambda\,\Phi_g + (1-\lambda)\,\Phi_l \qquad\qquad (13)$$

where Φ represent the mixture property (enthalpy, entropy, etc), Φ_g and Φ_l are the vapor and liquid saturated properties, and λ is the vapor-to-mixture mass ratio (quality).

The mixture density, which is by definition the inverse of the specific volume, is therefore given as:

$$\frac{1}{\rho} = \frac{\lambda}{\rho_g} + \frac{1-\lambda}{\rho_l} \qquad\qquad (14)$$

The mixture viscosity is treated separately in light of empirical evidence of a peculiar behavior of the viscosity for mixtures with low concentrations of a gaseous phase. The mixture viscosity models most commonly used in two-phase flow studies are those proposed by McAdams et al. (1942), Cicchitti et al. (1960) and Dukler (1964), as discussed by Carey (1992). These models consider that the mixture viscosity decreases between the value of saturated liquid viscosity to that of the saturated vapor viscosity as the mixture quality increases. However, some experimental data (Hayward, 1961, Zeidan et al., 1990) demonstrates that the mixture viscosity increases with respect to the viscosity of the liquid at low vapor concentrations (i.e. small qualities). Models for such variation are presented in Chamniprasart (1992) and they are attributed to Einstein (1906), Jeffery (1922) and Taylor (1932). According to these theoretical models, when the suspension (gaseous phase) is so diluted that the distances between contiguous particles are large compared with their dimensions (low vapor concentration), the presence of the disperse particles induces an excess of the rate of dissipation of energy over that which occur if the particles were removed and their space is filled with the base fluid. The increase in mixture viscosity is a result of this excess of energy dissipation.

These models state that the rise in viscosity is a function of mixture volume concentration and of the ratio of vapor-to-liquid viscosity. In order to include this effect in the proposed two-phase flow model a piece-wise continuous expression for mixture

viscosity is defined. Taylor's model is used for concentrations up to 30% in volume (void fraction $\Psi=0.3$). For higher mixture compositions the expression proposed by McAdams has been adapted to account for the variation of viscosity between its maximum value at $\Psi=0.3$ and the value for vapor ($\Psi=1$).

$$\frac{\mu}{\mu_l} = 1 + 2.5\left(\frac{n+0.4}{n+1}\right)\Psi \quad ; \quad n = \frac{\mu_g}{\mu_l} \qquad \textit{for} \quad \Psi \leq 0.3$$

$$\frac{1}{\mu} = \left[\left(\frac{\lambda_+}{\mu_g} - \frac{1}{\mu_+}\right) + \left(\frac{1}{\mu_+} - \frac{1}{\mu_g}\right)\lambda\right]\frac{1}{\lambda_+ - 1} \qquad \textit{for} \quad \Psi > 0.3 \tag{15}$$

where λ_+ and μ_+ are the quality and mixture viscosity at void fraction $\Psi=0.3$, given by:

$$\lambda_+ = \frac{0.3}{0.3 + 0.7\dfrac{\rho_l}{\rho_g}} \quad ; \quad \mu_+ = \frac{1.3\mu_l^2 + 1.75\mu_l\mu_g}{\mu_l + \mu_g} \tag{16}$$

For a homogeneous mixture, quality and void fraction are related by:

$$\lambda = \frac{\Psi}{\Psi + (1-\Psi)\dfrac{\rho_l}{\rho_g}} \quad ; \quad \Psi = \frac{\lambda}{\lambda + (1-\lambda)\dfrac{\rho_g}{\rho_l}} \tag{17}$$

The variation of mixture density and viscosity with mixture quality are presented in Figure 4 for oxygen at a pressure of 1.8 MPa ($T_{sat}=130.58$ °K). Density and viscosity are presented in dimensionless form, i.e. normalized with respect to the supply conditions given for the LOX example in Hughes (1987), (2.79 MPa and 139 °K) with $\rho_*=825.4$ kg/m^3, $\mu_*=62.94\mu$Pa-s .

Mixture Viscosity and Density
μ^*=62.94 mPa-s, ρ^*=825.4 kg/m^3
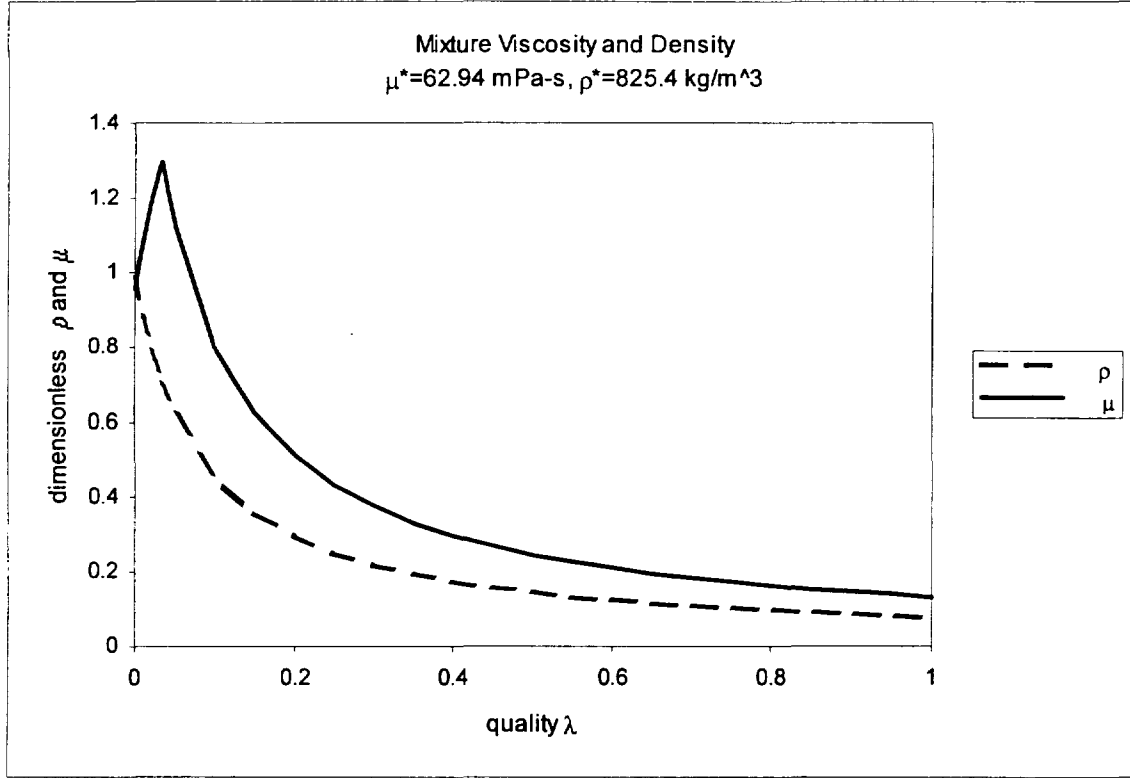
Figure 4. Variation of dimensionless mixture viscosity and density with quality for liquid oxygen (LOX) at P= 1.8 MPa (T_{sat}=130.58 °K).

4.6 Flow governing equations in dimensionless form

With the model's closure provided by the shear stress and boundary conditions expressions, the bulk-flow governing equations (1-4) can be expressed in dimensionless form by introducing the dimensionless coordinates and variables defined in the Nomenclature.

Continuity

$$\sigma\frac{\partial(\bar{\rho}h)}{\partial \tau} + \frac{\partial(\bar{\rho}hu)}{\partial x} + \frac{\partial(\bar{\rho}hv)}{\partial y} = 0 \tag{18}$$

Circumferential Momentum

$$\text{Re}_p^*\left[\sigma\frac{\partial(\bar{\rho}hu)}{\partial \tau} + \frac{\partial(\bar{\rho}hu^2)}{\partial x} + \frac{\partial(\bar{\rho}huv)}{\partial y}\right] = -h\frac{\partial p}{\partial x} - \frac{\bar{\mu}}{h}\left(k_x u - k_r \frac{\Lambda}{2}\right) \tag{19}$$

Axial Momentum

$$\mathrm{Re}_p^*\left[\sigma\frac{\partial(\bar{\rho}hv)}{\partial\tau}+\frac{\partial(\bar{\rho}huv)}{\partial x}+\frac{\partial(\bar{\rho}hv^2)}{\partial y}\right]=-h\frac{\partial p}{\partial y}-\frac{\bar{\mu}}{h}\left(k_y v\right) \tag{20}$$

Energy

$$\mathrm{Re}_p^*\,E_I\left[\sigma\frac{\partial(\bar{\rho}h\bar{i})}{\partial\tau}+\frac{\partial(\bar{\rho}hu\bar{i})}{\partial x}+\frac{\partial(\bar{\rho}hv\bar{i})}{\partial y}\right]=\sigma\frac{\partial p}{\partial\tau}+\left(u+\frac{\Lambda}{2}\right)h\frac{\partial p}{\partial x}+vh\frac{\partial p}{\partial y}$$

$$+\frac{\bar{\mu}}{h}\left[\left(u^2+v^2+\frac{u\Lambda}{2}\right)k_x+\left(\frac{\Lambda^2}{4}-u\Lambda\right)k_r\right]$$

$$\tag{21}$$

where Re_p^* denotes the relation between inertia and viscous forces, i.e. is a typical advection flow Reynolds number, and $\mathrm{Re}_S=\mathrm{Re}_p^*\sigma$ is typical squeeze film Reynolds number based on a characteristic whirl frequency (ω). E_I is a dimensionless parameter relating characteristic enthalpy and the square of fluid characteristic velocity. The rest of dimensionless flow parameters are defined in the Nomenclature.

5. SOLUTION OF THE FLOW GOVERNING EQUATIONS FOR TWO-PHASE SEALS

A dynamic perturbation on the film thickness for small amplitude rotor motions (e_X, e_Y) of frequency ω about the seal concentric position is needed to determine the dynamic forced response of the seal, leading to sets of zeroth and first order bulk-flow equations. Solution of the zeroth order equation provides the seal static characteristics such as leakage, drag torque, and velocity, pressure, temperature and mixture composition fields within the seal. Numerical integration of the first order pressure field provides the rotordynamic force coefficients. A concentric seal operation is assumed not only as a first stage in the process of increasing understanding of two-phase flow in annular pressure seals, but also because externally pressurized bearings show force coefficients with little dependency on rotor eccentricity.

The small amplitude rotor harmonic motion assumption allows the film thickness and the flow variables to be expressed as a superposition of a zeroth and first order fields representing the steady state and the dynamic components, respectively, i.e.,

$$h = h_o + \epsilon_\alpha \, h_\alpha e^{i\omega t} \quad ; \quad i = \sqrt{-1}$$

$$\Phi = \Phi_o + \epsilon_\alpha \, \Phi_\alpha e^{i\omega t}$$

(22)

where α represents the direction of the rotor motion (X,Y) as shown in Figure 1 - Theoretical model section. The dimensionless film thickness (h_o) is generally a function of the axial coordinate (y), and $h_X=\cos\theta$, $h_Y=\sin\theta$. Φ_α represents the perturbation of the given flow variable (velocity, pressure, enthalpy, density, viscosity) due to changes of the rotor position.

Introducing these perturbed flow variables into the dimensionless governing equations, equations 18 through 21, renders the zeroth and first order sets of equations given below. Note that no variation of the zeroth order flow variables in the circumferential direction occurs since concentric rotor operation within the cylindrical seal is assumed.

5.1 Dimensionless zeroth order equations for centered operation

<u>Continuity</u>

$$\frac{d}{d\bar{y}}(\bar{\rho}_o h_o v_o) = 0 \tag{23}$$

<u>Circumferential Momentum</u>

$$\text{Re}_p^* \frac{d(\bar{\rho}_o h_o u_o v_o)}{d\bar{y}} = -\frac{\bar{\mu}_o}{h_o}\left(k_{xo} u_o - k_{ro} \frac{\Lambda}{2}\right) \tag{24}$$

<u>Axial Momentum</u>

$$\text{Re}_p^* \frac{d(\bar{\rho}_o h_o v_o^2)}{d\bar{y}} = -h_o \frac{dp_o}{d\bar{y}} - \frac{\bar{\mu}_o}{h_o}\left(k_{yo} v_o\right) \tag{25}$$

<u>Energy</u> (adiabatic)

$$\text{Re}_p^* E_I \frac{d(\bar{\rho}_o h_o v_o \bar{i}_o)}{d\bar{y}} = h_o v_o \frac{dp_o}{d\bar{y}} + \frac{\bar{\mu}_o}{h_o}\left[\left(u_o^2 + v_o^2 + \frac{u_o \Lambda}{2}\right)k_{xo} + \left(\frac{\Lambda^2}{4} - u_o \Lambda\right)k_{ro}\right] \tag{26}$$

The boundary conditions for these equations are the same as those given by equations (7) through (10), which in dimensionless form are :

At seal inlet ($\bar{y} = 0$):

$$p_i = 1 - \frac{(1+\xi)}{2} \text{Re}_p^{*} \, \bar{\rho}_i \, v_i^2 \tag{27}$$

$$\bar{i}_i = 1 - \frac{(1+\xi)}{2} \frac{v_i^2}{E_i} \tag{28}$$

$$u = \alpha \Lambda \tag{29}$$

Seal exit (subsonic flow):

$$p_{(\bar{y}=L/R)} = 0 \tag{30}$$

5.2 Dimensionless first order equations for centered seal

Continuity

$$i\sigma \, (\bar{\rho}_o h_\alpha + h_o \bar{\rho}_\alpha) + \frac{\partial}{\partial \theta}\left(\bar{\rho}_o h_o u_\alpha + \bar{\rho}_o u_o h_\alpha + h_o u_o \bar{\rho}_\alpha\right)$$

$$+ \frac{\partial}{\partial \bar{y}}\left(\bar{\rho}_o h_o v_\alpha + \bar{\rho}_o v_o h_\alpha + h_o v_o \bar{\rho}_\alpha\right) = 0 \tag{31}$$

Circumferential Momentum

$$\text{Re}_p^{*}\left[\frac{\partial}{\partial \theta}(\bar{\rho}_o h_o u_o u_\alpha) + \frac{\partial}{\partial \bar{y}}(\bar{\rho}_o h_o v_o u_\alpha)\right] = \left(\Gamma_{uu} - i\sigma \text{Re}_p^{*} \, \bar{\rho}_o h_o\right)u_\alpha + \Gamma_{uv}v_\alpha + \Gamma_{uh}h_\alpha$$

$$+ \Gamma_{u\mu}\bar{\mu}_\alpha + \Gamma_{up}\bar{p}_\alpha - h_o \frac{\partial p_\alpha}{\partial \theta} \tag{32}$$

Axial Momentum

$$\text{Re}_p^{*}\left[\frac{\partial}{\partial \theta}(\bar{\rho}_o h_o u_o v_\alpha) + \frac{\partial}{\partial \bar{y}}(\bar{\rho}_o h_o v_o v_\alpha)\right] = \left(\Gamma_{vv} - i\sigma \text{Re}_p^{*} \, \bar{\rho}_o h_o\right)v_\alpha + \Gamma_{vu}u_\alpha + \Gamma_{vh}h_\alpha$$

$$+ \Gamma_{v\mu}\bar{\mu}_\alpha + \Gamma_{vp}\bar{p}_\alpha - h_o \frac{\partial p_\alpha}{\partial \bar{y}} \tag{33}$$

Energy

$$\text{Re}_p^* E_I \left[\frac{\partial}{\partial \theta}(\bar{\rho}_o h_o u_o \bar{i}_\alpha) + \frac{\partial}{\partial \bar{y}}(\bar{\rho}_o h_o v_o \bar{i}_\alpha) \right] = -i\sigma \text{Re}_p^* E_I \bar{\rho}_o h_o i_\alpha + i\sigma \bar{\rho}_o h_o p_\alpha + \Gamma_{iv} v_{\alpha\alpha}$$

$$+ \Gamma_{iu} u + \Gamma_{ih} h_\alpha + \Gamma_{i\mu} \bar{\mu}_\alpha + \Gamma_{i\rho} \bar{\rho}_\alpha \qquad (34)$$

$$+ \left(u_o + \frac{\Lambda}{2} \right) h_o \frac{\partial p_\alpha}{\partial \theta} + v_o h_o \frac{\partial p_\alpha}{\partial \bar{y}}$$

The coefficients Γ_{ij}, defined as functions of the zeroth order flow fields and shear stresses, are given in Appendix 1.

In the equations above, the coefficients of the first order flow variables are not functions of the circumferential coordinate (θ) and the flow variables must satisfy periodicity in the circumferential direction. Thus, the perturbed flow variables are expressed in terms of sine and cosine functions.

$$\text{Say for,} \qquad h_\alpha = h_\chi = \cos\theta$$

$$\text{then,} \qquad \Phi_\alpha = \Phi_{\alpha c} \cos\theta + \Phi_{\alpha s} \sin\theta \qquad (35)$$

where $\Phi_\alpha = f(\bar{y})$ represents any given perturbed variable (velocity, pressure, enthalpy, density, etc) as varying along the axial coordinate only. Thus the first order governing equations can be rewritten in terms of harmonic components as:

Continuity:

$$i\sigma (\bar{\rho}_o + h_o \bar{\rho}_{\alpha c}) + \bar{\rho}_o h_o u_{\alpha s} + h_o u_o \bar{\rho}_{\alpha s} + \frac{d}{dy}\left(\bar{\rho}_o h_o v_{\alpha c} + \bar{\rho}_o v_o + h_o v_o \bar{\rho}_{\alpha c}\right) = 0$$

$$(36)$$

$$i\sigma h_o \bar{\rho}_{\alpha s} - \bar{\rho}_o u_o + \bar{\rho}_o h_o u_{\alpha c} - h_o u_o \bar{\rho}_{\alpha c} + \frac{d}{dy}\left(\bar{\rho}_o h_o v_{\alpha s} + h_o v_o \bar{\rho}_{\alpha s}\right) = 0$$

Circumferential Momentum:

$$\operatorname{Re}_p^* \frac{d}{d\bar{y}}(\bar{\rho}_o h_o v_o u_{\alpha c}) + \operatorname{Re}_p^* \bar{\rho}_o h_o u_o u_{\alpha s} = \left(\Gamma_{uu} - i\sigma \operatorname{Re}_p^* \bar{\rho}_o h_o\right) u_{\alpha c} + \Gamma_{uv} v_{\alpha c} + \Gamma_{uh} + \Gamma_{u\mu} \bar{\mu}_{\alpha c}$$

$$+ \Gamma_{u\rho} \bar{\rho}_{\alpha c} + h_o p_{\alpha s}$$

$$\operatorname{Re}_p^* \frac{d}{d\bar{y}}(\bar{\rho}_o h_o v_o u_{\alpha s}) - \operatorname{Re}_p^* \bar{\rho}_o h_o u_o u_{\alpha c} = \left(\Gamma_{uu} - i\sigma \operatorname{Re}_p^* \bar{\rho}_o h_o\right) u_{\alpha s} + \Gamma_{uv} v_{\alpha s} + \Gamma_{u\mu} \bar{\mu}_{\alpha s}$$

$$+ \Gamma_{u\rho} \bar{\rho}_{\alpha s} - h_o p_{\alpha c}$$

(37)

Axial Momentum:

$$\operatorname{Re}_p^* \frac{d}{d\bar{y}}(\bar{\rho}_o h_o v_o v_{\alpha c}) + \operatorname{Re}_p^* \bar{\rho}_o h_o u_o v_{\alpha s} = \left(\Gamma_{vv} - i\sigma \operatorname{Re}_p^* \bar{\rho}_o h_o\right) v_{\alpha c} + \Gamma_{vu} u_{\alpha c} + \Gamma_{vh} + \Gamma_{v\mu} \bar{\mu}_{\alpha c}$$

$$+ \Gamma_{v\rho} \bar{\rho}_{\alpha c} - h_o \frac{dp_{\alpha c}}{d\bar{y}}$$

$$\operatorname{Re}_p^* \frac{d}{d\bar{y}}(\bar{\rho}_o h_o v_o v_{\alpha s}) - \operatorname{Re}_p^* \bar{\rho}_o h_o u_o v_{\alpha c} = \left(\Gamma_{vv} - i\sigma \operatorname{Re}_p^* \bar{\rho}_o h_o\right) v_{\alpha s} + \Gamma_{vu} u_{\alpha s} + \Gamma_{v\mu} \bar{\mu}_{\alpha s}$$

$$+ \Gamma_{v\rho} \bar{\rho}_{\alpha s} - h_o \frac{dp_{\alpha s}}{d\bar{y}}$$

(38)

Energy:

$$\operatorname{Re}_p^* E_I \frac{d}{d\bar{y}}(\bar{\rho}_o h_o v_o i_{\alpha c}) + \operatorname{Re}_p^* E_I \bar{\rho}_o h_o u_o i_{\alpha s} = -i\sigma \operatorname{Re}_p^* E_I \bar{\rho}_o h_o i_{\alpha c} + i\sigma \bar{\rho}_o h_o p_{\alpha c} + \Gamma_{iv} v_{\alpha c} + \Gamma_{iu} u_{\alpha c} + \Gamma_{ih}$$

$$+ \Gamma_{i\mu} \bar{\mu}_{\alpha c} + \Gamma_{i\rho} \bar{\rho}_{\alpha c} + \left(u_o + \frac{\Lambda}{2}\right) h_o p_{\alpha s} + v_o h_o \frac{\partial p_{\alpha c}}{\partial \bar{y}}$$

(39)

$$\operatorname{Re}_p^* E_I \frac{d}{d\bar{y}}(\bar{\rho}_o h_o v_o i_{\alpha s}) - \operatorname{Re}_p^* E_I \bar{\rho}_o h_o u_o i_{\alpha c} = -i\sigma \operatorname{Re}_p^* E_I \bar{\rho}_o h_o i_{\alpha s} + i\sigma \bar{\rho}_o h_o p_{\alpha s} + \Gamma_{iv} v_{\alpha s} + \Gamma_{iu} u_{\alpha s}$$

$$+ \Gamma_{i\mu} \bar{\mu}_{\alpha s} + \Gamma_{i\rho} \bar{\rho}_{\alpha s} - \left(u_o + \frac{\Lambda}{2}\right) h_o p_{\alpha c} + v_o h_o \frac{\partial p_{\alpha s}}{\partial \bar{y}}$$

The perturbed fluid properties are determined considering that they are functions of the perturbed pressure and enthalpy, i.e.

$$\overline{\rho}_{\alpha k} = \left(\frac{\partial \overline{\rho}}{\partial p}\right)_{T_o} p_{\alpha k} + \left(\frac{\partial \overline{\rho}}{\partial \overline{i}}\right)_{P_o} \overline{i}_{\alpha k}$$

$$\overline{\mu}_{\alpha k} = \left(\frac{\partial \overline{\mu}}{\partial p}\right)_{T_o} p_{\alpha k} + \left(\frac{\partial \overline{\mu}}{\partial \overline{i}}\right)_{P_o} \overline{i}_{\alpha k}$$

(40)

The boundary conditions for the first order equations are obtained by perturbing

the expressions for entrance and discharge conditions given in section 4.3.

Entrance Conditions:

$$p_{i\alpha c} = -\frac{(1+\xi)}{2}\text{Re}_p^{\bullet}\left[2\overline{\rho}_o v_o v_{i\alpha c} + v_o^2 \overline{\rho}_{i\alpha c}\right]$$

(41)

$$p_{i\alpha s} = -\frac{(1+\xi)}{2}\text{Re}_p^{\bullet}\left[2\overline{\rho}_o v_o v_{i\alpha s} + v_o^2 \overline{\rho}_{i\alpha s}\right]$$

(42)

$$\overline{i}_{i\alpha c} = -\frac{(1+\xi)}{2}\frac{2v_o}{E_I}v_{i\alpha c}$$

(43)

$$\overline{i}_{i\alpha s} = -\frac{(1+\xi)}{2}\frac{2v_o}{E_I}v_{i\alpha s}$$

(44)

$$u_{i\alpha c} = u_{i\alpha s} = 0$$

(45)

Exit Condition: ($\overline{y}$ = L/R, unchoked flow)

$$p_{\alpha c} = p_{\alpha s} = 0$$

(46)

In summary, a bulk-flow model to predict the static and dynamic characteristics

of annular pressure seals working with a real properties fluids has been developed. Flow

turbulence is accounted for through the use of turbulent shear stress parameters and

Moody's friction factors. Two-phase flow conditions within the seal are modeled as a

homogeneous mixture in thermodynamic equilibrium and with fluid based in the mixture quality. The rotordynamic force coefficients are obtained from the integration of the first order pressure field by means of the following expression.

$$K_{\alpha\beta} + i\omega C_{\alpha\beta} = -\frac{(P_s - P_a)R^2}{c} \int_0^{L/R} \int_0^{2\pi} p_\beta h_\alpha \, d\theta \, d\bar{y} \tag{47}$$

where $\alpha, \beta = X, Y$, and the perturbed pressure(p_β) and film thickness (h_α) are as defined in equation 35. For concentric operation, equation (47a) further reduces to:

$$\begin{Bmatrix} K_{XX} + i\omega C_{XX} \\ K_{XY} + i\omega C_{XY} \end{Bmatrix} = -\frac{(P_s - P_a)R^2}{c} \pi \int_0^{L/R} \begin{Bmatrix} p_c \\ p_s \end{Bmatrix} d\bar{y} \tag{48}$$

Additionally, for concentric seal operation, $K_{XX} = K_{YY}$, $K_{XY} = -K_{YX}$, $C_{XX} = C_{YY}$, $C_{XY} = -C_{YX}$.

The impedances, force-to-rotor displacement ratios, given in equations (47) and (48) do not follow the usual model presented in the Introduction (section 1) with constant stiffness, damping and added mass rotordynamic coefficients. For compressible fluids and flow-mixtures, both stiffness and damping are functions of the excitation frequency ω.

6. NUMERICAL IMPLEMENTATION

6.1 Numerical solution of the zeroth order equations

The numerical solution of the governing equations is obtained using the SIMPLEC finite difference scheme of Van Doormal and Raithby (1984). The accuracy and effectiveness of this approach on solving the inertia dominated turbulent flow equations for thin fluid film bearings used in cryogenic turbomachinery has been demonstrated by the good agreement between predictions and experiments shown in San Andres (1992, 1996), Yang (1992), Yang et al. (1993b) for liquid-hybrid journal bearings and seals.

The fluid flow domain within the seal is divided into a series of staggered rectangular control volumes for the different flow variables, as shown in Figure 5. The most important characteristic of this finite difference approach is the used of staggered grids for velocities, pressure and enthalpy (or temperature), where the velocity nodes lie at the interfaces midway between pressure nodes. Thus, the pressure difference between adjacent nodes becomes the natural driving force for the velocity component at the interface (Patankar, 1980).

The flow governing partial differential equations are integrated over these finite control volumes to render a set of non-linear algebraic difference equations with local mass conservation. The resulting equations are further simplified by means of two considerations. First, since the seal is assumed to operate concentric within the stator, the bulk flow can be considered as axi-symmetric, i.e. the flow variables do not change in the circumferential direction even though the velocity of the fluid in that direction is different

from zero. Thus, all the primitive flow variables vary only in the axial direction. Second, the large pressure drop characteristic of annular pressure seals, makes the flow axially dominant and prevents any bulk flow reversals. Thus, the transport of momentum and energy from the downstream control volume is unimportant. With these considerations, the discrete difference equations have the following general form

$$A^P \Phi^P = A^S \Phi^S + S^P \qquad \qquad (49)$$

where Φ represents one of the fluid velocities, or the fluid enthalpy. A^P and A^S are the coefficients for the current (P) and the upstream (S) control volumes, respectively. S^P is the source term evaluated at the current control volume
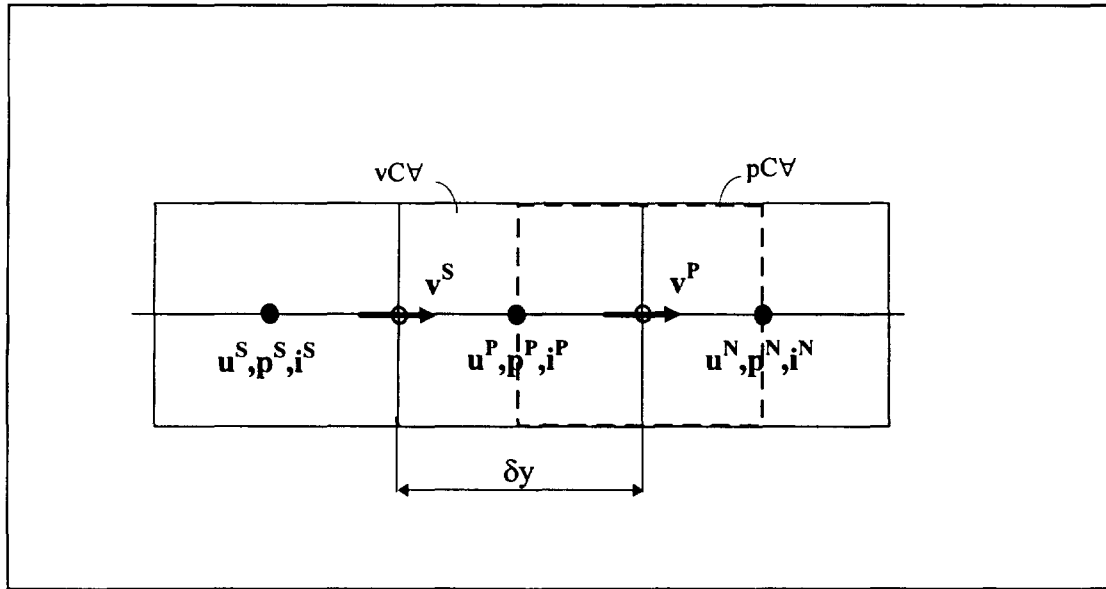

Figure 5. Schematic diagram of staggered grid sand control volumes used.

The contribution of the downstream control volume cannot be neglected in the pressure correction equation (derived from mass conservation) which is given by an expression of the form:

$$- A^N p^N + A^P p^P - A^S p^S = S^P \tag{50}$$

where the superscript N denotes conditions downstream form the current grid point. The discrete difference equations for momentum, energy and pressure are given in Appendix 2.

The numerical algorithm consists of a series of estimation-and-corrections steps to solve the difference governing equations. A guessed or initial pressure field is used to estimate velocities satisfying the momentum equations. Next, the energy equation is solved for fluid enthalpy which is then used to determine the fluid temperature or mixture quality, depending on whether single or two-phase flow conditions prevail at the control volume. A pressure correction field is calculated by enforcing mass conservation, and rectifications for the velocities are calculated as functions of these pressure corrections. A fluid density correction step is added to improve convergence when the fluid is very compressible. Fluid properties are updated and velocities are corrected before repeating the same procedure at the next axial location until the seal exit is reached.

The main steps in the numerical solution procedure are summarized as follows:

1) An initial guess of the flow fields is calculated based on a simplified solution

2) Discretized momentum and energy equations are solved to obtain velocities and fluid enthalpy, respectively.

3) If the fluid pressure is below the critical point, the calculated enthalpy is compared against the corresponding saturated liquid and saturated vapor enthalpies to check for two-phase flow condition. If the enthalpy is between those saturated values the flow is considered as a mixture and its quality is calculated based on the enthalpy. Otherwise the fluid is either a liquid or a gas and then the fluid temperature is calculated based on the current pressure and enthalpy.

4) The pressure corrections are calculated by solving the discretized form of the continuity equation by means of a tri-diagonal matrix solution procedure, TDMA (Patankar, 1980).

5) Velocity corrections are calculated, and the pressure and velocity fields are updated by adding the corresponding correction fields. Fluid properties are updated to account for pressure variations and to account for possible phase change.

6) Steps 2 to 5 are repeated at all axial location until the seal exit plane is reached. The inlet velocities are then obtained by satisfying continuity considerations, and the entrance pressure and enthalpy are calculated according to equations (27) and (28) presented in section 5.

7) The procedure described above is repeated until the global mass residual falls below a predetermined value , typically 0.1% of the inlet flow to the seal.

start

Initial calculations

Fluid Properties
(one or two-phase)

Check for two-phase
flow conditions

T=Tsat, λ=f(i)

λ=0 or 1, T=f(i)

Update fluid properties

Solve for u velocity
v velocity
enthalpy, i

Seal exit ? N

Y

Next
axial
point

Next
itera-
tion

Correct pressure and flow fields

Update fluid properties

Calculate inlet conditions

N Convergence

Y

Calculate static characteristics

Solve for force coefficients
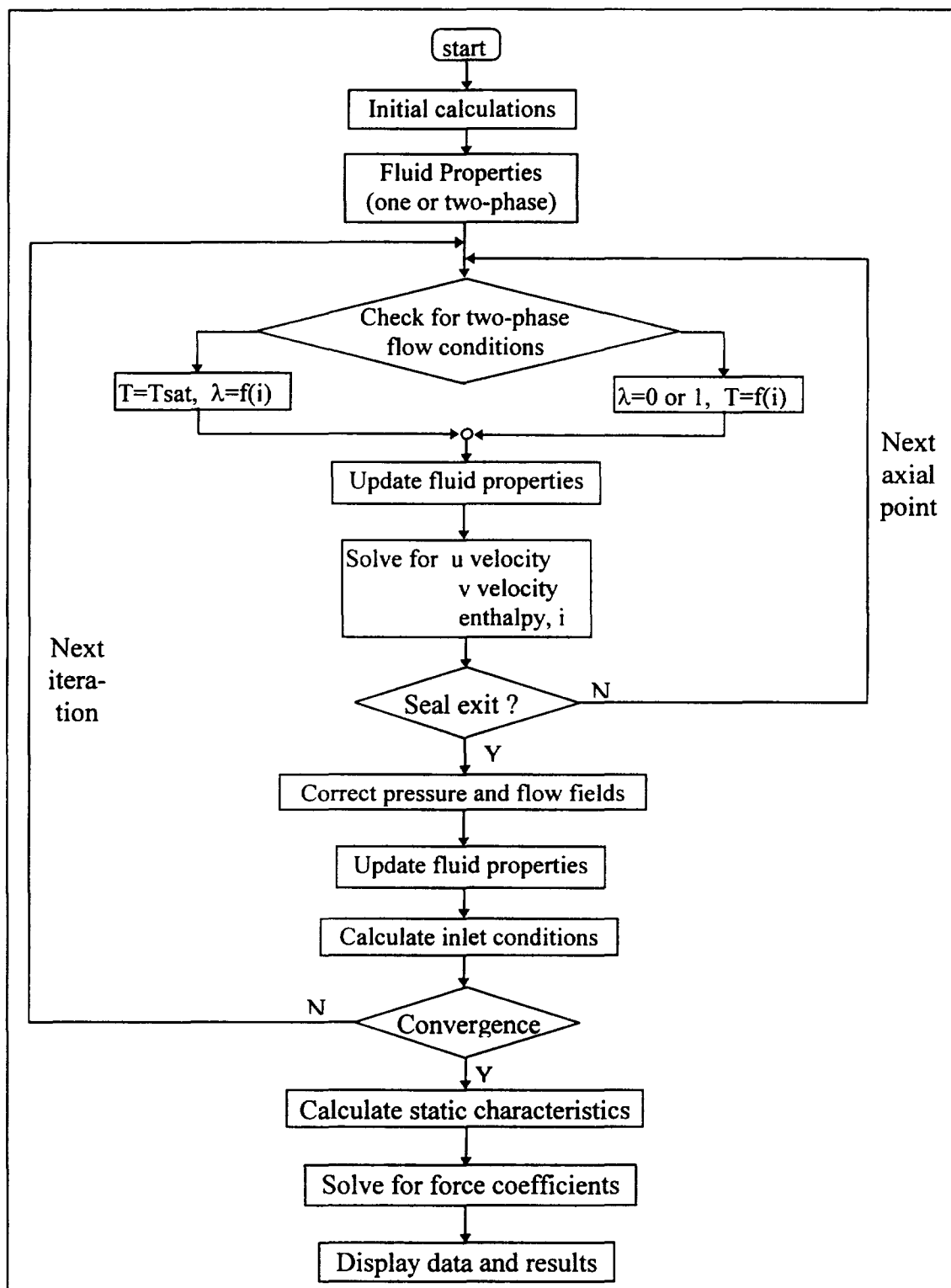
Display data and results

Figure 6. Flow chart illustrating numerical algorithm.

6.2 Numerical solution of the first order equations

Integration of the first order governing equations over the discretized control volumes renders a set of algebraic difference first order equations which have the same form as (49) and (50), with the only difference that the first order variables are expressed as vectors in terms of their harmonic components (cosine and sine), i.e. $\Phi=[\Phi_c ,\Phi_s]^T$ and $p=[p_c , p_s]^T$. The coefficients A's and source terms are, of course, (2x2) matrices. Since the coefficients in these equations are functions of the zeroth order flow variables (already solved) the resulting discrete difference equations are linear. The complete discretized first order equations for momentum, energy and pressure are also presented in Appendix 2.

The computer code developed based on the algorithm presented above is described in the flow chart presented in Figure 6.

6.3 Single phase fluid properties

Fluid properties for the cryogenic fluids (N_2, O_2 and H_2) under single phase conditions are obtained using a NBS database through a computer program named "miprops" (McCarty, 1986). The equilibrium properties are based on a 32-term modified Bennedict-Webb-Rubin (MBWR) equation of state. A series of subroutines provide fluid properties such as enthalpy, entropy, internal energy, viscosity, density, sonic velocity, and saturation conditions using the pairs temperature and density, or temperature and pressure as known inputs. Since fluid enthalpy is used as primitive flow variable instead

of temperature, an iterative method to calculate fluid temperature using known pressure and enthalpy as inputs was developed using the basic routines given in the NBS program.

6.4 Closure

A finite difference scheme based in the SIMPLEC semi-implicit method has been implemented to solve both the zeroth and first order flow equations. Convergence of the solution is achieved when the pressure field has converged and mass conservation is satisfied within a predetermined error margin (0.1%). Fluid film forces and rotordynamic coefficients are obtained by numerical integration of the first order pressure field over the journal surface as given in equations (47) and (48).

Numerous simulations for different seal configurations and working fluids have shown that the numerical algorithm is stable and efficient. A grid independence study shows that the calculation of the static seal characteristics like leakage, drag torque, temperature rise and mixture composition (zeroth order solution) requires very few grid points to achieve a grid independent solution. When the mesh is refined from a 14 node grid to a 28 node grid the maximum variation of the static seal parameters is 1.3%. If the grid is further refined to 56 nodes the maximum variation is 0.52%. Thus for the simulations requiring only static seal characteristics a mesh with 14 nodes along the seal length has been used. The rotordynamic force coefficients are quite sensitive to the extent of the two-phase region which (of course) is dependent on the grid distribution. The finer the mesh, the more accurate prediction of the two-phase region extent. Thus, under two-phase flow conditions the maximum variation of the rotordynamic coefficients when

comparing results from a 14 node and a 28 node grid is about 8%, and when the mesh is

further refined to 56 nodes the variation is about 4%. Although these values are higher

than those for the static seal characteristics they are still the same as observed in similar

codes dealing with gaseous annular seals (Yang et al., 1993a). The predictions for seal

rotordynamic force coefficients presented in the current analysis are based on a 28 node

mesh.

The comparisons with existing experimental and theoretical data presented in the

next section verify the accuracy and reliability of the model.

7. THEORETICAL PREDICTIONS AND DISCUSSION

This section presents theoretical predictions for the static and dynamic forced response of damper seals used in cryogenic turbomachinery and working under two-phase flow conditions. First, theoretical predictions are compared to experimental results for straight cylindrical seals with liquid nitrogen (LN2) (Hendricks, 1987). The validity of the model, at least for the static characteristics, is confirmed through these comparisons. Second, a parametric study of the seal static characteristics is performed on a configuration similar to the damper seal designed for the High Pressure Oxygen Turbopump (HPOTP) of the Space Shuttle Main Engine (SSME). The effect of two-phase flow conditions on these static parameters is studied through this example. Finally, simulations for static and dynamic seal characteristics are carried out for a seal configuration similar to that presented by Beatty and Hughes (1988). The closeness of the supply conditions to the saturation values makes this seal to operate with two-phase flow conditions all along the seal, and therefore renders a good example case to study the effect of two-phase flow on the seal static and dynamic forced response.

7.1 Validation

The scarce experimental data available for thin fluid film bearings used in cryogenic turbomachinery in general, and for their operation near or at two-phase flow conditions in particular, has limited the validation of the proposed model to the seal static conditions. Hendricks (1987) presents experimental results for a straight cylindrical seal

working with liquid and gaseous nitrogen. The seal configuration, similar to the one proposed for the space shuttle main engine oxidizer turbopump (SSME-HPOTP) was tested under non-rotating conditions and for concentric and fully eccentric seal positions. The experimental data includes mass flow rate and pressure profiles for different fluid supply conditions. The seal geometry and operating conditions are given in Table 2. A schematic view of the seal geometry as well as the locations for pressure readings are shown in Figure 6 (as extracted directly from Hendricks, 1987).

Table 2. Seal geometry and operating conditions for Hendricks seal example.

Diameter, D [m]	0.0842
Length, L [m]	0.0428
Radial Clearance, c [mm]	134.6
rotor and stator roughness	0.0 (smooth)
Rotational Speed [rpm]	0
Supply Pressure [MPa]	1 - 6
Supply temperature [$^{\circ}$K]	85 - 280
Discharge Pressure [MPa]	0.1 - 1.2

Fluid pressure is measured at seven axial locations, six within the seal and one beyond the seal exit, as shown in Figure 7. Predictions from the model are compared with the measurements within the seal, i.e. at locations P1 to P6.
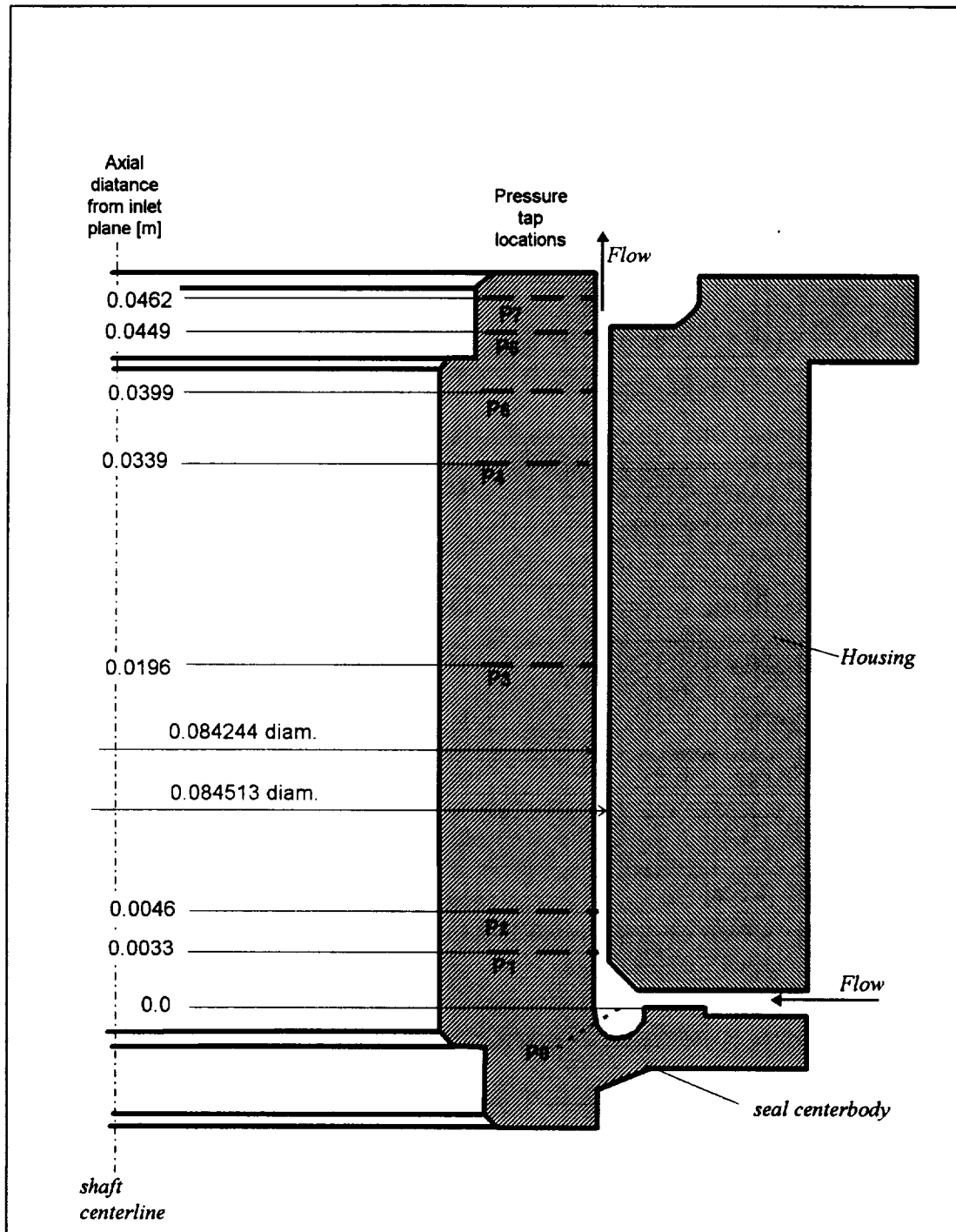
Figure 7. Schematic view of the seal geometry for the Hendricks (1987) example.
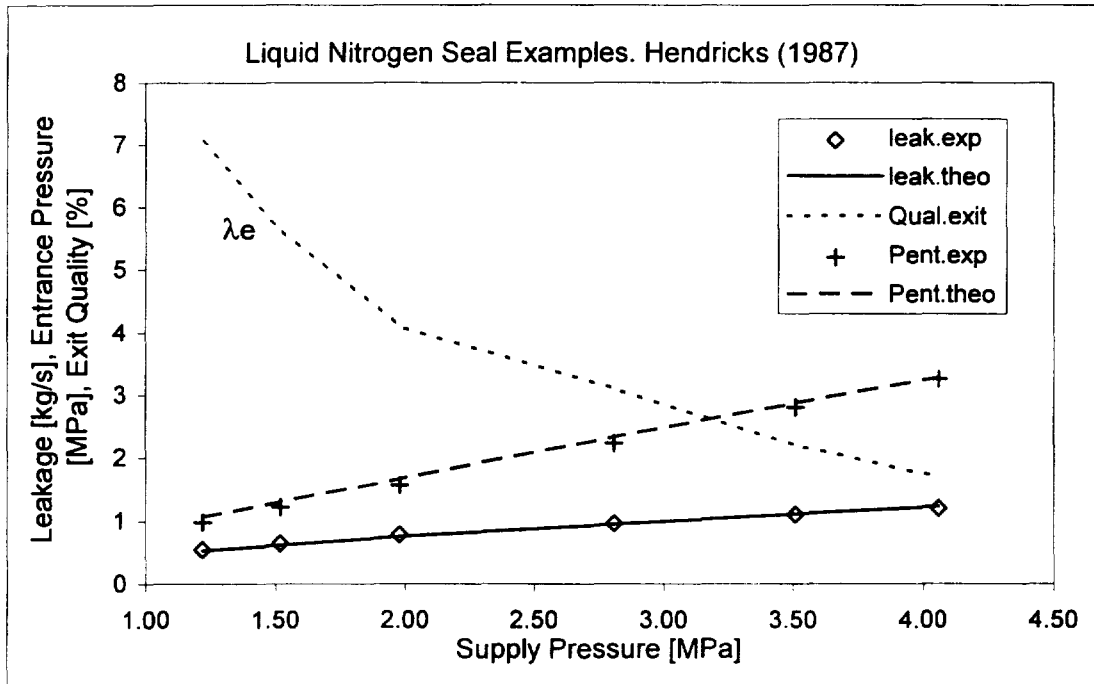
<u>Results</u>

Experimental and theoretical predictions for several cases of liquid and gaseous

nitrogen are presented in Tables 3 and 4. Leakage flow rates and fluid pressure at the seal

entrance (P1) are shown in the tables, along with deviation in percentage between model

predictions and experiments. The predicted exit quality (λ_{exit}) is also presented for the

inlet liquid seal cases. These results are depicted in graphical form in Figure 8 where

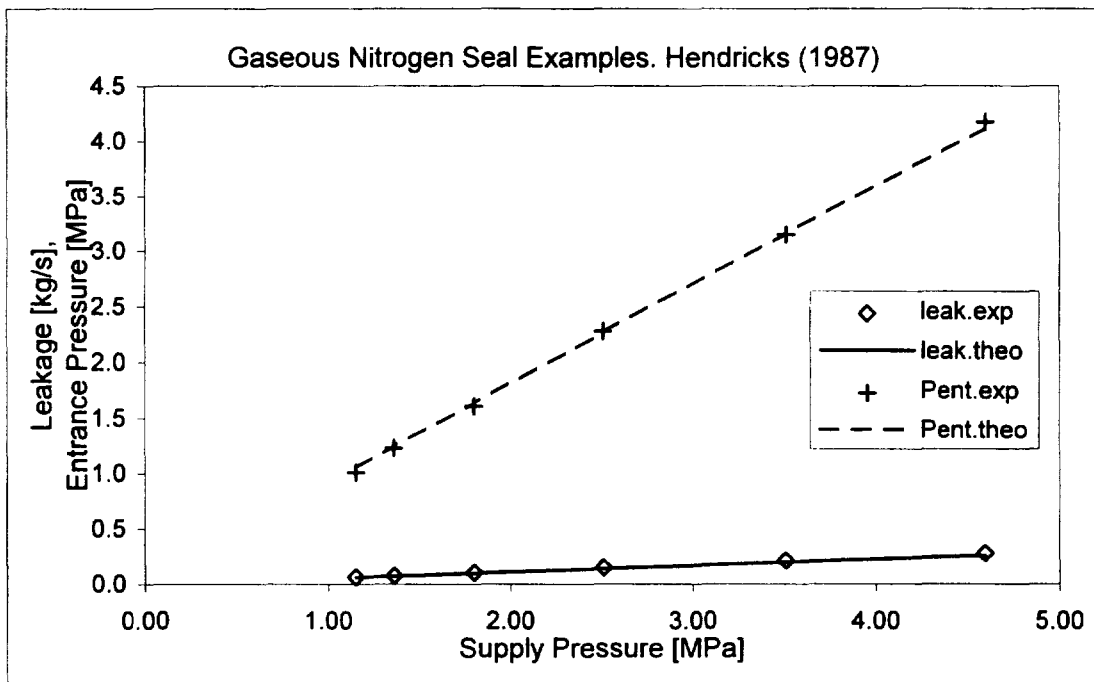symbols represent the experiments and lines denote the theoretical predictions[1].

Table 3. Experimental and theoretical results for liquid nitrogen.

run	P_s [MPa]	T_s [°K]	leakage$_{exp}$ [kg/s]	leakage$_{theo}$ [kg/s]	dev [%]	λ_{exit} [%]	P1$_{exp}$ [MPa]	P1$_{theo}$ [MPa]	dev [%]
592	2.68	89.00	0.943	0.944	0.10	2.40	2.18	2.22	1.83
591	3.33	88.30	1.083	1.085	0.18	2.10	2.71	2.72	0.37
590	3.99	88.00	1.215	1.241	2.14	1.40	3.27	3.20	-2.14
589	4.58	87.90	1.317	1.348	2.35	1.30	3.79	3.65	-3.69
587	4.80	86.90	1.354	1.393	2.88	1.20	3.99	3.81	-4.51
586	4.91	86.70	1.378	1.424	3.34	1.04	4.11	3.88	-5.60
588	5.00	88.20	1.357	1.425	5.01	1.26	4.08	3.96	-2.94
585	5.08	86.40	1.414	1.440	1.84	1.16	4.26	4.03	-5.40
584	5.56	87.50	1.455	1.532	5.29	1.03	4.59	4.37	-4.79
615	1.22	92.30	0.547	0.531	-2.93	7.05	0.98	1.07	9.18
614	1.52	91.10	0.648	0.623	-3.86	5.64	1.22	1.31	7.38
613	1.98	88.90	0.784	0.754	-3.83	4.10	1.57	1.68	7.01
612	2.81	88.80	0.964	0.953	-1.14	3.10	2.23	2.34	4.93
611	3.51	88.50	1.101	1.111	0.91	2.20	2.80	2.87	2.50
610	4.06	88.40	1.200	1.232	2.67	1.70	3.25	3.28	0.92

---

[1] *Table 2 also shows good agreement for runs 584-592. However, the exit quality presents a strange behavior for the points with supply pressure near 5 MPa. This is due to the non-uniform variation of supply temperature in those runs*

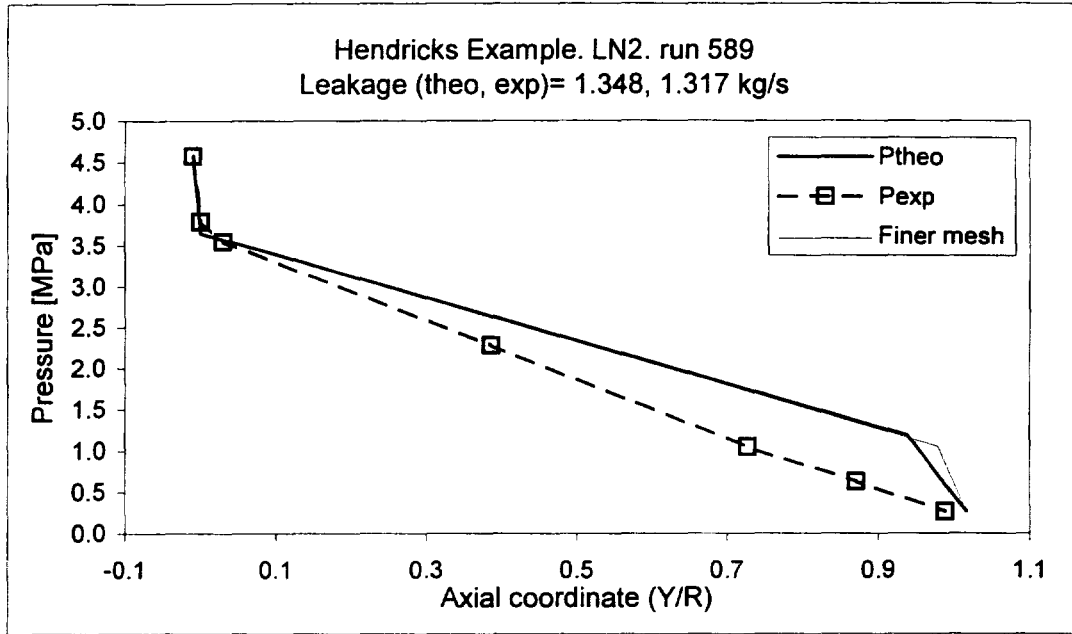**Figure 8.** Comparison of theoretical predictions with experimental results from Hendricks (1987). (a) N2 Liquid Ts~88 K (b) N2 Gaseous Ts~247 K

**Table 4.** Experimental and theoretical results for gaseous nitrogen.

run	P_s [MPa]	T_s [$^\circ$K]	leakage$_{exp}$ [kg/s]	leakage$_{theo}$ [kg/s]	dev [%]	$P1_{exp}$ [MPa]	$P1_{theo}$ [MPa]	dev [%]
533	1.15	239.50	0.064	0.061	-4.38	1.01	1.05	4.36
532	1.36	239.80	0.077	0.074	-4.55	1.23	1.24	1.06
531	1.80	2.39	0.107	0.100	-6.54	1.61	1.64	1.68
530	2.51	245.00	0.150	0.141	-5.80	2.28	2.27	-0.39
529	3.51	254.90	0.213	0.198	-6.90	3.15	3.16	0.29
528	4.60	267.00	0.279	0.258	-7.63	4.17	4.12	-1.20

Comparisons for leakage rate and seal entrance pressure (P1) show that the current theoretical model predicts accurately the static conditions of the seal. Part of the deviations may be attributed to the fact that the experimental values taken as entrance and discharge pressures are slightly inside the seal (as reported by Hendricks, 1987).

Samples of the comparisons for the axial pressure distribution for both liquid and gaseous cases are presented in Figure 9. The agreement between predictions and experiments is very good. The different character of the predicted pressures near the seal exit in the liquid nitrogen case arises from the discretization of the seal flow domain. The model assumes that entire last control volume element of the seal is under two-phase flow conditions when the actual transition from all-liquid to two-phase mixture may take place anywhere between the last two pressure nodes, or even just at the seal exit plane as Hendricks also explains. As the mesh is refined the extent of the two-phase region is predicted more accurately and the shape of the pressure curve approaches to that shown by the experimental results. This is illustrated by the curved shown thin line which represents a solution where the number of nodes in the mesh has been doubled.
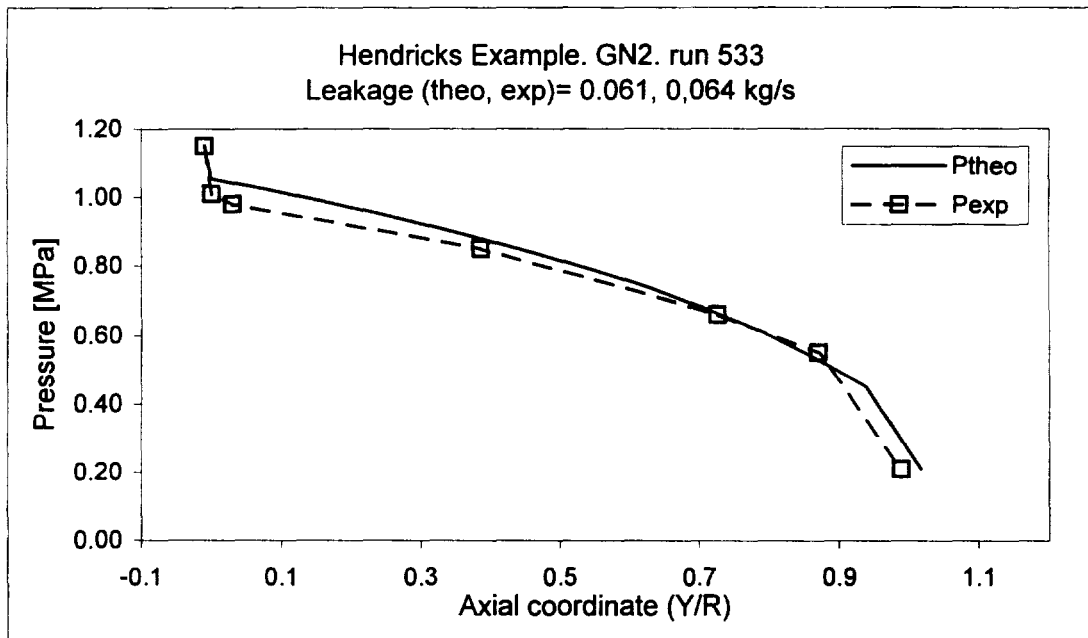
Figure 9. Comparison of theoretical axial pressure drop with experiments from Hendricks (1987). (a) N2 Liquid Ts~88 K (b) N2 Gaseous Ts~239 K.

Recall that due to the continuous drop in pressure across the seal, the discharge or exit plane is the most likely to present two-phase flow conditions, and depending on the supply conditions, the two-phase flow region grows from the exit toward the seal entrance plane. Although a comprehensive treatment of the second law of thermodynamics for mixtures is not available, it has been observed that, as a consequence of the continuos drop of pressure along the seal and the adiabatic character of the flow, the entropy is increasing along the seal in all the cases analyzed.

The theoretical model predicts two-phase flow conditions at the seal discharge for the liquid nitrogen cases as denoted by the values of mixture quality at the exit. This agrees with Hendricks observations that the changes in pressure between seal exit and the point downstream the seal discharge where very similar to those found in two-phase choked flows in long tubes. The increase of the exit quality with decreasing supply pressure is explained by the fact that as the supply pressure is lowered a larger portion of the seal is operating close to saturation conditions and therefore the two-phase flow region is extended. Since the mixture is assumed to be in thermodynamic equilibrium the mixture quality can only increase as it approaches the seal exit. Thus, the larger the two-phase region the higher the mixture quality at the discharge.

In summary, very good agreement exists between the experimental results for the static characteristics of concentric straight seals presented by Hendricks and the predictions from the proposed model. The predictions from the current analysis also show very good agreement with the seal static characteristic predictions presented by Beatty and Hughes (1988) for a liquid oxygen seal operating under two-phase flow conditions.

This provides confidence in the predictions from the current theoretical model when the supply and discharge conditions are known accurately.

7.2 Study of damper seal for the HPOTP-SSME

A parametric study of the static characteristics on a seal configuration similar to the damper seal designed for the High Pressure Oxygen Turbopump (HPOTP) of the Space Shuttle Main Engine (SSME) is presented in this section. No analysis of the rotordynamic force coefficients is presented for this example since the occurrence of two-phase flow conditions is limited to the seal discharge plane. Therefore the effect of two-phase flow on the dynamic response of the damper seal is addressed in detail in the next seal example where two-phase flow conditions are present throughout the entire seal length. The seal stator for the current seal example has a rough surface of the knurled type and comprises of two parallel annular seals of convergent tapered clearance separated by a deep feeding central groove. The seal geometry and operating conditions presented in Tables 5 and 6 have been taken from San Andres (1995). A schematic view of the seal geometry is shown in Figure 10.

Table 5. Damper seal geometry for SSME-HPOTP seal example.

Diameter, D [m]	0.0851
Length, L [m]	0.0222
Inlet Clearance, C_i [μm]	221.3
Exit Clearance, C_e [μm]	129.1
Average Clearance, C [μm]	175.2
Rotor surface relative roughness, r_r/c	0.0 (smooth)
Stator surface relative roughness, r_s/c	0.044 (knurled)
Seal entrance loss coefficient, ξ	0.25
Inlet Swirl Ratio, α	0.5

Table 6. HPOTP-SSME damper seal operating conditions.

Speed [rpm]	P_{supply}, P_s [MPa]	P_{exit}, P_a [MPa]	T_{supply}, T_s [°K]	T_{sat} at P_{exit} [°K]	Average Clearance, c [μm]
14,035	16.00	1.654	102.77	128.9	180.0
26,000	39.60	2.089	110.55	133.7	175.2
30,367	55.69	2.551	115.00	138	173.2
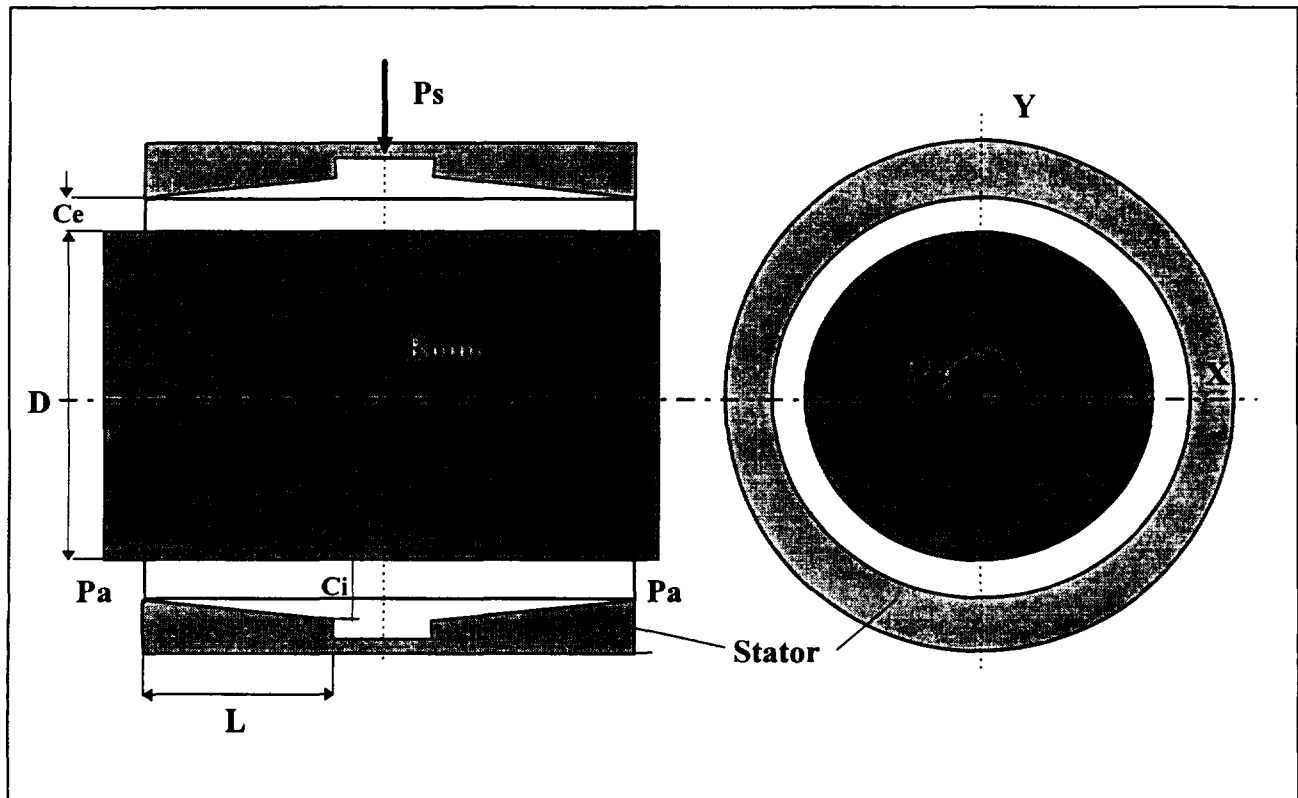
Figure 10. Schematic view of the seal geometry for the HPOTP-SSME seal example.

The stator relative roughness coefficient given in Table 5 does not represent the actual dimensions of the indentations of the knurled surface. Recall that the friction factors are based on a microscopic roughness. The value of 0.044 (r_s/c)chosen for this

seal is an empirical value based on test data for seals with similar surface roughness (Childs, 1993).

The effect of several parameters such as supply conditions (pressure and temperature), seal length, stator roughness and seal entrance loss coefficient on the main static performance characteristics of the parallel seals are studied. The results of interest are leakage or flow rate, drag torque, temperature rise across the seal (T_{exit}-T_s), pressure drop at the seal entrance (P_s-P_{inlet}), and mixture quality at the seal exit if the seal reaches two-phase flow conditions. The numerical predictions are for a seal concentric within its housing.

The total flow rate, torque, temperature rise and pressure drop at the seals entrance for the operating conditions listed above are shown in Figure 11. The agreement of these results with those presented by San Andres (1995) is very good. The results show that as the supply conditions (temperature and in particular pressure) and rotor speed are increased the seal flow rate (leakage) and the drag torque increase accordingly. The extra levels of energy added to the fluid when the supply conditions are raised can be seen also in the increase of temperature across the seal (T_{exit}-T_{supply}).

The pressure drop at the seal inlet (P_s-P_{inlet}), which is instrumental in the magnitude of the seal direct stiffness, also increases as the supply conditions and rotor speed are raised. None of the cases studied approach two-phase flow conditions within the seals.

The average seal clearance was reduced to 84 μm (C_i=99 μm, C_e=69 μm) in order to explore the possibility of two-phase flow conditions occurring within the seals. This radial clearance is still in the range of practical applications (Palazzolo, 1992). A parametric study was then performed on this new configuration. Since the purpose of this study is to explore the conditions under which two-phase flow appears, the case with largest supply pressure (55.69 MPa) and rotor speed (30,367 rpm) presented above is chosen as the base condition. In this case the supply temperature is the closest to the exit saturation condition (138 °K) and it also presents the largest amount of energy dissipated by the fluid as seen from the temperature rise shown in Figure 11.
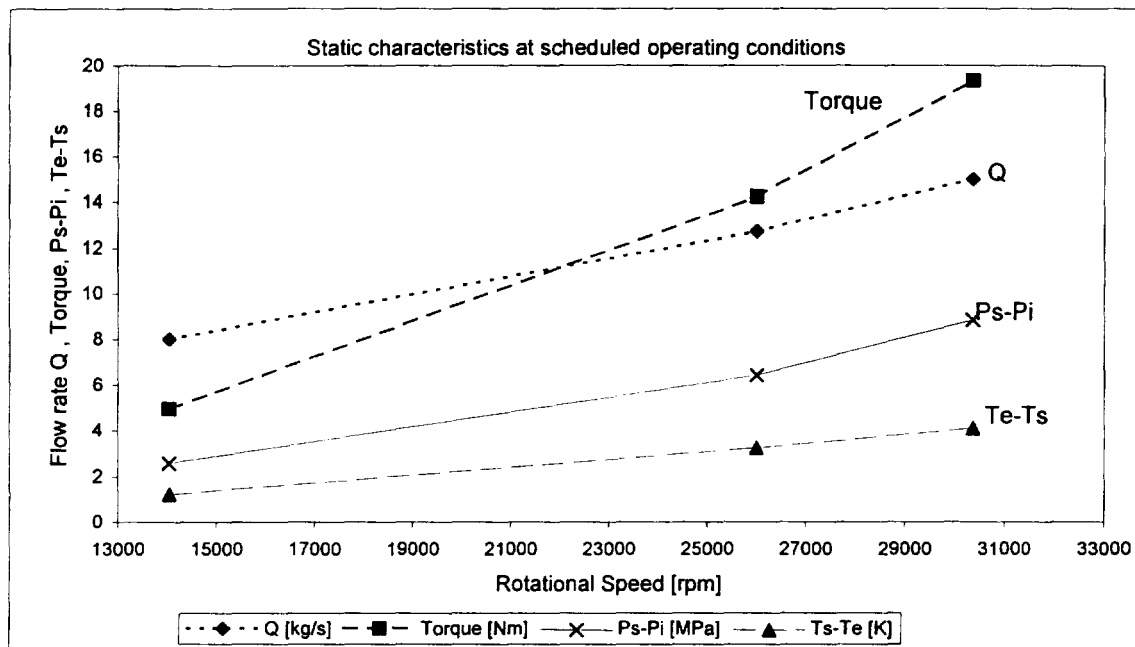
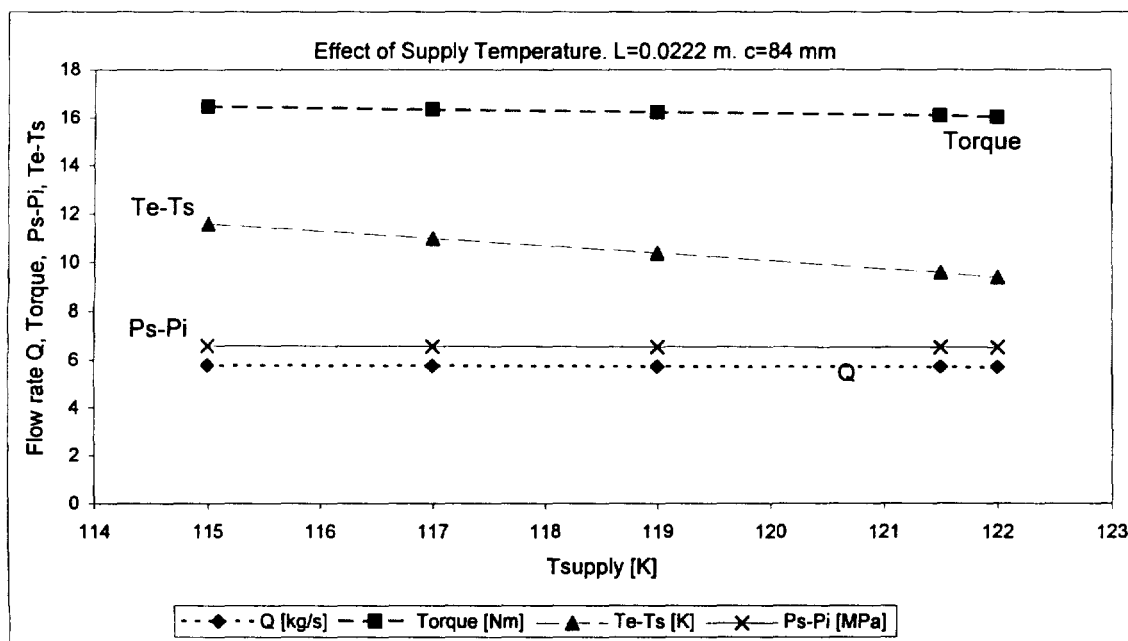**Figure 11.** Static characteristics at scheduled operating conditions for nominal configuration.

Figure 12. Static characteristics for reduced clearance configuration and increasing supply temperature.

Simulations for increasing values of seal length, bearing surface roughness and entrance loss coefficient are performed. For this high rotational speed and supply pressure condition the supply temperature is increased from 115 °K to a value of 122 °K which is the maximum temperature allowed at the boost pump discharge in the SSME HPOTP (Heshmat, 1991).

Effect of supply temperature

Results for leakage, torque, entrance pressure drop and temperature rise across the parallel seals with increasing values of supply temperature are presented in Figure 12. The effect of supply temperature on the static characteristics of the seal is found to be small. Slight reductions on leakage, torque and pressure drop are shown for increasing supply temperature, mainly due to the small change in fluid properties, particularly density. The only noticeable effect can be seen on the temperature rise across the seals. Due to the slight change in fluid properties as the supply temperature is increased the amount of energy supplied to the fluid does not increases at the same rate, and therefore the temperature rise across the seal decreases as shown in the figure. No two-phase flow is predicted for any of these conditions.

Effect of seal length:

The seal length is increased up to approximately three times its original value (L=22.2 cm) seeking to increase the dissipation effects and therefore increase the amount of energy supplied to the fluid. Figures 13a and 13b show the changes in the static parallel seals characteristics with increasing seal length for cases with supply temperature equal to 115 and 122 °K, respectively. Recall that from Figure 12 it was established that this change in supply temperatures had very little effect on the static characteristics of the seal. However, the operating conditions of the seal are brought closer to saturation conditions by increasing the supply temperature. The leakage (Q) and the entrance pressure drop (Ps-Pi) decrease with increasing seal length as a result of the additional resistance to the flow created when the parallel seals are lengthened. This
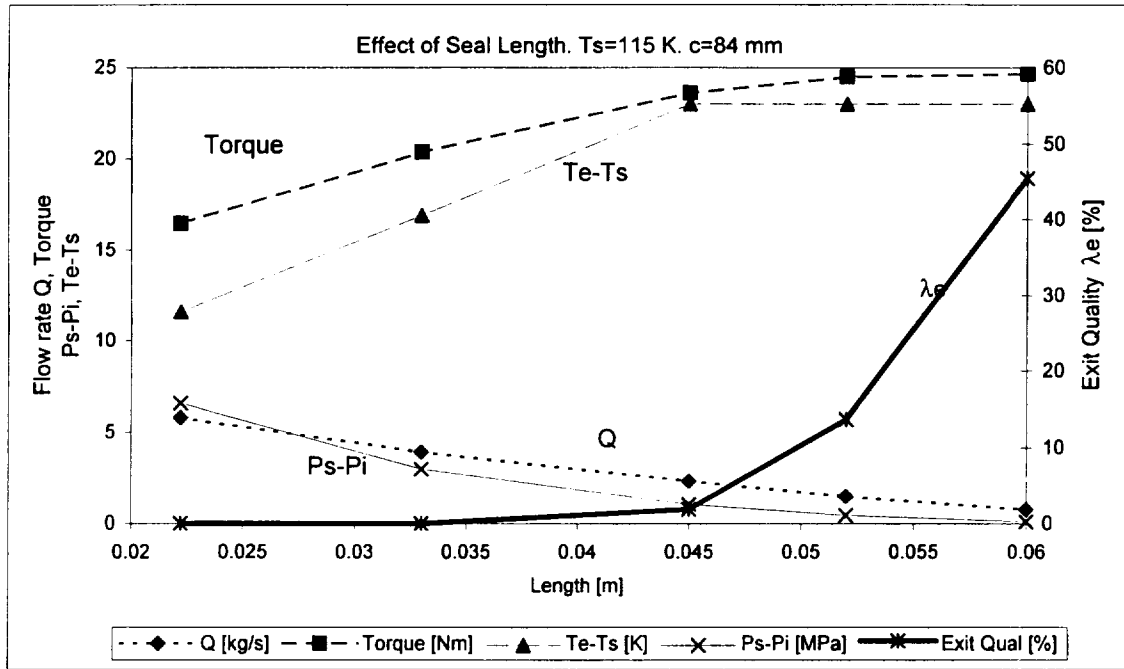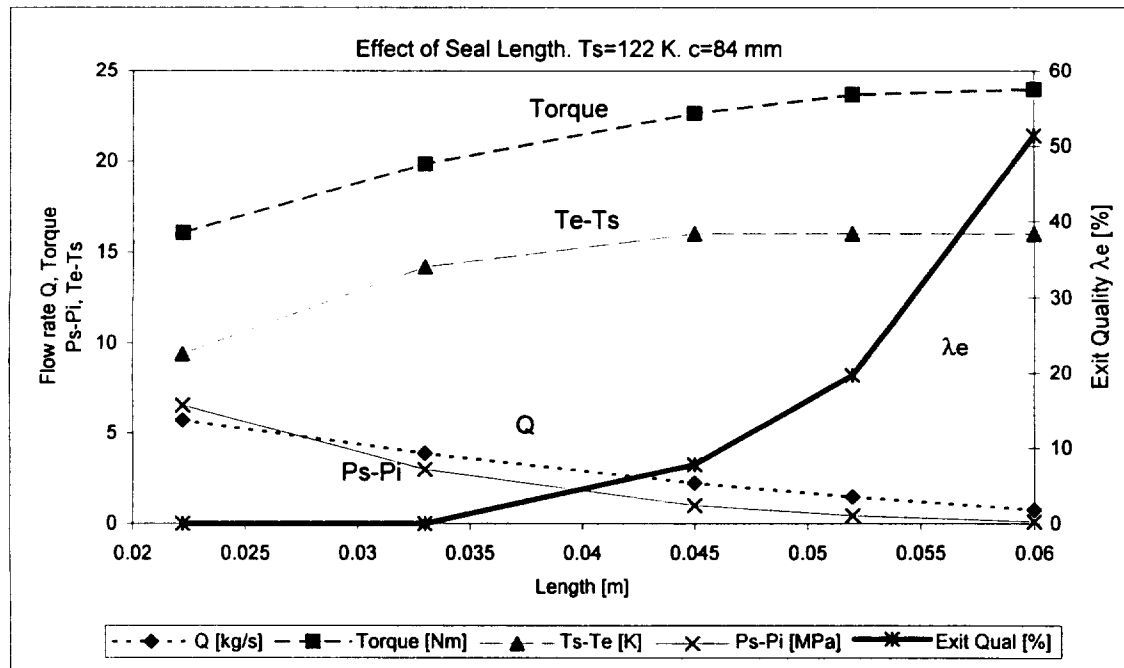
Figure 13. Static characteristics for reduced clearance configuration and increasing seal length. **(a)** Ts=115 K. **(b)** Ts=122 K.

increase in dissipation also produces an increase in drag torque and in temperature rise across the seals. The temperature rise across the seals which reflects the fact that when two-phase flow condition is reached the fluid temperature remains at its saturation value (138 °K) in accordance to the model assumption of a mixture in thermodynamic equilibrium. The energy added to the fluid cannot increase its temperature past its saturation value, but it is instead directed to sustain the phase change (vaporization in this case). Figure 13a shows that for seal lengths above 0.045 m. (L/D=0.529) the energy added to the flow is enough to reach saturation conditions at the seal exit (T_{sat}=138 °K) inducing a phase change, as denoted by the value of mixture quality. The longest seal presented in the Figure 13a shows a value of mixture quality λ=45.5% at the seal exit.

No significant changes in flow rate, torque or entrance pressure drop are noted for the cases with higher supply temperature conditions depicted in Figure 13b. However larger qualities at the seal exit are observed due to the increased proximity to the saturation conditions. At this level of supply temperature the energy added to the fluid is enough to produce two-phase flow conditions at the exit of the seals with length equal to 0.033 m. (L/D=0.388). A value of mixture quality λ=51.4% is predicted at the exit for the longest seals. It should be noted that, due to the fixed supply and discharge conditions, the fluid is below its critical pressure only at the exit, therefore the phase change occurs only at the seal discharge plane.

Effect of stator surface roughness:

The effect of stator surface roughness is illustrated in Figure 14. The relative roughness parameter, defined as the surface roughness-to-radial clearance ratio, was increased from its original value of 0.044, corresponding to a knurled surface, to values as high as 0.1. Two different sets of operating conditions were simulated. Figure 14a shows the results for a supply temperature of 115 °K and a seal length equal to 45 mm.

Under these conditions two-phase flow is predicted for all the cases although the quality at the exit reaches only about 5% for the seals with the roughest stator. The
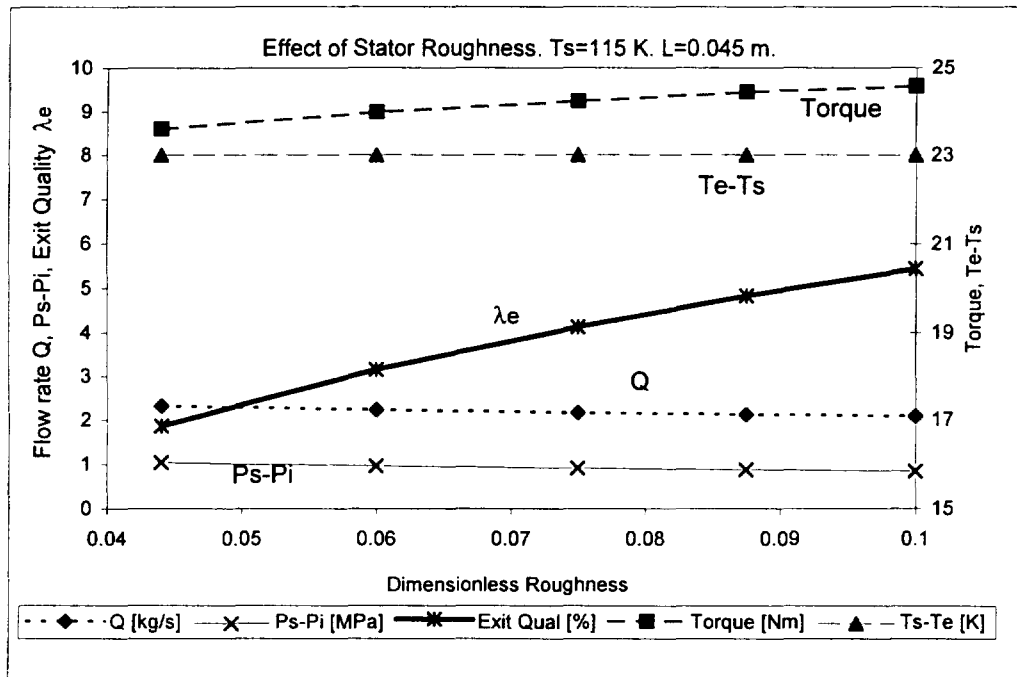
(a)
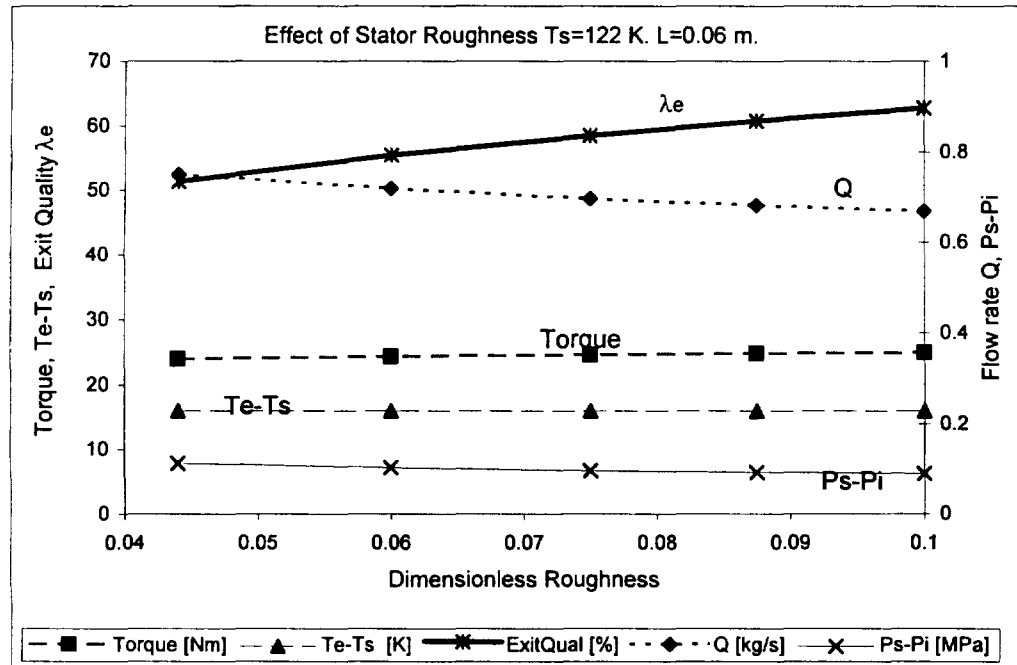
(b)

Figure 14. Static characteristics for reduced clearance configuration and increasing stator roughness. **(a)** Ts=115 K, L=0.045 m. **(b)** Ts=122 K, L=0.06 m.

second case with a larger supply temperature ($T_s=122°K$) and increased seal length ($L=60$ mm.), as presented in Figure 14b, showed significantly larger values of exit mixture quality, which shows the combined effect of increasing the seal length and bringing the operation conditions closer to the saturation region. The behavior of flow rate, torque and entrance pressure drop is the same with increasing surface roughness for both seal cases. Flow rate and inlet pressure drop decrease, and torque increases as the stator roughness increases. Figure 14a present smaller values for these parameters as expected due to the smaller seal length, but the qualitative behavior is the same. The variation of exit or discharge quality with increasing surface roughness is a result of the increment in mechanical energy dissipation generated by the increased friction and turbulence resulting from the larger surface roughness. Once the fluid has reached two-phase conditions its temperature remains at its saturation value ($T_{sat}=138$ °K), and consequently the temperature rise across the seal remains constant as shown in Figure 14b.

Effect of entrance loss coefficient:

The effect of increasing the entrance loss coefficient (ξ) is shown in Figure 15. As expected the main effect can be seen in the pressure drop at the seal entrance which is directly proportional to the loss coefficient. However variations in (ξ) have no significant effect on leakage, torque and temperature rise across the seals. All of these parameters decrease slightly with increasing entrance loss coefficient due to the reduction of pressure drop between inlet and exit when the loss coefficient increases. The variation of the entrance loss coefficient was explored since a larger pressure drop at the entrance results in a less steep drop in pressure along the seal and therefore the region where the fluid has a pressure below its critical value is extended. Consequently a larger region within the seal has the potential to reach saturation conditions and experience a phase change.

A parametric study of the static characteristics of an annular damper seal arrangement for cryogenic applications has been carried out . The effects of varying supply conditions (P_s, T_s), seal geometry, surface roughness and entrance loss coefficient on the seal static performance characteristics, namely leakage, torque, temperature rise, entrance pressure drop , and presence of two-phase flow conditions were analyzed.
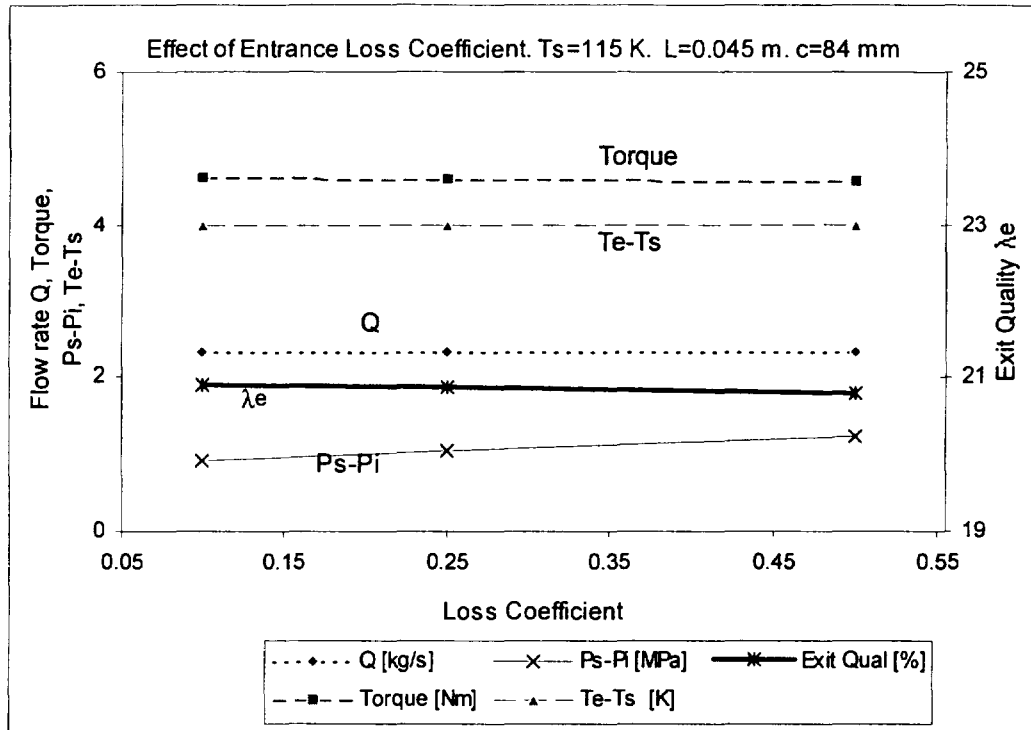
Figure 15. Static characteristics for reduced clearance configuration and increasing entrance loss coefficient.

The numerical results show that for the operating conditions studied the occurrence of two-phase flow is linked to the amount of energy absorbed by the fluid. For applications such as in a cryogenic turbomachinery where the heat transfer to the solid surfaces can be neglected due to the high velocities of the fluid (i.e. as adiabatic flow process), all the energy dissipated by shear phenomena, extrusion work, etc, is carried away by the fluid. When this energy is large enough bring the fluid into saturation condition the flow undergoes a phase change. Therefore, any factor that increases the energy dissipated by the fluid will favor the occurrence of two-phase flow. This is the case of increasing seal length or increasing surface roughness as shown in the analysis.

Working in conjunction with the amount of energy dissipated by the fluid is the proximity of the operating conditions to the saturation region. It has been shown that by increasing the supply temperature, bringing operation close to saturation conditions, the amount of liquid -vapor mixture is increased. For concentric operation two-phase flow is

not possible for conditions above the fluid critical pressure. However, for seal eccentric operations is more likely to have two-phase flow even though the pressures are above the critical value (Hendricks, et al. 1987). The drop in pressure occurring at the location of maximum film thickness when the journal performs eccentric excursions may bring the fluid pressure below its critical value and close to the saturation condition, thus creating the potential for phase change to occur.

7.3 LOX seal under two-phase conditions

Predictions for the static and dynamic forced response of a liquid oxygen damper seal operating under two-phase flow conditions are presented in this section. Beatty and Hughes (1988) present a seal example with geometry similar to that of the damper seal for the oxygen pump of the space shuttle main engine. The supply conditions were decreased to bring the seal operation close to the saturation region and to induce two-phase flow conditions throughout all the seal. Beatty and Hughes results include theoretical predictions for the static response of the seal, i.e. mass flow rate and pressure, temperature and mixture quality fields. Although the supply conditions are not realistic for the proposed application (Space Shuttle Main Engine), this is a good example case to study the effect of two-phase flow conditions on the seal forced response.

Table 7. Geometry and operating conditions for Beatty and Hughes seal example.

Diameter D [m]	0.065
Length L [m]	0.026
Radial clearance, c [mm]	174
Rotor and stator roughness	0.0 (smooth)
Rotational speed [rpm]	30,000
Supply pressure [MPa]	2.79
Supply temperature [°K]	139
Discharge pressure [MPa]	1.8 (T_{sat}=140.02 °K)
Entrance loss and swirl coefficients ξ, α	0.5

For these conditions the predictions from the model proposed in this dissertation show very good agreement with those given earlier by Beatty and Hughes (1988). The deviations detected are caused mainly by the circumferential flow development in the present model and the use of a improved model for novel formulation of mixture viscosity as given earlier.

Numerical predictions are presented for a range of supply temperatures between 125 and 150 °K in order to study the effect of two-phase flow on the seal response. The examples then show different flow structures within the seal like all-liquid, liquid-mixture, all mixture, mixture-vapor, and all-vapor. The numerical simulations revealed that several values of supply temperature have a special significance. At a supply temperature approximately equal to 129.5 °K the theoretical model predicts that the transition from liquid to a mixture occurs just at the seal exit plane. The change from liquid to mixture along the entire seal occurs at the seal entrance for a supply temperature equal to 138.5 °K. Finally, the transition from flow mixture to all-vapor occurs at the seal entrance when the supply temperature is around 145 °K. The significance of these transition zones is illustrated in the following sections.

Static Seal Characteristics

A study of the variation of the main seal static characteristics, namely mass flow rate (leakage), torque, seal entrance pressure and mixture quality at the exit, over a range of supply temperatures is presented next. Figures 16 and 17 presents the summary of the theoretical predictions versus supply temperature and supply enthalpy, respectively. When the fluid is fed to the seal as a mixture the supply temperature is equal to the
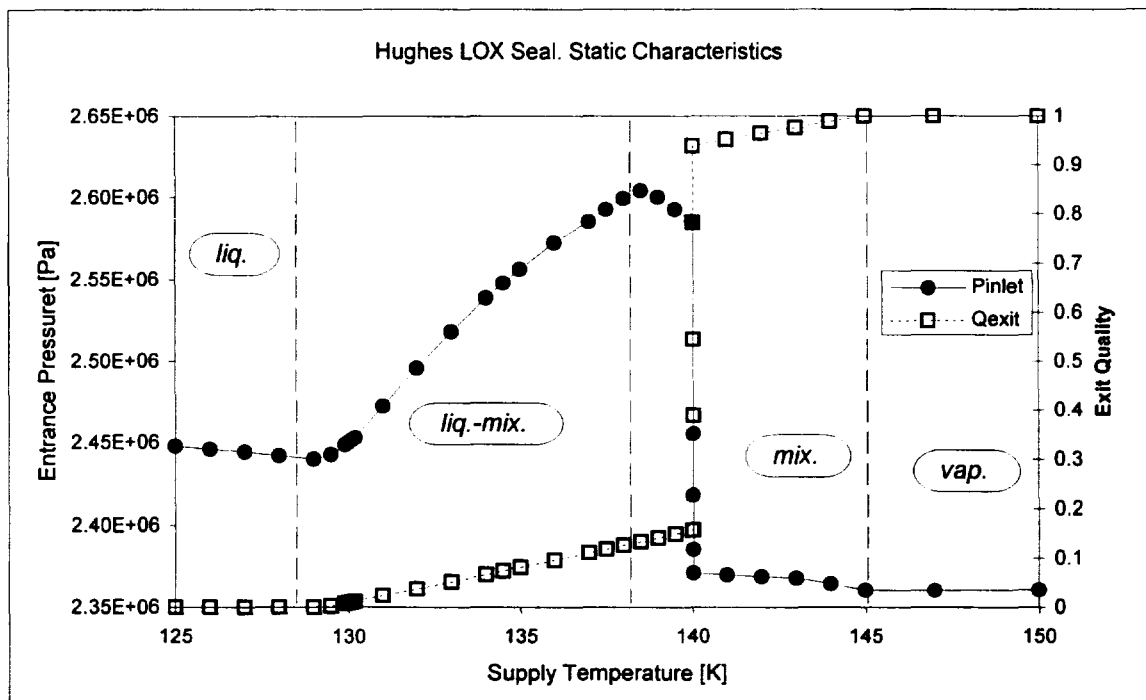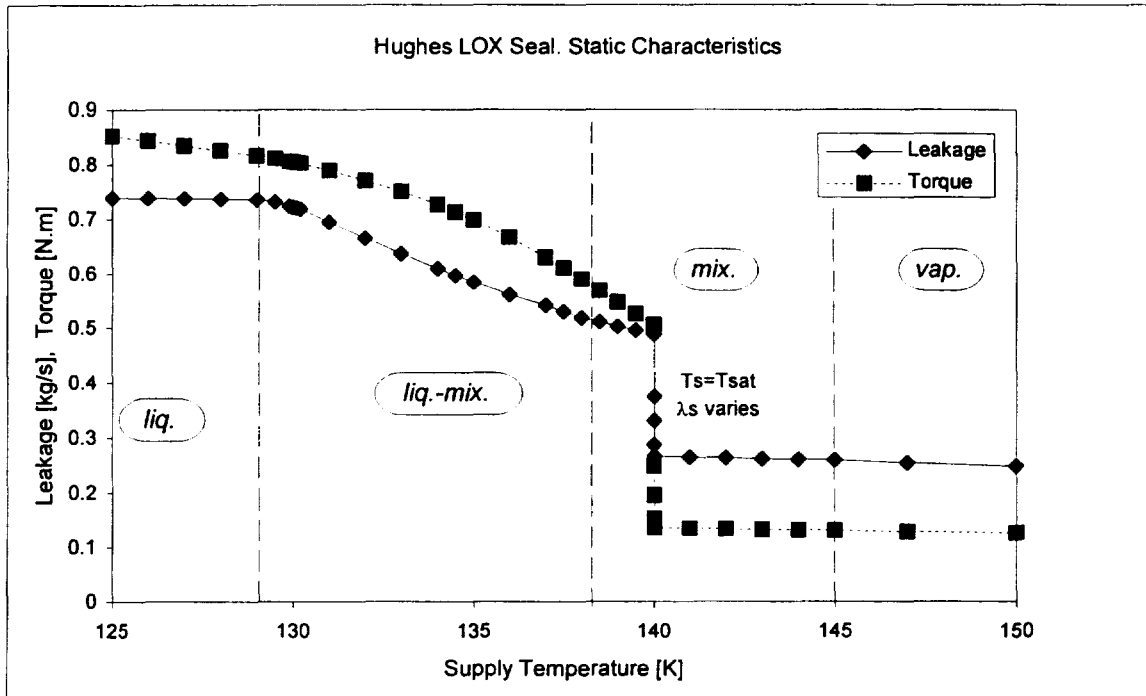
Figure 16. Leakage, torque, entrance pressure and exit quality for different supply temperatures.
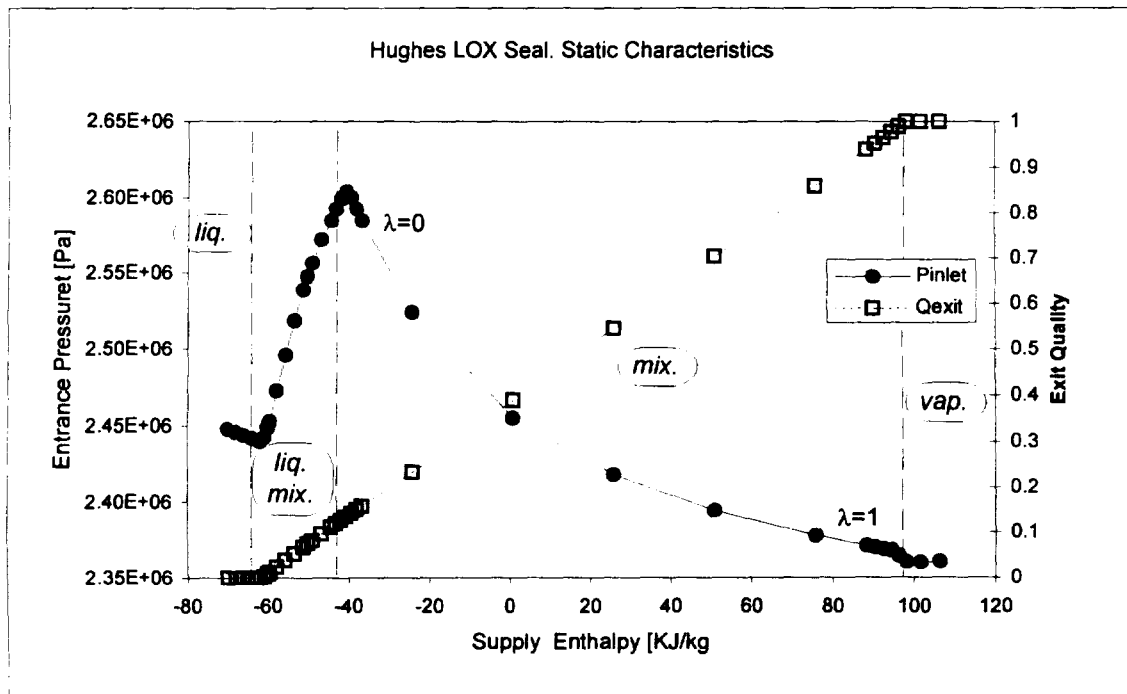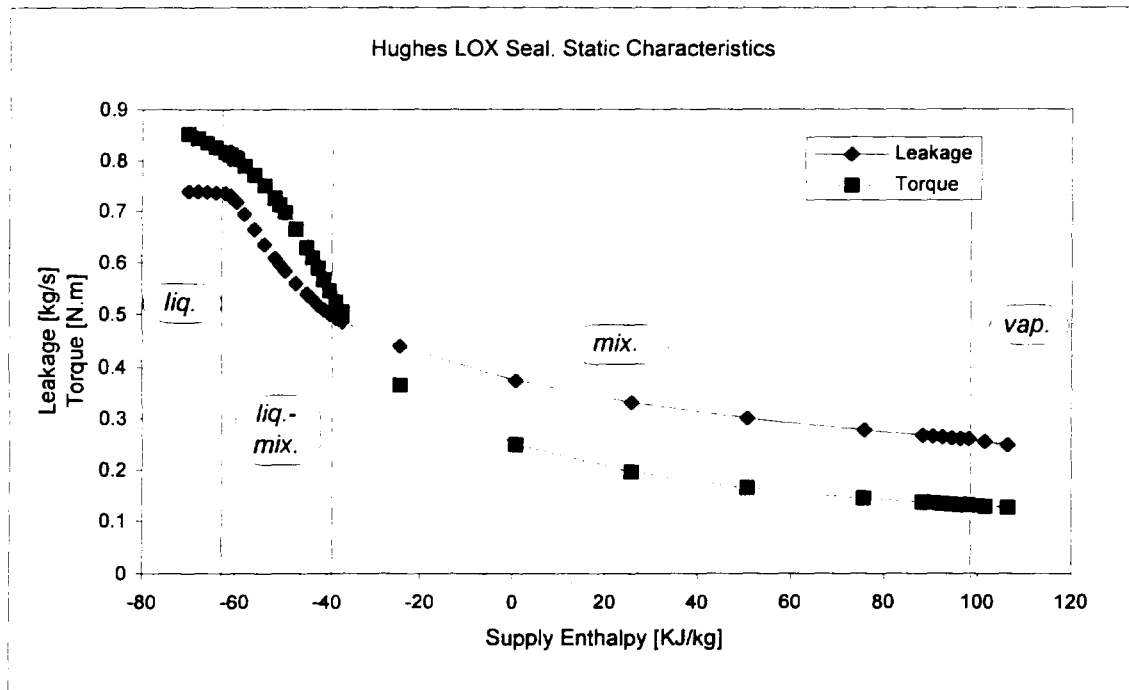
Figure 17. Leakage, torque, entrance pressure and exit quality for different supply enthalpies.

saturation temperature (140 °K) corresponding to the supply pressure. Then, mixture quality is varied to simulate different supply conditions, and a different physical property, such as enthalpy, is needed to identify the supply conditions and avoid the multi-valued conditions shown at 140 °K in Figure 16.

The behavior of leakage, torque and exit quality agrees with experimental observations and theoretical results presented in the literature (Beatty and Hughes, 1988). That is, torque and leakage decrease monotonically from the all-liquid condition $(T_s<130°K, i_s<-60$ KJ/kg) to the all-vapor condition $(T_s>145$ °K, $i_s>98$ KJ/kg), while the mixture quality at the seal discharge increases linearly between $\lambda=0$ (all-liquid) to $\lambda=1$ (all-vapor) in the same range. However, the pressure at the seal entrance (P_{inlet}) presents a different behavior and its variation is not bounded by the all-liquid and all-vapor cases. Opposite variations with increasing supply temperature are observed in the liquid-mixture range $(130 < T_s < 138.5$ °K) and all-mixture range $(138.5 < T_s < 145$ °K) denoting the large change in the compressibility character of the flow at the seal entrance.

The axial variation of the dimensionless pressure and enthalpy along the seal is presented in Figure 18. The all-liquid (Ts=125 K) and all vapor (Ts=150 K) cases are presented in thick lines, while the cases presenting two-phase flow conditions are shown with lines and symbols. Since the supply and discharge pressures are the same for all the cases presented, Figure 18a represents also the variation of the actual fluid pressure. As depicted in this figure, if the fluid is all-liquid the pressure decreases almost linearly within the seal, and if it is all gas the variation is non linear. However, if a phase change occurs the seal leakage is reduced and the pressure is higher than the single phase cases.
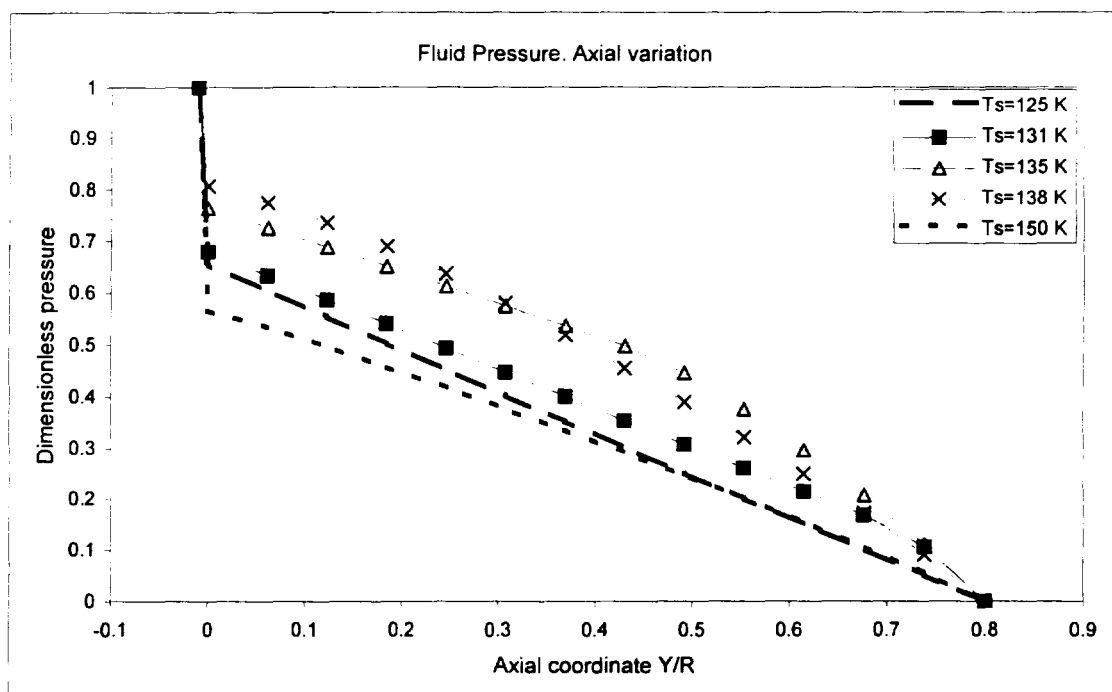
(a)
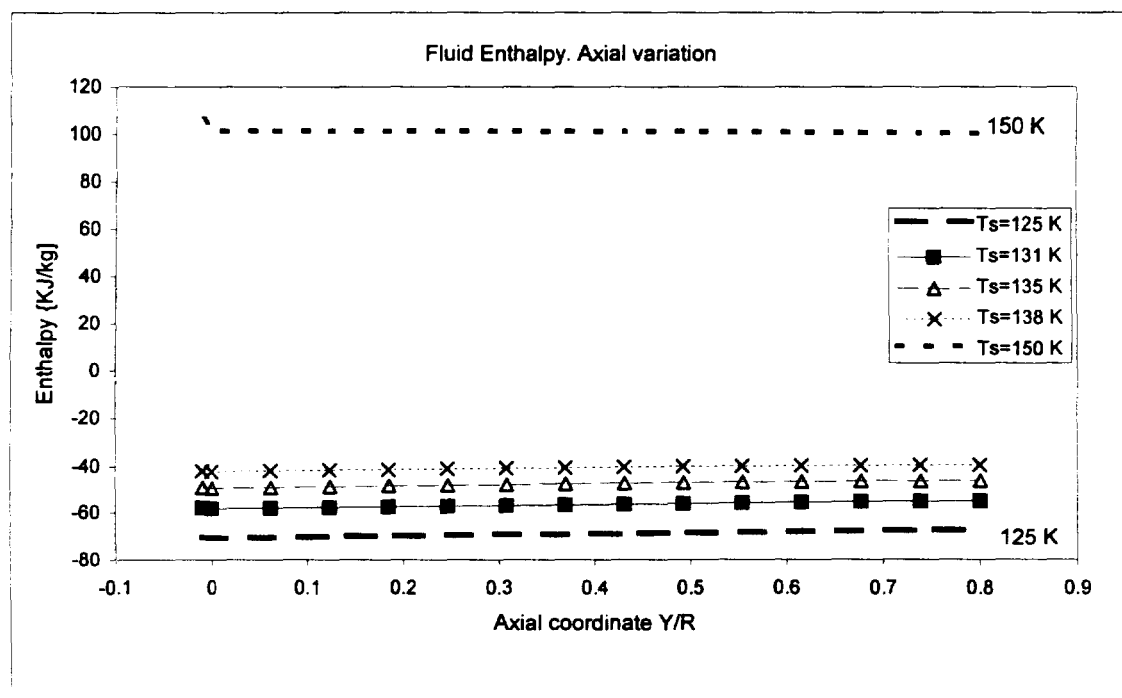
(b)

Figure 18. Variation of fluid properties along the seal for different supply conditions. (a) dimensionless pressure. (b) enthalpy.

The examples with supply temperatures equal to 131, 135 and 138 °K show two-phase flow conditions at the exit, middle and entrance of the seal, respectively. The presence of two-phase flow condition is denoted by the change in pressure variation from linear in the liquid region to nearly quadratic in the two-phase region. Note that for the two-phase flow cases (Ts=131, 135 and 138 K) the pressure drops more rapidly in the two-phase region than in the liquid region. These observations agree with those presented by Pinkus (1990) for face seals.

Figure 18b shows the variation of fluid enthalpy along the seal for different supply temperatures. Note that only a small increment of enthalpy between seal inlet and exit is predicted. As the supply temperature is increased, and the flow within the seal changes from all-liquid to two-phase mixture to all-vapor, the fluid enthalpy increases steadily without any dramatic changes due to the presence of two-phase flow conditions.

Dynamic Force Characteristics

The study of variation of the rotordynamic force coefficients under two-phase flow operation is the purpose of this subsection. Theoretical predictions for dynamic stiffness and damping coefficients are presented for different supply conditions (enthalpy/temperature) and increasing excitation frequencies (ω). As explained in section 5, the fluid film forces are described by damping coefficients (C_{ij}) and frequency dependent or dynamic stiffness coefficients (K_{ij}).

Two types of results are presented. The first of them, shown in Figures 19 through 23, represents the effect of supply enthalpy on the seal force coefficients. The

second set of results, shown in Figures 24 and 25, depicts the relation between the rotordynamic coefficients and the excitation frequency.

The variation of the direct ($K_{XX}=K_{YY}$) and cross-coupled dynamic stiffness ($K_{XY}=-K_{YX}$) with supply enthalpy and for three levels of excitation frequency is presented in Figures 19a and 19b, respectively. The same plots are presented in Figure 20 in terms of supply temperature. The predictions for the lowest excitation frequency ($\omega/\Omega=0.01$, 5Hz) can be safely regarded as the proper stiffness, i.e. with no excitation frequency effects. Both stiffnesses (K_{XX} and K_{XY}) appears to be unaffected by changes in supply conditions and excitation frequency on the all-vapor range ($i_s>98$ KJ/kg, $T_s>145$ °K). The behavior within the all-liquid range ($i_s<-60$ KJ/kg, $T_s<130$ °K) is the typical of an incompressible fluid which includes a positive inertia coefficient. For two-phase flow conditions the stiffnesses present different behavior depending on whether the flow has a liquid-mixture ($130 <T_s<138.5$ °K, $-60<i_s<-40$ KJ/kg) or an all-mixture structure ($138.5<T_s< 145$ °K , $-40<i_s<98$ KJ/kg).

The direct dynamic stiffness(K_{XX}) increases with increasing supply enthalpy in the liquid-mixture "regime" reaching values significantly larger than those predicted for the all-vapor case. This behavior denotes a continuous rise of the fluid mixture compressibility effects as the enthalpy increases. Direct stiffness seems to be independent of the excitation frequency at the supply conditions corresponding to 133 °K ($\sim$-50 KJ/kg). From the transition point between liquid-mixture and all mixture ($i_s=-40$ KJ/kg, $T_s=138.5$ °K), as the mixture density drops to a value close to the vapor density, the direct
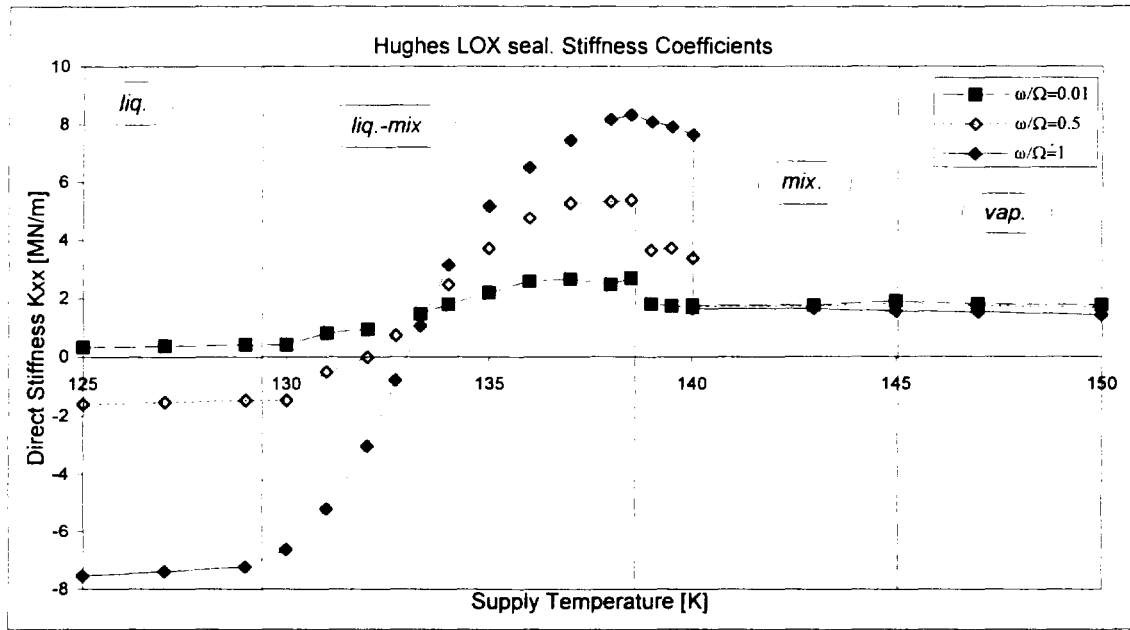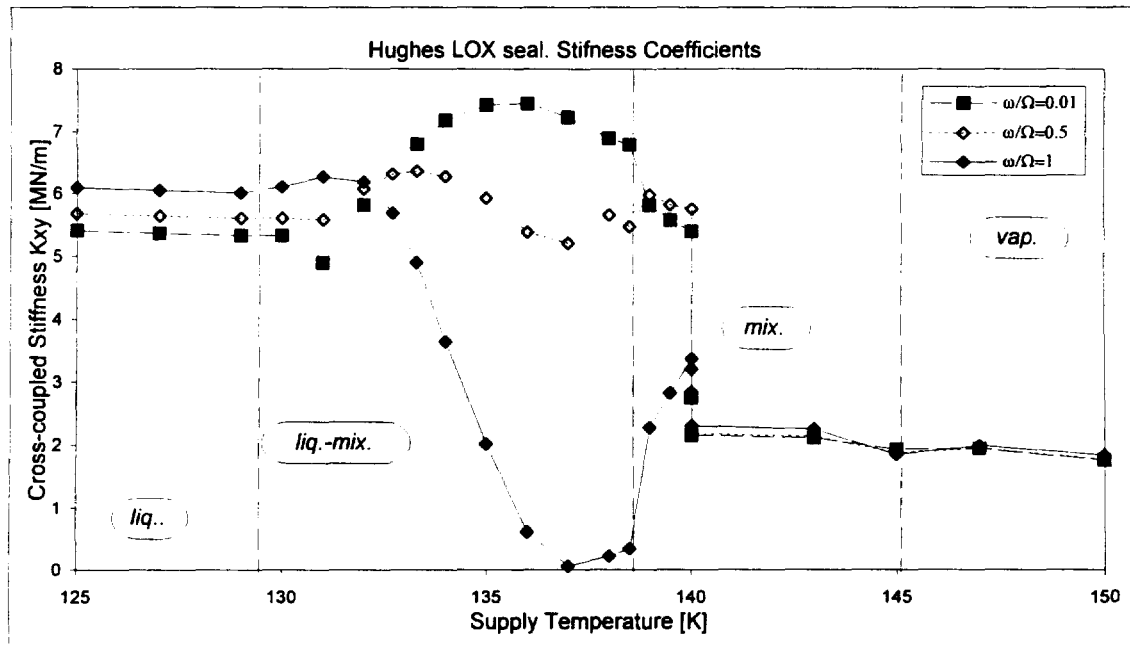
72
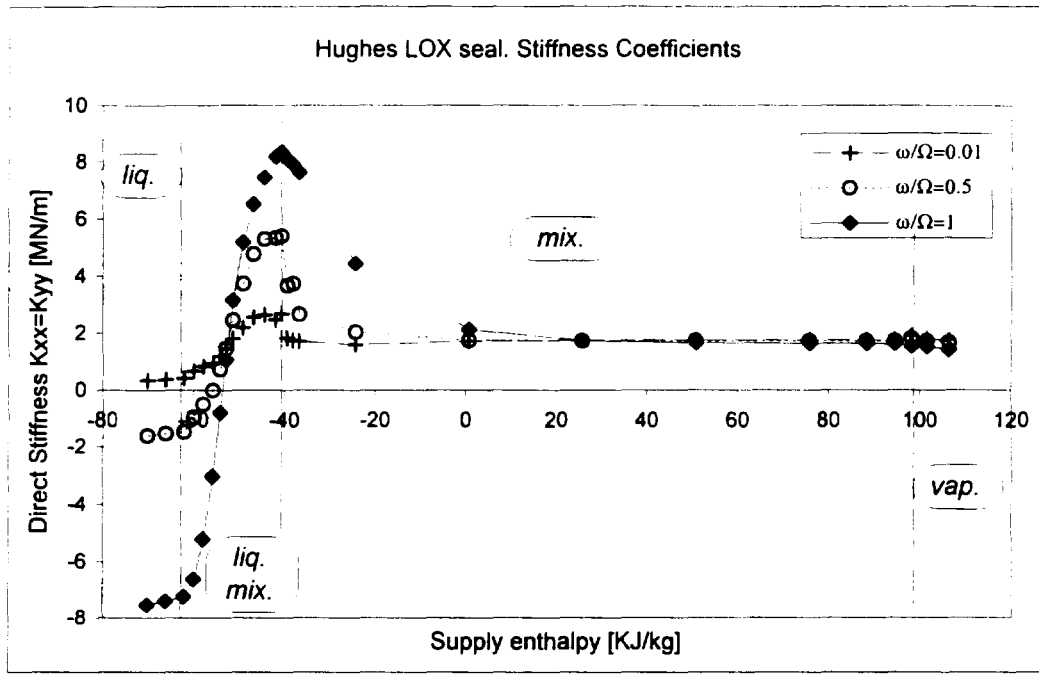
(a)
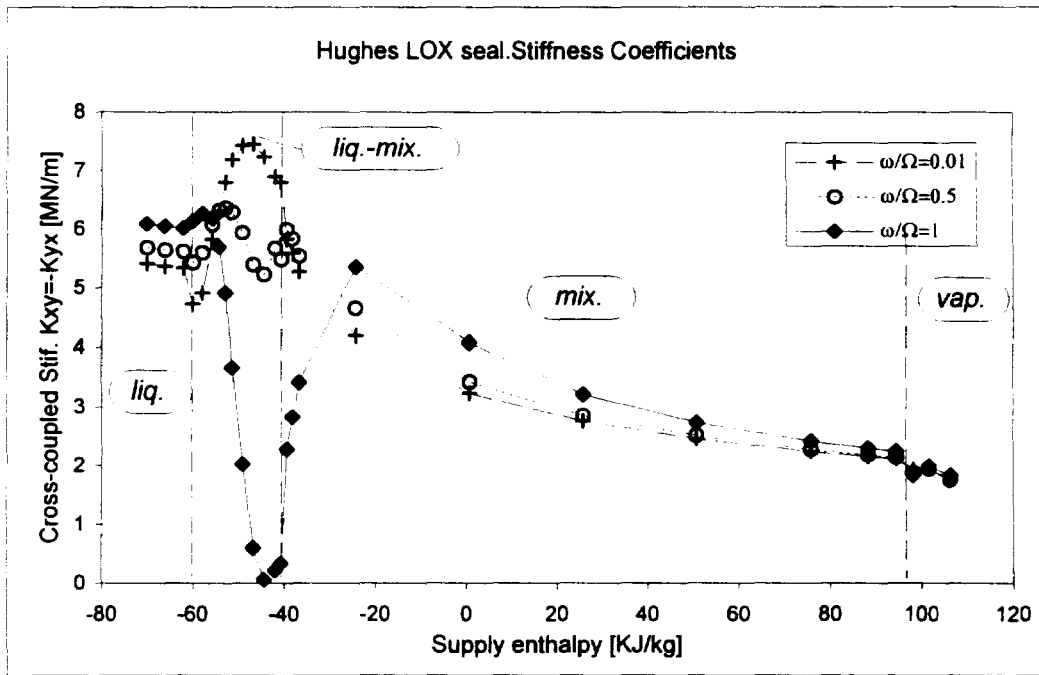
(b)

Figure 19. Variation of dynamic stiffness with supply enthalpy for different excitation frequencies. (a) Direct stiffness, Kxx. (b) Cross-coupled stiffness, Kxy.

(a)

(b)

Figure 20. Variation of dynamic stiffness with supply temperature for different excitation frequencies. (a) Direct stiffness, Kxx. (b) Cross-coupled stiffness, Kxy.

dynamic stiffness decreases with increasing supply enthalpy until it reaches the all-vapor condition.

The cross-coupled dynamic stiffness (K_{XY}) also decreases as the supply temperature increases in the all-mixture regime. However, the variation in the liquid-mixture regime shows a rather complex dependency of cross-coupled stiffness on excitation frequency and supply temperature with a minimum at around i_s=-44 KJ/kg (137 °K), and for the case with excitation frequency equal to 500 Hz, it even shows cross-coupled stiffnesses smaller than those predicted for the all-vapor case. Again this behavior is attributed to the rise in fluid compressibility effects mentioned above.

Figure 21 depicts the variation of direct (C_{XX}) and cross-coupled (C_{XY}) damping coefficients (21a and 21b, respectively) with supply enthalpy for three different excitation frequencies. The same plots are presented in terms of supply temperature in Figure 22. The figures show again that the behavior in the all-liquid and all-vapor regimes are the ones expected for single phase liquid and a gaseous seals, with little dependency on the excitation frequency and independent of the supply temperature for the all-vapor cases. The results under two-phase flow conditions show that the direct damping decreases as the excitation frequency increases. More importantly, an increment in direct damping with respect to its all-liquid value is observed when liquid and mixture are present along the seal. For high frequencies the direct damping shows the same type of dependency on frequency and temperature as the one shown by the cross-coupled stiffness. In the all-mixture regime the damping coefficients decrease steadily to reach the all-vapor values. The cross-coupled damping (C_{XY}) shows a large drop in the liquid-mixture regime
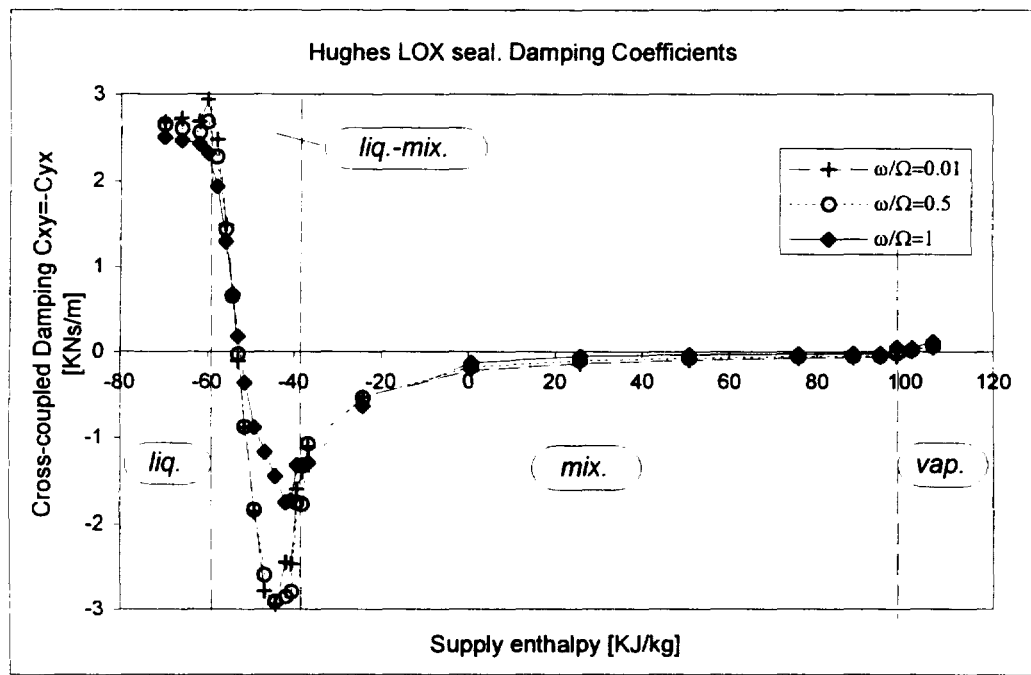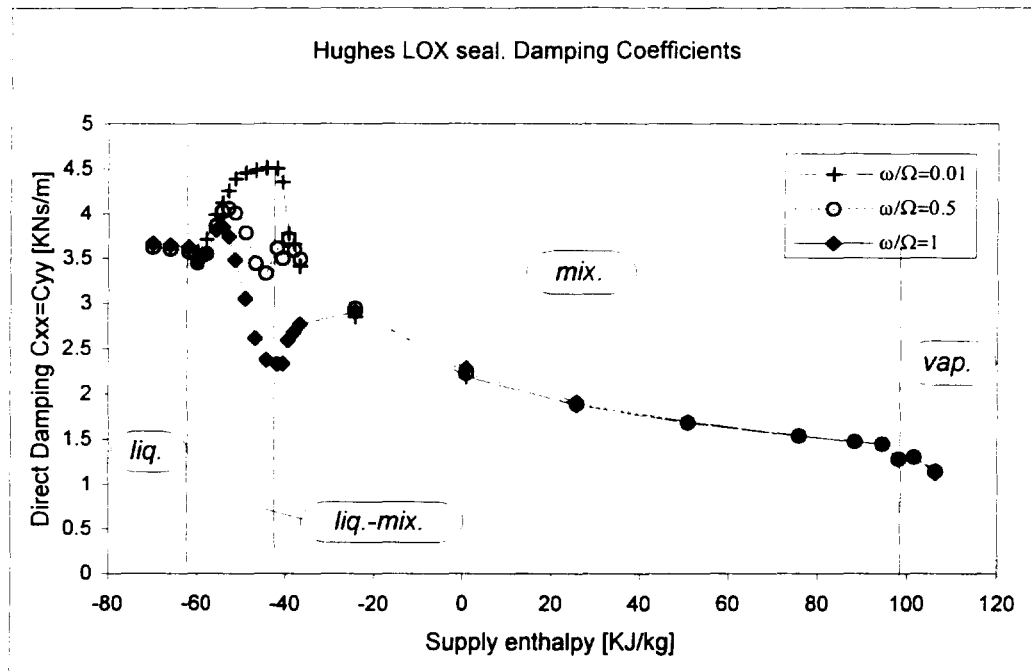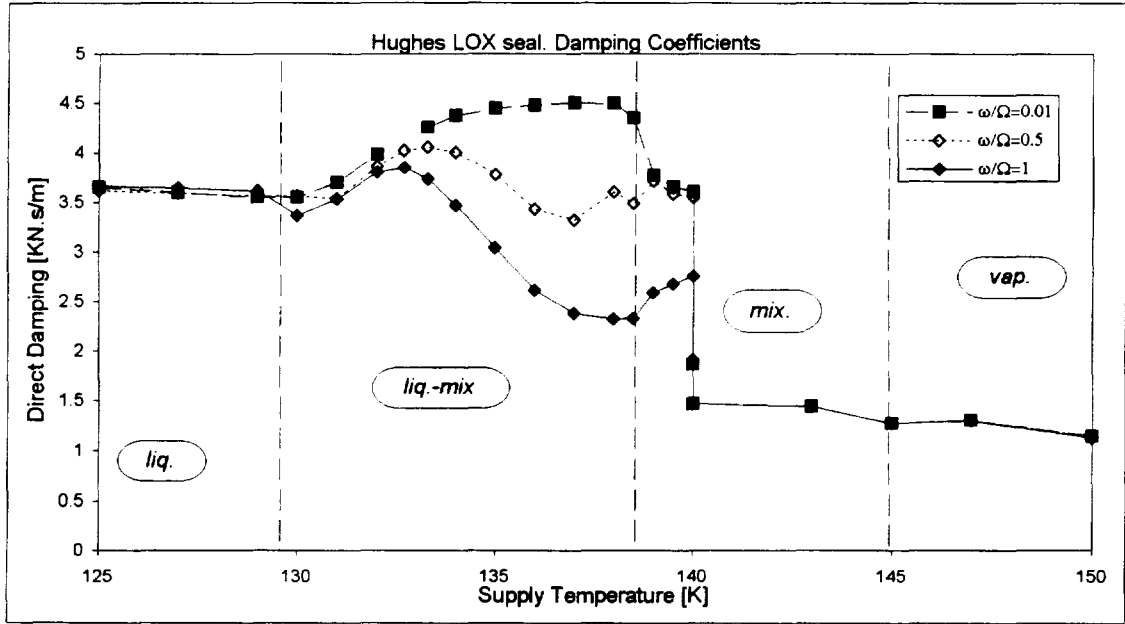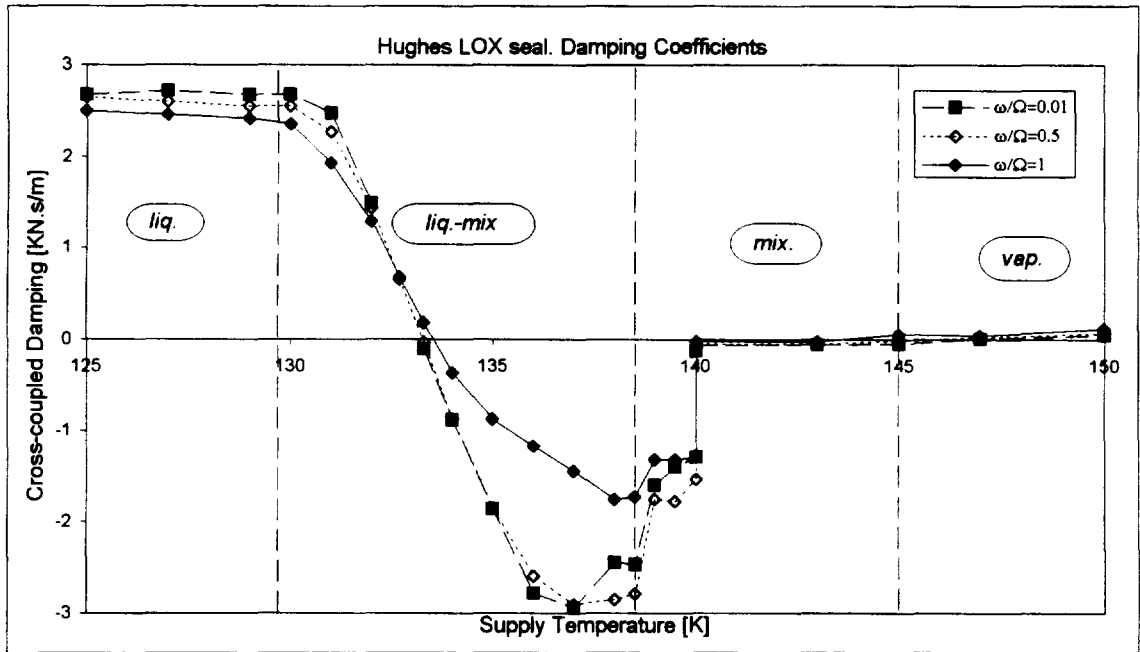
(a)

(b)

Figure 21. Variation of damping with supply enthalpy for different excitation frequencies. frequencie (a) Direct damping, Cxx. (b) Cross-coupled damping, Cxy.

(a)

(b)

Figure 22. Variation of damping with supply temperaute for different excitation frequencies.
(a) Direct damping, Cxx. (b) Cross-coupled damping, Cxy.

reaching even negative values of the same order of magnitude as those for the all-liquid conditions. When all the fluid within the seal is a mixture the cross-coupled damping increases steadily approaching the values for the all-vapor cases.

The whirl frequency ratio (WFR=K_{XY} /$C_{XX}\Omega$) is a parameter commonly used in rotordynamics to describe the rotor stability. It can be described as the ratio between destabilizing-to-stabilizing forces. A WFR equal to 1 denotes a system on the verge of instability, i.e. destabilizing and stabilizing forces are equal. On the other hand, a WFR equal to zero denotes an inherently stable system (no destabilizing forces). Typical WFR for damper seals without preswirl working with either liquid or gaseous fluids is approximately equal to 0.5 which corresponds to the average tangential fluid velocity within the seal (0.5 $R\Omega$).

When combining the variation of direct damping and cross-coupled stiffness a reduction of whirl frequency ratio is predicted, as shown in Figure 23, implying an improvement on stability characteristics, which is a suspect result until validated by experimental data. Figure 23 shows that the WFR can be very close to zero (inherently stable condition) for the case when the cross-oupled stiffness is at its minimum (i_s=44 KJ/kg, T_s=137 °K).
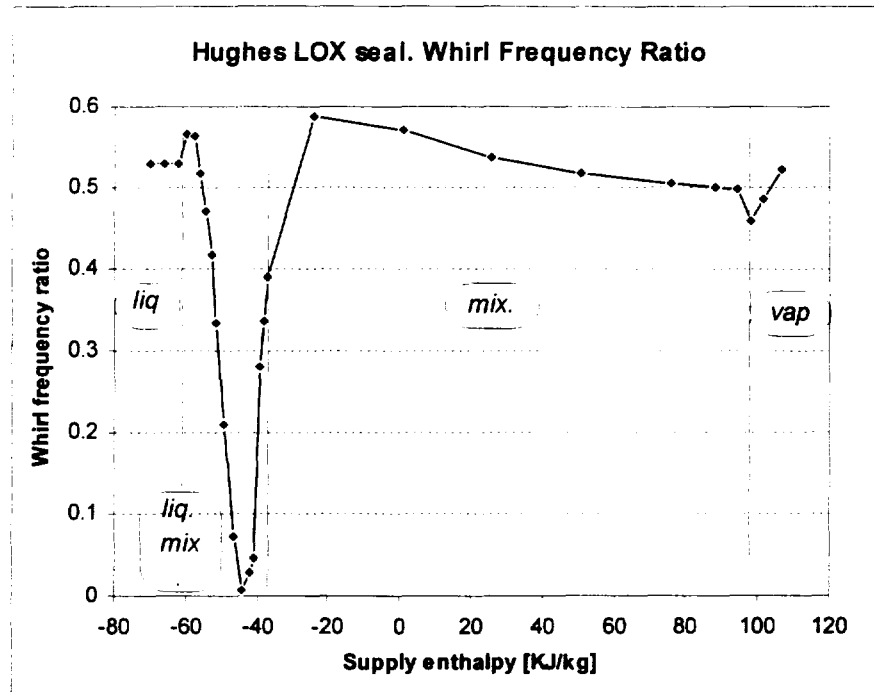
Figure 23. Variation of whirl frequency ratio, WFR, with supply conditions.

Some corroboration to the important WFR phenomena described may be found in the experimental results presented by Iwatsubo et al. (1993). This is an experimental study of the dynamic force response of annular seals working with a mixture of water and air with void fractions (gas-to-mixture volume ratio) up to 70%. The mixture compositions in terms of quality are just below 1%, i.e. very low mass concentration of gaseous phase. The experimental results show, due to a yet non-explained behavior of the cross-coupled stiffness, a reduction of the whirl frequency ratio for these low concentration mixtures.

A more detailed study of the variation of the rotordynamic force coefficients with excitation frequency is presented in figures 24 and 25. All-liquid (T_s=125 °K) and all-vapor (T_s=150 °K) cases are shown in dotted lines in all the plots.

In general, when the fluid is an all two-phase mixture within the seal (T_s>T_{sat}=140 °K) the variation of the rotordynamic force coefficients is similar to those of the all-vapor case. The figures also show that for conditions where the two-phase or mixture region within the seal is small (T_s=131 °K) the behavior of the coefficients is similar to that of the all-liquid case. However, as the two-phase region grows, significant changes in the dependency of the coefficients with frequency is observed.

The direct stiffness (K_{XX}) shows an stiffening effect with increasing excitation frequency and supply temperature for the cases with liquid-mixture conditions (T_s=135 °K, T_s=138 °K). As seen in Figure 24a, this behavior is significantly different to that exhibit by the all-liquid or all-vapor cases also depicted.

The variation of cross-coupled stiffness (K_{XY}) presented in Figure 24b also shows a peculiar behavior for the cases with liquid-mixture conditions. At low excitation frequencies the cross-coupled stiffness are higher than the ones for all-liquid cases, and then they decrease with increasing frequency approaching the values for the gaseous case, and showing a more distinct dependency on the supply conditions.

Figure 25a presents the variation of direct damping (C_{XX}) with excitation frequency and supply temperature. For the cases in the liquid-mixture regime the damping appears to be independent of supply conditions for low frequencies. As the excitation frequency increases direct damping decreases and the dependency on supply conditions is
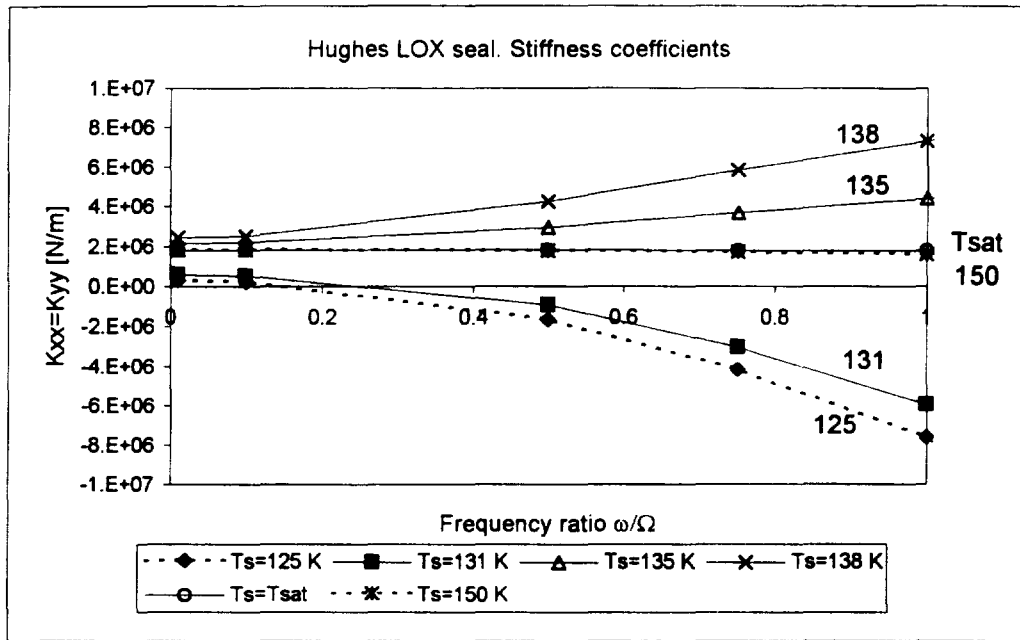
(a)
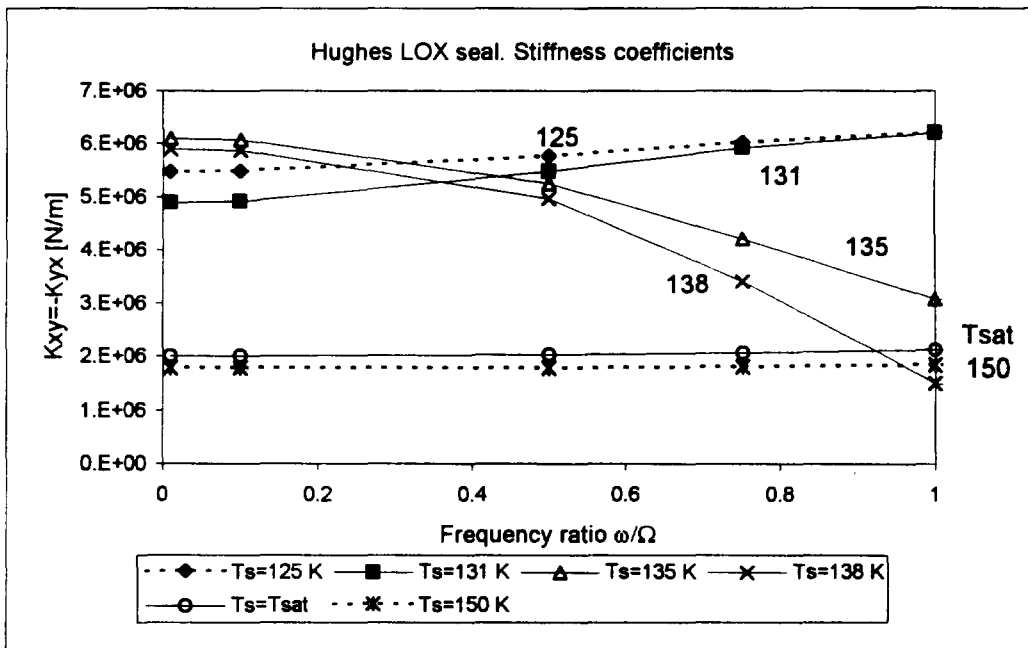
(b)

Figure 24. Variation of dynamic stiffness with excitation frequency for different supply temperatures (Ts). (a) Direct stiffness, Kxx. (b) Cross-coupled stiffness, Kxy.

(a)

(b)

Figure 25. Variation of damping with excitation frequency for different supply temperatures (Ts). (a) Direct damping, Cxx. (b) Cross-coupled damping, Cxy.

accentuated. Note the drastic drop in damping if the fluid goes from liquid-mixture (T_s=138 °K) to an all-mixture conditions (T_s=T_{sat}= 140 °K) within the seal. According to these predictions this may happen with a change in supply temperature of just 2 °K.

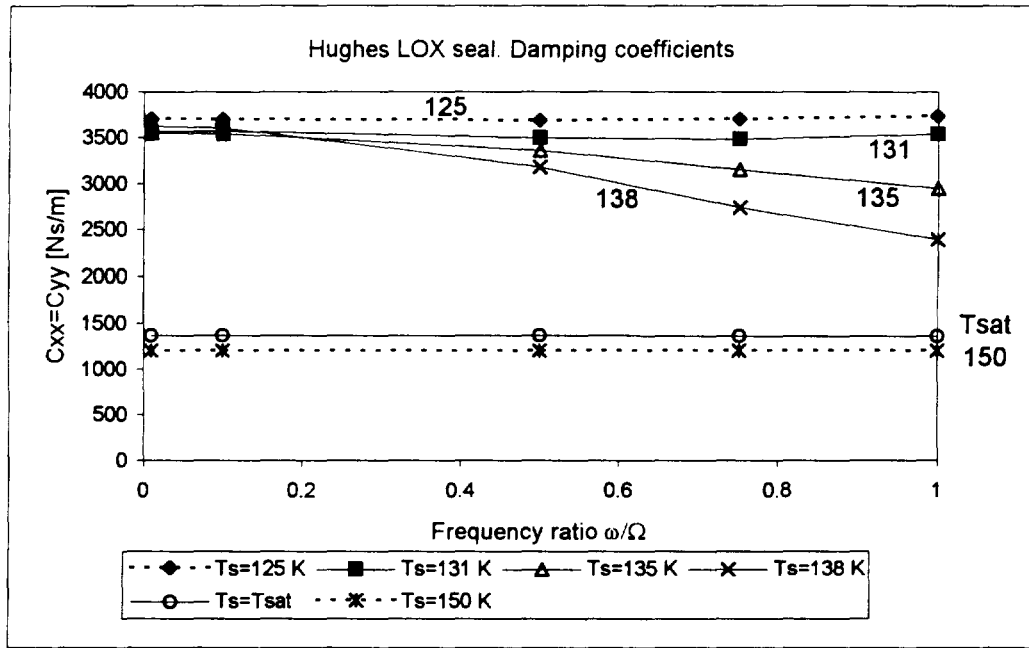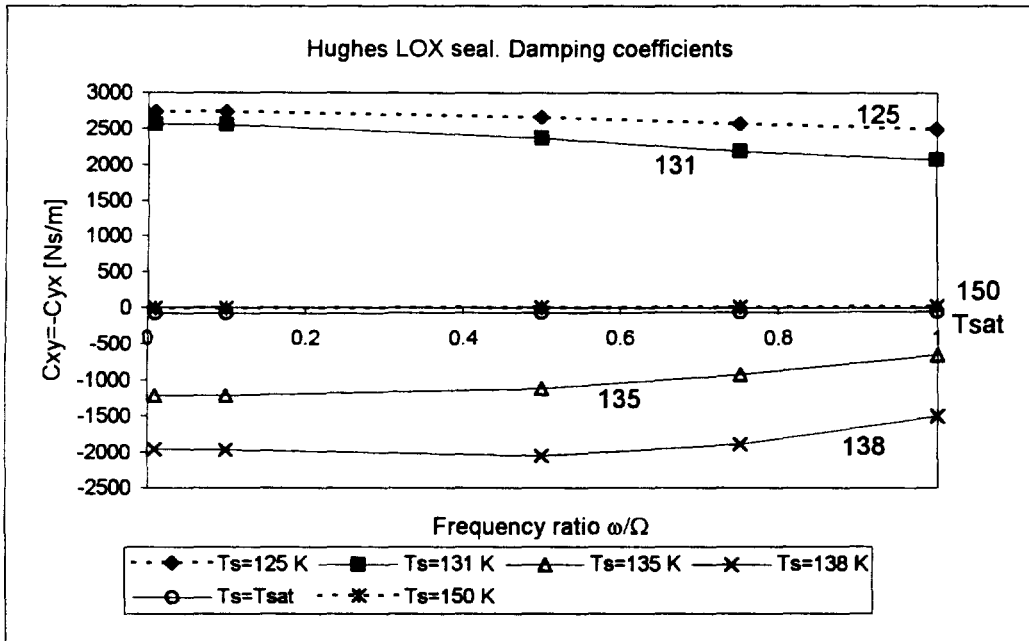Figure 25b shows again that the cross-coupled damping (C_{XY}) coefficients for the cases with liquid-mixture conditions have a different frequency dependency compared to the rest of cases presented. The cross-coupled damping is lower than the all-vapor case and it increases with increasing frequency for seal cases in the liquid-mixture regime.

The dramatic changes in the variation of rotordynamic coefficients for cases where a liquid-mixture flow structure is present within the seal can be explained by the large compressibility exhibited by the mixture, particularly for low vapor mass contents ($\lambda \rightarrow 0$). This can be seen not only from the steep variation of mixture density in the transition from liquid to mixture as observed in Figure 26, but more clearly, by the drastic changes in the derivative of mixture density with respect to pressure shown in Figure 27.

Figure 27 shows that the mixture compressibility ($\partial\rho/\partial p$) is several orders of magnitude larger for the cases where liquid and two-phase mixture co-exist within the seal (131, 135, and 138 °K) than the all-liquid case Although the change in compressibility is about the same for all the liquid-mixture cases, the fact that the levels of fluid density are higher in the cases with smaller two-phase regions explains why this compressibility effect is more significant in the cases with lower supply temperatures.

Another example of the peculiar character of a mixture with a low vapor content can be seen in the pressure-density diagram of Figure 28. Density has been used instead of specific volume (as is commonly used in thermodynamics) since this is the fluid
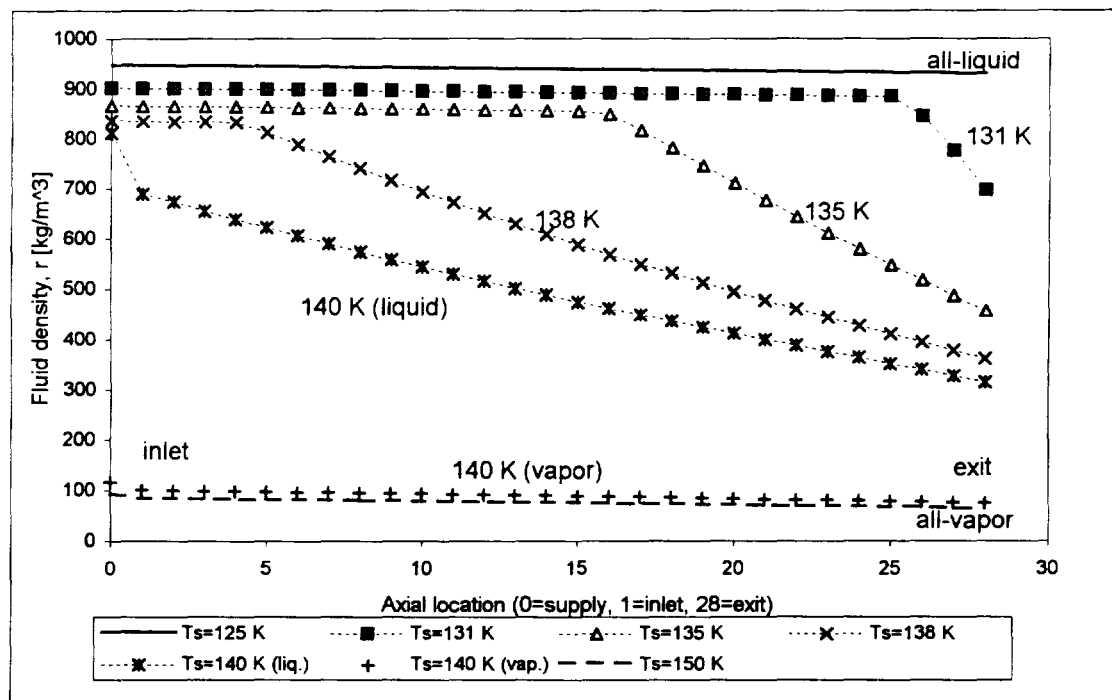
Figure 26. Variation of fluid density along the seal for different supply temperatures (Ts).
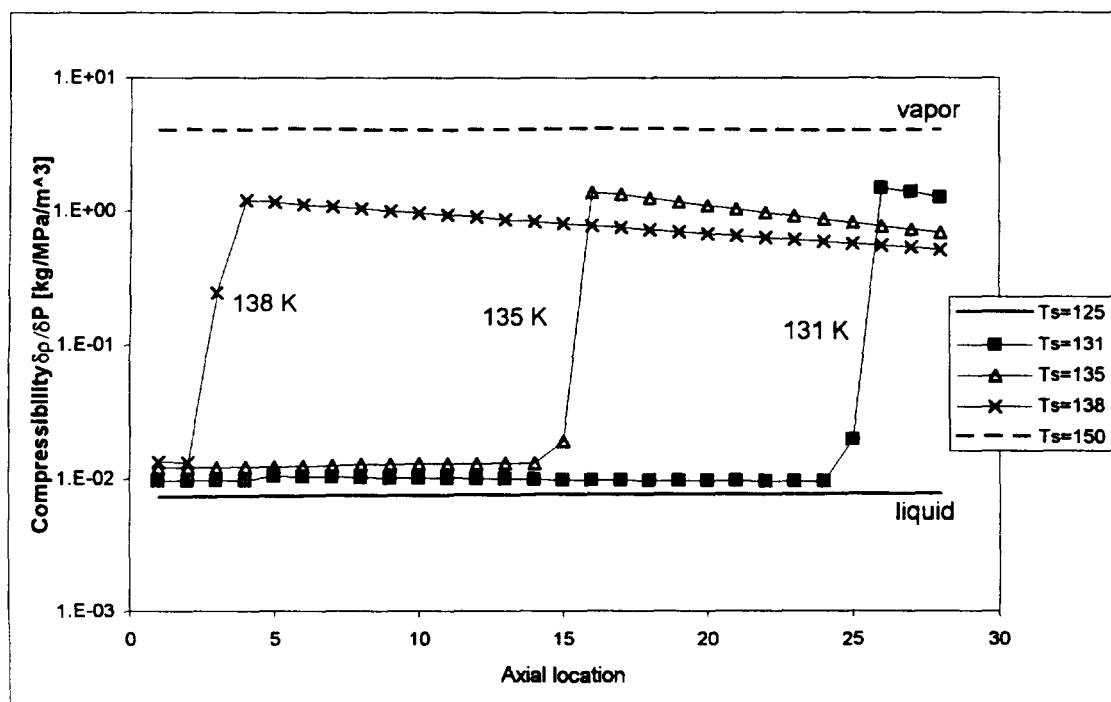
Figure 27. Variation of the derivative of density with respect to pressure along the seal for different supply temperatures (Ts).

property used in the theoretical model. Within this framework, the liquid region is located to the right of the saturation pressure curve (P_{sat}), while the vapor region is located to the left of saturation curve. Three different curves of constant enthalpy are presented in addition to the isothermal curves. The constant enthalpy curves lying in the vapor region (i=93.1 KJ/kgl) and in the high quality mixture region (i=62.5 KJ/kg) have very similar shapes and can be regarded as similar to the portion of the lowest enthalpy curve (i=-59.7 KJ/kg) that lies in the liquid region. However the portion of the latter curve that lies within the liquid-vapor region shows a very strong dependency of enthalpy with mixture quality and present a very different shape in the region of low mixture quality.
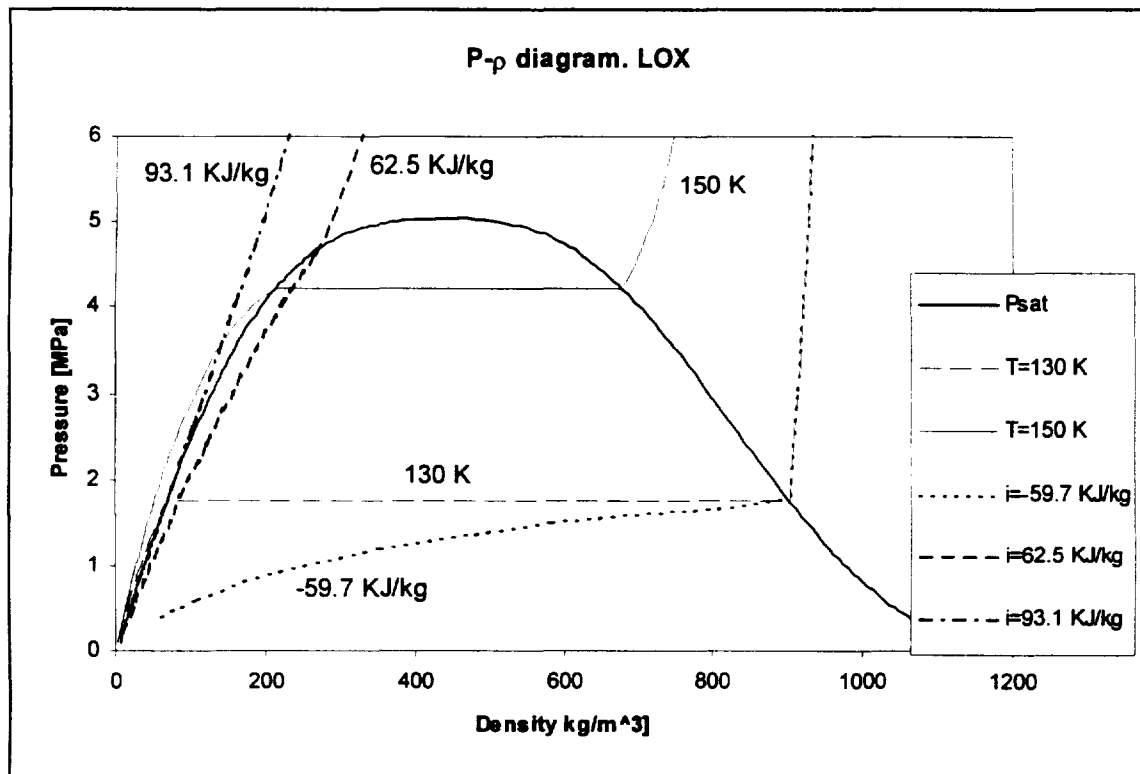
Figure 28. Pressure-density diagram for liquid oxygen with isothermal and constant enthalpy curves.

In summary, the theoretical predictions for a seal case operating under two-phase flow conditions show that the seal leakage and torque decrease monotonically from the all-liquid to the all-vapor conditions as the supply enthalpy rises and the two-phase region grows towards the inlet. In regard to the rotordynamic force coefficients, when the flow shows a two-phase mixture structure throughout the entire seal, the force coefficients vary steadily between the all-liquid and all-vapor values as the supply conditions (temperature or enthalpy) increase. However, when liquid and a low quality two-phase mixture region co-exist within the seal the fluid exhibits a sudden compressibility producing force coefficients beyond the bounds of the liquid and vapor cases with peculiar consequences such as a stiffening effect or a reduction of the whirl frequency ratio. These increased fluid compressibility effects are also denoted by the strongest dependency on excitation frequency shown by the liquid-mixture cases compared to the all mixture configurations.

8. CONCLUSIONS AND RECOMENDATIONS

8.1 Conclusions

A bulk-flow analysis for the prediction the dynamic forced response of centered damper seals for cryogenic turbopumps operating under two-phase flow conditions has been developed. The two-phase flow region is regarded as a homogeneous mixture in thermodynamic equilibrium. In addition to important seal static characteristics such as leakage rate, drag torque, velocities, pressure, temperature and mixture composition fields, the theoretical model predicts the rotordynamic force coefficients that characterize the seal dynamic forced response.

Predictions for the seal static characteristics are validated against existing liquid nitrogen experimental results from Hendricks (1987) which show two-phase flow conditions at the seal exit. The excellent agreement between experiment and results from the current model gives relevance to the analysis. The scarce experimental data available for thin film bearings used in cryogenic turbomachinery in general, and for rotordynamic force coefficients in particular, precludes a proper validation of the predictions for the seal dynamic force response. Qualitative assurance is found from a unique seal experimental data (Iwatsubo, 1993) which covers mixtures (gaseous nitrogen and dissolved oil) with very low mass gas contents.

A parametric study of the static characteristics of an annular seal for cryogenic applications, where the flow process is typically regarded as adiabatic, show that the occurrence of two-phase flow is linked to the amount of energy dissipated by the fluid. When this energy is large enough to bring the fluid into saturation condition the flow

undergoes a phase change. Therefore, any factor that increases the energy dissipated by the fluid, such as increased stator roughness or seal length, will favor the occurrence of two-phase flow.

The most important effect of two-phase flow conditions on the dynamic response of the seals studied occurs when the transition from liquid to mixture of takes place within the seal. In such conditions, the large changes in fluid density (compressibility) when the fluid goes form liquid to low quality mixture within a short physical zone induce a significant change in the nature of the rotordynamic force coefficients. This fluid compressibility effect is stronger in the cases where the mixture portion of the fluid has larger mixture density, i.e. when the mixture mass vapor content is low.

8.2 Recommendations

Important effects have been shown to occur when the seal operates under two-phase flow conditions. The author wishes these predictions will motivate experimental tests for validation and/or a more judicious selection of the seal operating conditions. Phenomena such as the stiffening effect and the reduction of whirl frequency ratio for cases with low quality mixtures can be qualitatively corroborated against results from research on two-component mixtures with low gas content. This research is currently under development at the Texas A&M Turbomachinery Laboratory.

The theoretical analysis is not yet able to simulate seals working with liquid hydrogen due to lack of fluid viscosity data in the thermophysical properties database used. This problem will be corrected when the new version of such database is

incorporated to the model. Although a model for mixture sound velocity has been developed, the current model does not account for sonic flow. Under choked flow conditions the fluid velocity has to be set equal to the sonic speed, and the discharge pressure is no longer an appropriate boundary condition.

The next logical step in the analysis of two-phase flow in damper seals is eccentric rotor operation. The possibility of two-phase flow regions "trapped" in the low pressure regions opposite to the minimum film thickness location will make necessary to reexamine the homogeneous mixture assumption.

REFERENCES

Al-Sharif, A., 1992, "Hydrodynamic Lubrication with Emulsion," Ph.D. Dissertation, Department of Mechanical Engineering, University of Pittsburgh.

Al-Sharif, A., Chamniprasart, K., Rajagopal K.R., Szeri A.Z., 1993, "Lubrication with Binary Mixtures: Liquid-Liquid Emulsion," *ASME Journal of Tribology*, Vol.115, pp.46-55.

Atkin, R.J., Craine, R.E., 1976, "Continuum Theories of Mixtures: Basic Theory and Historical Development," *Quarterly Journal of Mechanics and Applied Mathematics*, Vol. 28, pp. 209-244.

Beatty, P.A., and Hughes, W.F., 1987, "Turbulent Two-Phase Flow in Annular Seals," *ASLE Transactions*, Vol. 30, pp. 11-18.

Beatty, P.A., and Hughes, W.F., 1990, "Stratified Two-Phase Flow in Annular Seals," *ASME Journal of Tribology*, Vol. 112, pp.372-381.

Braun, M. and Hendricks, R., 1981, "An Experimental Investigation of the Vaporous / Gaseous Cavity Characteristics of an Eccentric Journal Bearing," *ASLE Transactions*, Vol. 27, pp.1-14.

Cameron, A., 1966, *Principles of Lubrication*, Longman, Harlow, Essex, England.

Carey, V., 1992, *Liquid-Vapor Phase-Change Phenomena*, Taylor & Francis, Bristol, Pennsylvania, USA.

Chamniprasart, K., 1992, "A Theoretical Model of Hydrodynamic Lubrication with Bubbly Oil," Ph.D. Dissertation, Department of Mechanical Engineering, University

of Pittsburgh.

Chamniprasart, K., Al-Sharif, A., Rajagopal K.R., Szeri A.Z., 1993, "Lubrication with Binary Mixtures: Bubbly Oil," *ASME Journal of Tribology*, Vol.115, pp. 253-260.

Childs, D., 1993, *Turbomachinery Rotordynamics:, Modeling, and Analysis*, John Wiley & Sons, Inc., New York, New York, pp. 40-71.

Cicchitti, A., et al., 1960, "Two-Phase Cooling Experiments- Pressure Drop, Heat Transfer and Burnout Measurements," *Energia Nucleare*, Vol.7,6. pp. 407-425.

Dukler, A.E., Wicks, M.III, and Cleveland, R.G., 1964, "Pressure Drop and Hold-Up in Two-Phase Flow, Part A- A Comparison of Existing Correlations; and Part B- An Approach Through Similarity Analysis, *AIChE Journal*, Vol. 10, pp. 38-51.

Einstein, A., 1906, "Eine neue Bestimmung der Molekul-Dimension." *Ann. Physik*, Vol. 19, p. 289-306.

Feng, N.S., and Hahn, E.J., 1986, "Density and Viscosity Models for Two-Phase Homogeneous Hydrodynamic Damper Fluids," *ASLE Transactions*, Vol. 29, pp. 361-369.

Gray, W.G., 1975, "A Derivation of the Equations for Multi-phase Transport, " *Chemical Engineering Science*, Vol.30, pp. 229-233.

Gross D'Aillon, L., and Jeandey, C., 1981, "Two Phase Flow under Steep Pressure Gradients, " *Proceedings of the Third CSNI Specialist Meeting on Transient Two-Phase Flow*, Pasadena, California, Mar. 23-25, 1981, pp. 123-132.

Hayward, A., 1961, "Viscosity of Bubbly Oil," *Fluids Report*, No Phenomena 99, National Engineering Laboratory.

Hendricks, R.C., 1987, "Straight Cylindrical Seals for High Performance

Turbomachinery," NASA TP-1850.

Hendricks, R.C., Braun, M.J., and Mullen, R.L., 1987, "Two-Phase Flows and Heat Transfer Within Systems with Ambient Pressure Above the Thermodynamic Critical Pressure," NASA TM-87228.

Heshmat, H, 1991, "Investigation of Foil Bearings for Use in High-Thrust Liquid Rocket Engines," NASA Contractor Report CR-187099.

Hughes, W.F., Winowich, N.S., Birchak, M.J., Kennedy, W.C., 1978, "Phase Change in Liquid Face Seals," *ASME Journal of Tribology*, Vol.100, pp. 74-80.

Iwatsubo, T., and Nishino, T., 1993, "An Experimental Study on the Static and Dynamic Characteristics of Pump Annular Seals, " *7th Workshop on Rotordynamic Instability Problems in High Performance Turbomachinery*, held at Texas A&M University, College Station, Texas, May 10-12.

Jeffery, G.B., 1922, "The Motion of Ellipsoidal Particles Immersed in a Viscous Fluid," *Proceedings of the Royal Society*, Series A102, p. 161-179.

Khalil, M.F., and Rhodes, E., 1980, "Effect of Air Bubbles on Externally Pressurized Bearing Performance," *WEAR*, Vol. 65, pp.113-123.

Look, D., Sauer, H., 1986, *Engineering Thermodynamics*, PWS Publishers, Boston, Massachusets.

Mc Adams, W.H., Woods, W.K., and Heroman, L.C., Jr., 1942, "Vaporization Inside Horizontal Tubes- II -Benzene-Oil Mixtures," *ASME Transactions*, Vol. 64, p.193.

McCarty, R.D., NBS Standard Reference Data Base 12, 1986, "Thermophysical Properties of Fluids, MIPROPS-86," Thermophysics Division, Center for Chemical Engineering, National Bureau of Standards, Colorado.

Meirovitch, L., 1986, *Elements of Vibration Analysis*, Wiley, New York.

Muller, I., 1968, "A Thermodynamic Theory of Mixture of Fluids," *Archive of Rational Mechanics and Analysis*, Vol. 28, pp.1-39.

Nakahara, T., Makino, T., Jyogoku, K., 1988, "Observations of Liquid Droplet Behavior and Oil Film Formation in O/W Type Emulsion Lubrication," *ASME Journal of Tribology*, Vol. 110, pp. 348-353.

Palazzolo, A., 1992, personal communication.

Patankar, S.V., 1980, *Numerical Heat Transfer and Fluid Flow*, Hemisphere Publishing Corporation, McGraw-Hill Book Company, New York.

Pinkus, O., 1990, *Thermal Aspects of Fluid Film Tribology*, ASME Press, New York, pp. 326-340.

San Andres, L., 1991, "Analysis of Variable Fluid Properties, Turbulent Annular Seals," *ASME Journal of Tribology*, Vol. 113, pp. 694-702.

San Andres, L., 1992, "Analysis of Turbulent Hydrostatic Bearings with a Barotropic Cryogenic Fluid," *ASME Journal of Tribology*, Vol. 114, pp. 755-765.

San Andres, L. 1995, "Thermohydrodynamic Analysis of Fluid Film Bearings for Cryogenic Applications," *Journal of Propulsion and Power*, Vol. 11,5, pp.964-972.

San Andres, L. 1996, "Angled Injection-Hydrostatic Bearings Analysis and Comparisons to Test Results," ASME Paper No. 96-TRIB-10.

Salhi, A., Rey, C., and Rosant, J.M., 1992, "Pressure Drop in Single-Phase and Two-Phase Couette-Poiseuille Flow," *ASME Journal of Fluids Engineering*, Vol. 114, pp.80-84.

Taylor, G.I., 1932, "The Viscosity of a Fluid Containing Small Drops of Another Fluid," *Proceedings of the Royal Society*, Series A138, p. 41-48.

Tonder, K., 1975, "Parallel Surfaces Lubricated by a Bubbly Oil," *WEAR*. Vol. 35, pp. 23-34.

Tonder, K., 1976a, "Thermal Model of Effects of Gas Bubbles on the Lubrication of Parallel Surfaces," *WEAR*, Vol. 40, pp. 37-50.

Tonder, K., 19776b, "Effect on Bearing Performance of a Bubbly Lubricant," *JSLE-ASLE International Lubrication Conference*, Tokyo, 1975, Elsevier, Amsterdam, 1976.

Van Doormaal, J.P., and Raithby, D., 1984, "Enhancements of the SIMPLE Method for Predicting Incompressible Fluid Flows," *Numerical Heat Transfer*, Vol. 7, pp.144-163.

Vance, J.M., 1988, *Rotordynamics of Turbomachinery*, Wiley and Sons, New York.

Wang, S.H., Al-Sharif, A., Rajagopal K.R., Szeri A.Z., 1993, "Lubrication with Binary Mixtures: Liquid-Liquid Emulsion in an EHL Conjunction," *ASME Journal of Tribology*, Vol. 115, pp. 515-522.

Yang, Z., 1992, "Thermohydrodynamic Analysis of Product-Lubricated Hydrostatic Bearings in Turbulent Regime," Ph.D Dissertation, Mechanical Engineering

Dept., Texas A&M University.

Yang, Z, San Andres, L, Childs, D., 1993a, "Thermal Effects in Cryogenic Liquid Annular Seals - Part II: Numerical Solution and Results," *ASME Journal of Tribology*, Vol. 115, pp. 277-284.

Yang, Z, San Andres, L, Childs, D., 1993b, "Thermal Effects in Cryogenic Liquid Annular Seals - Part I: Theory and Approximate Solution," *ASME Journal of Tribology*, Vol. 115, pp. 267-276.

Yasuna, J.A., Hughes, W.F., 1990, "A Continuous Boiling Model for Face Seals," *ASME Journal of Tribology*, Vol. 112, pp. 266-274.

Yasuna, J.A., Hughes, W.F., 1992, "Squeeze Film Dynamics of Two-Phase Seals," *ASME Journal of Tribology*, Vol. 114, pp. 236-247.

Zeidan, F.Y., Vance, J.M., 1989, "Cavitation Leading to a Two Phase Fluid in Squeeze Film Damper," *ASLE Transactions*, Vol. 32, pp. 100-110.

Zeidan, F.Y., Vance, J.M., 1990, "A Density Correlation for a Two Phase Lubricant and its Effect on the Pressure Distribution," *ALSE Transactions*, Vol. 33, pp. 641-647.

Zuber, N., and Dougherty, D.E., 1982, "The Field Equations for Two-Phase Reynolds Film Flow with a Change of Phase," *ASLE Trans.*, Vol. 25, pp. 108-116.

APPENDIX 1

COEFFICIENTS FOR FIRST ORDER EQUATIONS

The following are the coefficients for equations (31) through (39).

Circumferential Momentum

$$\Gamma_{uu} = \gamma_{uu} \; ; \quad \Gamma_{uh} = \gamma_{uh}$$

$$\Gamma_{u\mu} = \gamma_{u\mu} \; ; \quad \Gamma_{up} = \gamma_{up}$$

$$\Gamma_{uv} = \gamma_{uu} - \text{Re}_p^\bullet \, \bar{\rho}_o h_o \frac{du_o}{d\bar{y}} \qquad \textbf{(a1.1)}$$

$$\Gamma_{up} = \gamma_{u\mu} \left.\frac{\partial \bar{\mu}}{\partial p}\right|_{\bar{i}} + \gamma_{up} \left.\frac{\partial \bar{\rho}}{\partial p}\right|_{\bar{i}}$$

$$\Gamma_{ui} = \gamma_{u\mu} \left.\frac{\partial \bar{\mu}}{\partial \bar{i}}\right|_{p} + \gamma_{up} \left.\frac{\partial \bar{\rho}}{\partial \bar{i}}\right|_{p}$$

Axial Momentum

$$\Gamma_{vu} = \gamma_{vu} \; ; \quad \Gamma_{vh} = \gamma_{vh}$$

$$\Gamma_{v\mu} = \gamma_{v\mu} \; ; \quad \Gamma_{vp} = \gamma_{vp}$$

$$\Gamma_{vv} = \gamma_{vv} - \text{Re}_p^\bullet \, \bar{\rho}_o h_o \frac{dv_o}{d\bar{y}} \qquad \textbf{(a1.2)}$$

$$\Gamma_{vp} = \gamma_{v\mu} \left.\frac{\partial \bar{\mu}}{\partial p}\right|_{\bar{i}} + \gamma_{vp} \left.\frac{\partial \bar{\rho}}{\partial p}\right|_{\bar{i}}$$

$$\Gamma_{vi} = \gamma_{v\mu} \left.\frac{\partial \bar{\mu}}{\partial \bar{i}}\right|_{p} + \gamma_{vp} \left.\frac{\partial \bar{\rho}}{\partial \bar{i}}\right|_{p}$$

Energy

$$\Gamma_{iu} = \gamma_{iu} \; ; \quad \Gamma_{i\mu} = \gamma_{i\mu}$$

$$\Gamma_{i\rho} = \gamma_{i\rho} - \mathrm{Re}_p^* \, E_I v_o h_o \frac{di_o}{d\bar{y}}$$

$$\Gamma_{iv} = \gamma_{iv} + h_o \frac{dp_o}{d\bar{y}} - \mathrm{Re}_p^* \, E_I \bar{\rho}_o h_o \frac{di_o}{d\bar{y}}$$

$$\Gamma_{ih} = \gamma_{ih} + v_o \frac{dp_o}{d\bar{y}} - \mathrm{Re}_p^* \, E_I \bar{\rho}_o v_o \frac{di_o}{d\bar{y}} \qquad \textbf{(a1.3)}$$

$$\Gamma_{ip} = i\sigma h_o + \Gamma_{i\mu} \frac{\partial \bar{\mu}}{\partial p}\bigg|_i + \Gamma_{i\rho} \frac{\partial \bar{\rho}}{\partial p}\bigg|_i$$

$$\Gamma_{ii} = i\sigma \, \mathrm{Re}_p^* \, E_I \bar{\rho}_o h_o + \Gamma_{i\mu} \frac{\partial \bar{\mu}}{\partial \bar{i}}\bigg|_p + \Gamma_{i\rho} \frac{\partial \bar{\rho}}{\partial \bar{i}}\bigg|_p$$

Shear Stress Coefficients

$$\gamma_{uu} = -\bar{\mu}_o \left[\frac{k_{xo}}{h_o} + f_{r1}(u_o - \Lambda)^2 + f_{s1}u_o^2 \right]$$

$$\gamma_{uv} = -\bar{\mu}_o v_o \left[f_{r1}(u_o - \Lambda) + f_{s1}u_o \right]$$

$$\gamma_{uh} = -\frac{\bar{\mu}_o}{h_o^2} \left[u_o(-k_{xo} + C_{cr} + C_{cs}) - \Lambda \left(C_{cr} - \frac{k_{ro}}{2} \right) \right] \qquad \textbf{(a1.4)}$$

$$\gamma_{u\rho} = -\frac{\bar{\mu}_o b_m}{2 h_o \bar{\rho}_o} \left[u_o(\gamma_r + \gamma_s) - \Lambda \gamma_r \right] + \frac{h_o}{\bar{\rho}_o} \frac{\partial p_o}{\partial \bar{x}}$$

$$\gamma_{u\mu} = \frac{b_m}{2 h_o} \left[u_o(\gamma_r + \gamma_s) - \Lambda \gamma_r \right]$$

$$\gamma_{vv} = -\overline{\mu}_o \left[\frac{k_{yo}}{h_o} + (f_{r1} + f_{s1})v_o^2 \right]$$

$$\gamma_{vu} = \gamma_{uv}$$

$$\gamma_{vh} = -\frac{\overline{\mu}_o v_o}{h_o^2} \left[-k_{yo} + C_{cr} + C_{cs} \right] \qquad \text{(a2.5)}$$

$$\gamma_{v\rho} = -\frac{\overline{\mu}_o b_m}{2h_o \overline{\rho}_o} \left[v_o(\gamma_r + \gamma_s) \right] + \frac{h_o}{\overline{\rho}_o} \frac{\partial p_o}{\partial \overline{y}}$$

$$\gamma_{v\mu} = \frac{b_m}{2h_o} \left[v_o(\gamma_r + \gamma_s) \right]$$

$$\gamma_{iu} = \frac{\overline{\mu}_o}{h_o} \left[\left(2u_o + \frac{\Lambda}{2} \right) k_{xo} - \Lambda k_{ro} \right] + \overline{\mu}_o \left[(u_{co} + 2u_{c1})(u_o - \Lambda) f_{r1} + u_{co} u_o f_{s1} \right]$$

$$\gamma_{iv} = \frac{\overline{\mu}_o}{h_o} (2v_o k_{xo}) + \overline{\mu}_o v_o \left[u_{co}(f_{r1} + f_{s1}) + 2u_{c1} f_{r1} \right]$$

$$\gamma_{ih} = \frac{\overline{\mu}_o}{h_o^2} \left[u_{co}(C_{cr} + C_{cs}) + 2u_{c1} C_{cr} \right] \qquad \text{(a1.6)}$$

$$\gamma_{i\rho} = \frac{\overline{\mu}_o}{h_o \overline{\rho}_o} \left\{ u_{co} \left[k_{xo} + \frac{b_m}{2}(\gamma_r + \gamma_s) \right] + u_{c1}(k_{ro} + b_m \gamma_r) \right\}$$

$$\gamma_{i\mu} = -\frac{b_m}{h_o} \left[\frac{u_{co}}{2}(\gamma_r + \gamma_s) + u_{c1} \gamma_r \right]$$

where

$$C_{cr} = \frac{1}{2}(\text{Re}_{ro} C_r + b_m)\gamma_r \quad ; \quad C_{cs} = \frac{1}{2}(\text{Re}_{so} C_s + b_m)\gamma_s$$

$$C_r = c_m \frac{r_r}{h_o c} \quad ; \quad C_s = c_m \frac{r_s}{h_o c}$$

$$\mathrm{Re}_{ro} = \mathrm{Re}_p \frac{h_o \bar{\rho}_o}{\bar{\mu}_o} \sqrt{(u_o - \Lambda)^2 + v_o^2} \quad ; \quad \mathrm{Re}_{so} = \mathrm{Re}_p \frac{h_o \bar{\rho}_o}{\bar{\mu}_o} \sqrt{u_o^2 + v_o^2}$$

$$\gamma_r = \frac{-a_m e_m}{\left[\dfrac{f_{ro}}{a_m} - 1 \right]^{\frac{1}{e_m} - 1}} \quad ; \quad \gamma_s = \frac{-a_m e_m}{\left[\dfrac{f_{so}}{a_m} - 1 \right]^{\frac{1}{e_m} - 1}}$$

$$f_{r1} = \frac{h_o}{2\,\mathrm{Re}_{ro}} \left(\frac{\mathrm{Re}_p \bar{\rho}_o}{\bar{\mu}_o} \right)^2 \left[f_{ro} + \frac{b_m}{\mathrm{Re}_{ro}} \gamma_r \right] \quad ; \quad f_{s1} = \frac{h_o}{2\,\mathrm{Re}_{so}} \left(\frac{\mathrm{Re}_p \bar{\rho}_o}{\bar{\mu}_o} \right)^2 \left[f_{so} + \frac{b_m}{\mathrm{Re}_{so}} \gamma_s \right]$$

$$u_{co} = u_o^2 + v_o^2 + u_o \frac{\Lambda}{2} \quad ; \quad u_{c1} = \frac{\Lambda^2}{4} - u_o \Lambda$$

APPENDIX 2

DISCRETIZATION EQUATIONS

Dimensionless zeroth order discretization equations

Circumferential momentum equation

$$A_P^u \, u_P = A_S^u \, u_S + S_P^u \qquad \text{(a2.1)}$$

where

$$A_S^u = \text{Re}_P^* \left(\bar{\rho}_o h_o u_o \right)_S$$

$$A_P^u = A_S^u + \left(\frac{\bar{\mu}_o k_{xo}}{h_o} \right)_P \delta \bar{y}$$

$$S_P^u = \left(\frac{\bar{\mu}_o k_{xo} \Lambda}{2 h_o} \right)_P \delta \bar{y}$$

Axial momentum equation

$$A_P^v \, v_P = A_S^v \, v_S + S_P^v \qquad \text{(a2.2)}$$

where

$$A_S^v = \text{Re}_P^* \left(\bar{\rho}_o h_o v_o \right)_S$$

$$A_P^v = A_S^v + \left(\frac{\bar{\mu}_o k_{xo}}{h_o} \right)_P^v \delta \bar{y}^v$$

$$S_P^v = h_P^v \left(p_S - p_P \right)$$

Energy

$$A_P^i \, \bar{i}_P = A_S^i \, \bar{i}_S + S_2^i + S_1^i \delta \bar{y} \qquad \text{(a2.3)}$$

where

$$A_P^t = A_S^t = \text{Re}_p^\bullet \, E_I \left(\bar{\rho}_o h_o v_o \right)^s$$

$$S_1^t = \frac{\bar{\mu}_o}{h_o} \left[\left(u_o^2 + v_o^2 + u_o \, \frac{\Lambda}{2} \right) k_{xo} + \left(\frac{\Lambda^2}{4} - u_o \Lambda \right) k_{ro} \right]_p$$

$$S_2^t = (h_o v_o)_p \left(p_N - p_S \right)$$

Pressure correction equation (based on continuity)

$$A_P^p \, p_P' = A_N^p \, p_N' + A_S^p \, p_S' - \left(F^n - F^s \right) \qquad \text{(a2.4)}$$

where

$$A_P^p = A_N^p + A_S^p + \beta_{po} \left(F^n - F^s \right)$$

$$A_N^p = \bar{\rho}_o^\bullet h_o D_P^v$$

$$A_S^p = \bar{\rho}_o^\bullet h_o D_P^v + \beta_{po} \, F^s$$

$$F^s = \left(\bar{\rho}_o h_o v_o \right)^s ; \quad F^n = \left(\bar{\rho}_o h_o v_o \right)^n$$

Velocity correction

$$v_P' = D_P^v \left(p_S' - p_P' \right) \qquad \text{(a2.5)}$$

with

$$D_P^v = \frac{h_P^v}{A_P^v - A_S^v}$$

Dimensionless first order discretization equations

The first order variables are defined as:

$$
\mathbf{u} = \begin{bmatrix} u_{\alpha c} \\ u_{\alpha s} \end{bmatrix}; \quad
\mathbf{v} = \begin{bmatrix} v_{\alpha c} \\ v_{\alpha s} \end{bmatrix}; \quad
\mathbf{p} = \begin{bmatrix} p_{\alpha c} \\ p_{\alpha s} \end{bmatrix};
$$

$$
\bar{\mathbf{i}} = \begin{bmatrix} \bar{i}_{\alpha c} \\ \bar{i}_{\alpha s} \end{bmatrix}; \quad
\bar{\rho} = \begin{bmatrix} \bar{\rho}_{\alpha c} \\ \bar{\rho}_{\alpha s} \end{bmatrix}; \quad
\mathbf{I} = \begin{bmatrix} 1 & 0 \\ 0 & 1 \end{bmatrix}
$$

(a2.6)

Circumferential momentum equation

$$
\mathbf{A}_P^u \, \mathbf{u}_P = \mathbf{A}_S^u \, \mathbf{u}_S + \mathbf{S}_P^u \qquad \text{(a2.7)}
$$

where

$$
\mathbf{A}_S^u = \mathrm{Re}_p^* \frac{\bar{\rho}_o h_o v_o}{\delta \bar{y}} \mathbf{I}
$$

$$
\mathbf{A}_P^u = \begin{bmatrix}
\Gamma_{uu} - i\sigma \mathrm{Re}_p^* \bar{\rho}_o h_o + \mathrm{Re}_p^* \dfrac{\bar{\rho}_o h_o v_o}{\delta \bar{y}} & \mathrm{Re}_p^*\left(\bar{\rho}_o h_o u_o\right) \\[4mm]
- \mathrm{Re}_p^*\left(\bar{\rho}_o h_o u_o\right) & \Gamma_{uu} - i\sigma \mathrm{Re}_p^* \bar{\rho}_o h_o + \mathrm{Re}_p^* \dfrac{\bar{\rho}_o h_o v_o}{\delta \bar{y}}
\end{bmatrix}_P
$$

$$
\mathbf{S}_P^u = -\left[\Gamma_{uv} - \mathrm{Re}_p^* \frac{\bar{\rho}_o h_o v_o}{\delta \bar{y}}\left(u_o^n - u_o^s\right) \right]\mathbf{v}_* - \begin{bmatrix} \Gamma_{uh} \\ 0 \end{bmatrix} - \begin{bmatrix} \Gamma_{up} & h_o \\ -h_o & \Gamma_{up} \end{bmatrix}\mathbf{p}_P - \Gamma_{ut}\mathbf{T}_P
$$

The coefficients Γ_{ij} are functions of the zeroth order solution only and they are defined in Appendix 1.

Axial momentum equation

$$\mathbf{A}_P^v \, \mathbf{v}_P = \mathbf{A}_S^v \, \mathbf{v}_S + \mathbf{S}_P^v \qquad \textbf{(a2.8)}$$

where

$$\mathbf{A}_S^v = \mathrm{Re}_p^{\bullet} \frac{\overline{\rho}_o h_o v_o}{\delta \overline{y}^v} \mathbf{I}$$

$$\mathbf{A}_P^v = \begin{bmatrix} \overline{\Gamma}_{vv} + \mathrm{Re}_p^{\bullet} \dfrac{\overline{\rho}_o h_o u_o}{\delta \overline{y}^v} + \|S_{P2}, 0\| & \mathrm{Re}_p^{\bullet}\left(\overline{\rho}_o h_o u_o\right). \\[2ex] - \mathrm{Re}_p^{\bullet}\left(\overline{\rho}_o h_o u_o\right). & \overline{\Gamma}_{vv} + \mathrm{Re}_p^{\bullet} \dfrac{\overline{\rho}_o h_o u_o}{\delta \overline{y}^v} + \|S_{P2}, 0\| \end{bmatrix}$$

$$S_{P2} = \mathrm{Re}_p^{\bullet} \frac{\overline{\rho}_o h_o}{\delta \overline{y}^v}\left(v_o^n - v_o^s\right); \qquad \overline{\Gamma}_{vv} = \Gamma_{vv} - \mathbf{i}\sigma \mathrm{Re}_p^{\bullet} \, \overline{\rho}_o h_o \; ; \qquad \|a, b\| = Max(a, b)$$

$$\mathbf{S}_P^v = -\Gamma_{vu}\mathbf{u}. - \begin{bmatrix} \Gamma_{uh} \\ 0 \end{bmatrix} - \Gamma_{vp}\mathbf{p}. - \Gamma_{ut}\mathbf{T}. + \left\|- S_{P2}, 0\right\| \mathbf{v}_P + \frac{h_o}{\delta \overline{y}^v}\left[\mathbf{p}_S - \mathbf{p}_P\right]$$

Energy

$$\mathbf{A}_P^i \, \overline{\mathbf{i}}_P = \mathbf{A}_S^i \, \overline{\mathbf{i}}_S + \mathbf{S}_P^i \qquad \textbf{(a2.9)}$$

where

$$\mathbf{A}_S^i = \mathrm{Re}_p^{\bullet} E_I \frac{\overline{\rho}_o h_o v_o}{\delta \overline{y}} \mathbf{I}$$

$$\mathbf{A}_P^i = \begin{bmatrix} \Gamma_{ii} + \mathrm{Re}_p^{\bullet} E_I \dfrac{\overline{\rho}_o h_o v_o}{\delta \overline{y}} & \mathrm{Re}_p^{\bullet}\left(\overline{\rho}_o h_o u_o\right) \\[2ex] - \mathrm{Re}_p^{\bullet}\left(\overline{\rho}_o h_o u_o\right) & \Gamma_{ii} + \mathrm{Re}_p^{\bullet} E_I \dfrac{\overline{\rho}_o h_o v_o}{\delta \overline{y}} \end{bmatrix}_P$$

$$S_P^u = \begin{bmatrix} \Gamma_{th} \\ 0 \end{bmatrix} + \Gamma_{tu}\mathbf{u}_P + \Gamma_{tv}\mathbf{v}_P + \begin{bmatrix} \Gamma_{tp} + \left(\dfrac{h_o v_o}{\delta\tilde{y}}\right) & \left(u_o + \dfrac{\Lambda}{2}\right)h_o \\ -\left(u_o + \dfrac{\Lambda}{2}\right)h_o & \Gamma_{tp} + \left(\dfrac{h_o v_o}{\delta\tilde{y}}\right) \end{bmatrix}_P \mathbf{p}_P - \left(\dfrac{h_o v_o}{\delta\tilde{y}}\right)_P \mathbf{p}_S$$

Pressure correction

$$\mathbf{A}_P^p\,\mathbf{p}_P' = \mathbf{A}_N^p\,\mathbf{p}_N' + \mathbf{A}_S^p\,\mathbf{p}_S' + \mathbf{S}_P^p \qquad \textbf{(a2.10)}$$

where

$$\mathbf{A}_N^p = \left(h_o\bar{\rho}_o\right)_P \mathbf{G}_N^v$$

$$\mathbf{A}_S^p = \left(h_o\bar{\rho}_o\right)_P \mathbf{G}_P^v + \beta_{pS}(v_o h_o)_P\mathbf{I}$$

$$\mathbf{A}_P^p = \left(h_o\bar{\rho}_o\right)_P \left[\mathbf{G}_N^v + \mathbf{G}_P^v\right] + \delta\tilde{y}\left(h_o\bar{\rho}_o\right)_P \underline{\underline{\mathbf{G}}}_P^u + \beta_p\mathbf{F}$$

$$\mathbf{S}_P^p = -\begin{bmatrix} \bar{\rho}_{oP}(v_{oN} - v_{oS}) + \mathrm{i}\sigma(\bar{\rho}_o\delta\tilde{y})_P \\ -\delta\tilde{y}(\bar{\rho}_o h_o)_P \end{bmatrix} + (\bar{\rho}_o h_o)_P(\mathbf{v}_N - \mathbf{v}_P). -(\bar{\rho}_o h_o)_P\begin{bmatrix} 0 & 1 \\ -1 & 0 \end{bmatrix}\mathbf{u}_P$$
$$- \mathbf{F}\bar{\mathbf{p}}_P + (v_o h_o)_P\bar{\mathbf{p}}_S$$

$$\mathbf{F} = \begin{bmatrix} (v_o h_o)_N + \mathrm{i}\sigma(h_o\delta\tilde{y})_P & \delta\tilde{y}(u_o h_o)_P \\ -\delta\tilde{y}(u_o h_o)_P & (v_o h_o)_N + \mathrm{i}\sigma(h_o\delta\tilde{y})_P \end{bmatrix}$$

$$\mathbf{G}^{u,v} = \left(\mathbf{A}^{u,v}\right)^{-1}\dfrac{h_o}{\delta\tilde{y}} \quad ; \quad given \quad \mathbf{G}^u = \begin{bmatrix} g_{11} & g_{12} \\ g_{21} & g_{22} \end{bmatrix} \Rightarrow \underline{\underline{\mathbf{G}}}^u = \begin{bmatrix} g_{22} & -g_{21} \\ -g_{12} & g_{11} \end{bmatrix}$$

The subscript * indicates that the quantity is evaluated at the center of a control volume.

VITA

Grigory Luis Alberto Arauz Rosero, the son of Luis Alberto Arauz and Fabiola Rosero, was born on ███████████, in ███████████. He began his college studies at the Escuela Politécnica Nacional, Quito-Ecuador, in 1983 and graduated, Cum Laude, in 1989 with a Mechanical Engineer degree. After working for over a year for the Army's Industries National Direction, Quito-Ecuador, as an specialist in project development, he enrolled the graduate program at Texas A&M University. He obtained his M.S. in Mechanical Engineering in 1993, and he is currently pursuing a Ph.D. degree. Mr. Arauz has written several technical reports and co-authored seven technical papers in the fields of tribology and rotordynamics. In January, 1989, he married Ximena Vinueza. In February, 1994, his son Luis Alberto, was born.

Permanent address:

Grigory L. Arauz
Mechanical Engineering Dept.
Texas A&M University
College Station, TX 77843